Statistical mechanics of two-dimensional and geophysical flows

Freddy Bouchet, Antoine Venaille

Statistical mechanics of two-dimensional and geophysical flows

Freddy Bouchet[a], Antoine Venaille[b]

[a] *Université de Lyon, Laboratoire de Physique de l'Ecole Normale Supérieure de Lyon, ENS-Lyon, CNRS, 46 allée d'Italie, 69364 Lyon cedex 07, France.* Freddy.Bouchet@ens-lyon.fr
[b] *GFDL-AOS Princeton University, Forrestal Campus, NJ 08542 Princeton, United States.*

Abstract

The theoretical study of the self-organization of two-dimensional and geophysical turbulent flows is addressed based on statistical mechanics methods. This review is a self-contained presentation of classical and recent works on this subject; from the statistical mechanics basis of the theory up to applications to Jupiter's troposphere and ocean vortices and jets. Emphasize has been placed on examples with available analytical treatment in order to favor better understanding of the physics and dynamics.

After a brief presentation of the 2D Euler and quasi-geostrophic equations, the specificity of two-dimensional and geophysical turbulence is emphasized. The equilibrium microcanonical measure is built from the Liouville theorem. Important statistical mechanics concepts (large deviations, mean field approach) and thermodynamic concepts (ensemble inequivalence, negative heat capacity) are briefly explained and described.

On this theoretical basis, we predict the output of the long time evolution of complex turbulent flows as statistical equilibria. This is applied to make quantitative models of two-dimensional turbulence, the Great Red Spot and other Jovian vortices, ocean jets like the Gulf-Stream, and ocean vortices. A detailed comparison between these statistical equilibria and real flow observations is provided.

We also present recent results for non-equilibrium situations, for the studies of either the relaxation towards equilibrium or non-equilibrium steady states. In this last case, forces and dissipation are in a statistical balance; fluxes of conserved quantity characterize the system and microcanonical or other equilibrium measures no longer describe the system.

Keywords: 2D Euler equations, large scales of turbulent flows, 2D turbulence, quasi-geostrophic equations, geophysical turbulence, statistical mechanics, long range interactions, kinetic theory, Jupiter's troposphere, Great Red Spot, ocean jets, ocean rings
PACS: 05.20.-y, 05.20.Jj, 05.45.-a, 05.45.Jn, 05.65.+b, 05.70.-a, 05.70.Fh, 05.70.Ln, 02.50.-r, 02.50.Ey, 47.10.-g, 47.10.ad, 47.20.-k, 47.20.Ky, 47.27.-i, 47.27.eb, 47.32.-y, 92.05.-x, 92.05.Bc, 92.10.-c, 92.10.A-, 92.10.ak, 96.15.-g, 96.15.Hy, 96.30.Kf

Contents

List of figure captions

Figure 1 page 11. Observation of the Jovian atmosphere from Cassini (Courtesy of NASA/JPL-Caltech). See figure 12 page 71 for more detailed legends.

Figure 2 page 11. Observation of the north Atlantic ocean from altimetry. See figure 19 page 79 for more detailed legends.

Figure 3 page 12. Example of an experimental realization of a 2D flow in a soap bubble, courtesy of American Physical Society. See [177] and [107] for further details.

Figure 4 page 12. Experimental observation of a 2D long lived coherent vortex on the 14m diameter Coriolis turntable (photo gamma production).

Figure 5 page 22. Vertical structure of the 1.5-layer quasi-geostrophic model: a deep layer of density $\rho + \Delta\rho$ and a lighter upper layer of thickness H and density ρ. Because of the inertia of the lower layer, the dynamics is limited to the upper layer.

Figure 6 page 33. Snapshot of electron density (analogous to vorticity field) at successive time from an initial condition with two vortices to a single large scale coherent structure via turbulent mixing (see [173, 174]). The best experimental realization of inviscid 2D Euler equations is probably so far achieved in those magnetized electron plasma experiments where the electrons are confined in a Penning trap. The dynamics of both systems are indeed isomorphic, where the electron density plays the role of vorticity. The major drawback of this experimental setting comes from its observation, since any measurement requires the destruction of the plasma itself.

Figure 7 page 58. Bifurcation diagram for the statistical equilibria of the 2D Euler equations in a doubly periodic domain with aspect ratio δ, in the limit where the normal form treatment is valid, in the g-a_4 parameter plane. The geometry parameter g is inversely proportional to the energy and proportional to the difference between the two first eigenvalues of the Laplacian (or equivalently to $\delta - 1$ in the limit of small $\delta - 1$), the parameter a_4 measures the non-quadratic contributions to the Casimir functional. The solid line is a second order phase transition between a dipole (mixed state) and a parallel flow along the y direction (pure state $X = 0$). Along the dashed line, a metastable parallel flow (along the x direction, pure state $X = 1$) loses its stability.

Figure 8 page 60. Bifurcation diagrams for statistical equilibria of the 2D Euler equations in a doubly periodic domain a) in the g-a_4 plane (see figure 7) b) obtained numerically in the $E - a_4$ plane, in the case of doubly periodic geometry with aspect ratio $\delta = 1.1$. The colored insets are streamfunction and the inset curve illustrates good agreement between numerical and theoretical results in the low energy limit.

Figure 9 page 65. The double well shape of the specific free energy $f(\phi)$ (see equation (80)).

The function $f(\phi)$ is even and possesses two minima at $\phi = \pm u$. At equilibrium, at zeroth order in R, the physical system will be described by two phases corresponding to each of these minima.

Figure 10 page 66. At zeroth order, ϕ takes the two values $\pm u$ on two sub-domains $A_{\pm}$. These sub-domains are separated by strong jets. The actual shape of the structure, or equivalently the position of the jets, is given by the first order analysis.

Figure 11 page 68. Illustration of the Plateau problem (or minimal area problem) with soap films: the spherical bubble minimizes its area for a given volume (Jean Simeon Chardin, *Les bulles de savon*, 1734).

Figure 12 page 71. Observation of the Jovian atmosphere from Cassini (Courtesy of NASA/JPL-Caltech). One of the most striking feature of the Jovian atmosphere is the self organization of the flow into alternating eastward and westward jets, producing the visible banded structure and the existence of a huge anticyclonic vortex $\sim 20,000$ *km* wide, located around 20 South: the Great Red Spot (GRS). The GRS has a ring structure: it is a hollow vortex surrounded by a jet of typical velocity $\sim 100\ m.s^{\{-1\}}$ and width $\sim 1,000\,km$. Remarkably, the GRS has been observed to be stable and quasi-steady for many centuries despite the surrounding turbulent dynamics. The explanation of the detailed structure of the GRS velocity field and of its stability is one of the main achievement of the equilibrium statistical mechanics of two dimensional and geophysical flows (see figure 13 and section 4).

Figure 13 page 73. Left: the observed velocity field is from Voyager spacecraft data, from Dowling and Ingersoll [63] ; the length of each line is proportional to the velocity at that point. Note the strong jet structure of width of order R, the Rossby deformation radius. Right: the velocity field for the statistical equilibrium model of the Great Red Spot. The actual values of the jet maximum velocity, jet width, vortex width and length fit with the observed ones. The jet is interpreted as the interface between two phases; each of them corresponds to a different mixing level of the potential vorticity. The jet shape obeys a minimal length variational problem (an isoperimetrical problem) balanced by the effect of the deep layer shear.

Figure 14 page 73. Left panel: typical vortex shapes obtained from the isoperimetrical problem (curvature radius equation (85)), for two different values of the parameters (arbitrary units). The characteristic properties of Jupiter's vortex shapes (very elongated, reaching extremal latitude y_m where the curvature radius is extremely large) are well reproduced by these results. Central panel: the Great Red Spot and one of the White Ovals. Right panel: one of the Brown Barge cyclones of Jupiter's north atmosphere. Note the very peculiar cigar shape of this vortex, in agreement with statistical mechanics predictions (left panel).

Figure 15 page 75. Phase diagram of the statistical equilibrium states versus the energy E and a parameter related to the asymmetry between positive and negative potential vorticity B, with a quadratic topography. The inner solid line corresponds to a phase transition, between vortex and straight jet solutions. The dash line corresponds to the limit of validity of the small

deformation radius hypothesis. The dot lines are constant vortex aspect ratio lines with values 2,10,20,30,40,50,70,80 respectively. We have represented only solutions for which anticyclonic potential vorticity dominate ($B > 0$). The opposite situation may be recovered by symmetry. For a more detailed discussion of this figure, the precise relation between E, B and the results presented in this review, please see [21].

Figure 16 page 76. Snapshot of surface velocity field from a comprehensive numerical simulation of the southern Oceans [90]. Left: coarse resolution, the effect of mesoscale eddies ($\sim 100km$) is parameterized. Right: higher resolution, without parameterization of mesoscale eddies. Note the formation of large scale coherent structure in the high resolution simulation: there is either strong and thin eastward jets or rings of diameter ~ 200 km. Typical velocity and width of jets (be it eastward or around the rings) are respectively ~ 1 $m.s^{-1}$ and ~ 20 km. The give a statistical mechanics explanation and model for these rings.

Figure 17 page 77. Vortex statistical equilibria in the quasi-geostrophic model. It is a circular patch of (homogenized) potential vorticity in a background of homogenized potential vorticity, with two different mixing values. The velocity field (right panel) has a very clear ring structure, similarly to the Gulf-Stream rings and to many other ocean vortices. The width of the jet surrounding the ring has the order of magnitude of the Rossby radius of deformation R.

Figure 18 page 78. Altimetry observation of the westward drift of oceanic eddies (including rings) from [52], figure 4. The red line is the zonal average (along a latitude circle) of the propagation speeds of all eddies with life time greater than 12 weeks. The black line represents the velocity $\beta_c R^2$ where β_c is the meridional gradient of the Coriolis parameter and R the first baroclinic Rossby radius of deformation. This eddy propagation speed is a prediction of statistical mechanics, when the linear momentum conservation, due to translational invariance, is taken into account (see section 4.4.2).

Figure 19 page 79. Observation of the sea surface height of the north Atlantic ocean (Gulf Stream area) from altimetry REF. As explained in section 2.1, for geophysical flows, the surface velocity field can be inferred from the see surface height (SSH): strong gradient of SSH are related to strong jets. The Gulf stream appears as a robust eastward jet (in presence of meanders), flowing along the east coast of north America and then detaching the coast to enter the Atlantic ocean, with an extension $L \sim 2000$ km. The jet is surrounded by numerous westward propagating rings of typical diameters $L \sim 200$ km. Typical velocities and widths of both the Gulf Stream and its rings jets are respectively 1 $m.s^{-1}$ and 50 km, corresponding to a Reynolds number $Re \sim 10^{11}$. Such rings can be understood as local statistical equilibria, and strong eastward jets like the Gulf Stream and obtained as marginally unstable statistical equilibria in simple academic models (see subsections 4.4-5).

Figure 20 page 80. b) and c) represent respectively a snapshot of the streamfunction and potential vorticity (red: positive values; blue: negative values) in the upper layer of a three layers quasi-geostrophic model in a closed domain, representing a mid-latitude oceanic basin, in

presence of wind forcing. Both figures are taken from numerical simulations [1], see also [7]. a) Streamfunction predicted by statistical mechanics, see section 5 on page 79 for further details. Even in an out-equilibrium situation like this one, the equilibrium statistical mechanics predicts correctly the overall qualitative structure of the flow.

Figure 21 page 81. a) Eastward jet: the interface is zonal, with positive potential vorticity $q = u$ on the northern part of the domain. b) Westward jet: the interface is zonal, with negative potential vorticity $q = -u$ in the northern part of the domain. c) Perturbation of the interface for the eastward jet configuration, to determine when this solution is a local equilibrium (see subsection 5.2). Without topography, both (a) and (b) are entropy maxima. With positive beta effect (b) is the global entropy maximum; with negative beta effect (a) is the global entropy maximum.

Figure 22 page 86. Phase diagrams of RSM statistical equilibrium states of the 1.5 layer quasi-geostrophic model, characterized by a linear $q - \psi$ relationship, in a rectangular domain elongated in the x direction. $S(E,\Gamma)$ is the equilibrium entropy, E is the energy and Γ the circulation. Low energy states are the celebrated Fofonoff solutions [80], presenting a weak westward flow in the domain bulk. High energy states have a very different structure (a dipole). Please note that at high energy the entropy is non-concave. This is related to ensemble inequivalence (see 3.3 page 50), which explain why such states were not computed in previous studies. The method to compute explicitly this phase diagram is the same as the one presented in subsection 3.5 page 52. See [197] for more details.

Figure 23 page 92. First experimental observation of the inverse energy cascade and the associated $k^{-5/3}$ spectrum, from [179]. The 2D turbulent flow is approached here by a thin layer of mercury and a further ordering from a transverse magnetic field. The flow is forced by an array of electrodes at the bottom, with an oscillating electric field. The parameter Rh is the ratio between inertial to bottom friction terms. At low Rh the flow has the structure of the forcing (left panel). At sufficiently high Rh the prediction of the self similar cascade theory is well observed (right panel, bottom), and at even higher Rh, the break up of the self similar theory along with the organization of the flow into a coherent large scale flow is observed (see right panel above).

Figure 25 page 98. $\omega - \psi$ scatter-plots (cyan) (see color figure on the .pdf version). In black the same after time averaging (averaging windows $1 \ll \tau \ll 1/\nu$, the drift due to translational invariance has been removed). Left: dipole case with $\delta = 1.03$. Right: unidirectional case $\delta = 1.10$.

Figure 26 page 99. Dynamics of the 2D Navier–Stokes equations with stochastic forces in a doubly periodic domain of aspect ratio δ, in a non-equilibrium phase transition regime. The two main plots are the time series and probability density functions (PDFs) of the modulus of the Fourier component $z_1 = \frac{1}{(2\pi)^2}\int_{\mathscr{D}} \mathrm{d}\mathbf{r}\, \omega(x,y)\exp(iy)$ illustrating random changes between dipoles ($|z_1| \simeq 0.55$) and unidirectional flows ($|z_1| \simeq 0.55$). As discussed in section 6.4.3, the existence of such a non-equilibrium phase transition can be guessed from equilibrium phase diagrams (see figure 8).

Figure 27 page 100. Bistability in a rotating tank experiment with topography (shaded area)[190, 201]. The dynamics in this experiment would be well modeled by a 2D barotropic model with topography (the quasi-geostrophic model with $R = \infty$). The flow is alternatively close to two very distinct states, with random switches from one state to the other. Left: the streamfunction of each of these two states. Right: the time series of the velocity measured at the location of the black square on the left figure, illustrating clearly the bistable behavior. The similar theoretical structures for the 2D Euler equations on one hand and the quasi-geostrophic model on the other hand, suggest that the bistability in this experiment can be explained as a non equilibrium phase transition, as done in section 6.4.3 (see also figure 26).

Figure 28 page 100. Kuroshio: sea surface temperature of the pacific ocean east of Japan, February 18, 2009, infra-red radiometer from satellite (AVHRR, MODIS) (New Generation Sea Surface Temperature (NGSST), data from JAXA (Japan Aerospace Exploration Agency)).
The Kuroshio is a very strong current flowing along the coast, south of Japan, before penetrating into the Pacific ocean. It is similar to the Gulf Stream in the North Atlantic. In the picture, The strong meandering color gradient (transition from yellow to green) delineates the path of the strong jet (the Kuroshio extension) flowing eastward from the coast of Japan into the Pacific ocean.
South of Japan, the yellowish area is the sign that, at the time of this picture, the path of the Kuroshio had detached from the Japan coast and was in a meandering state, like in the 1959-1962 period (see figure 29).

Figure 29 page 101. Bistability of the paths of the Kuroshio during the 1956-1962 period : paths of the Kuroshio in (left) its small meander state and (right) its large meander state. The 1000-m (solid) and 4000-m (dotted) contours are also shown. (figure from Schmeits and Dijkstraa [175], adapted from Taft 1972).

Figure 30 page 101. Bistability of the paths of the Kuroshio, from Qiu and Miao [161]: time series of the distance of the Kuroshio jet axes from the coast, averaged other the part of the coast between 132 degree and 140 degrees East, from a numerical simulation using a two layer primitive equation model.

Figure 31 page 106. Evolution of $\omega(x,y,t)$ from an initial vorticity perturbation $\omega(x,y,0) = \omega_1(y,0)\cos(x)$, by the linearized 2D Euler equations close to a shear flow $U(y) = \sigma y$ (colors in the .PDF document).

Figure 32 page 107. Evolution of the vorticity perturbation $\omega(x,y,t) = \omega(y,t)\exp(ikx)$, close to a parallel flow $\mathbf{v}_0(x,y) = U(y)\mathbf{e}_x$ with $U(y) = \cos(y)$, in a doubly periodic domain with aspect ratio δ. The figure shows the modulus of the perturbation $|\omega(y,t)|$ as a function of time and y. One clearly sees that the vorticity perturbation rapidly converges to zero close to the points where the velocity profile $U(y)$ has extrema ($U'(y_0) = 0$, with $y_o = 0$ and π). This *depletion of the perturbation vorticity* at the stationary streamlines y_0 is a new generic self-consistent

mechanism, understood mathematically as the regularization of the critical layer singularities at the edge of the continuous spectrum (see [23]).

Figure 33 page 127. The space-time series of perturbation velocity components, $|v_{\delta,x}(y,t)|$ (a) and $|v_{\delta,y}(y,t)|$ (b), for the initial perturbation profile $\cos(x/\delta)$ in a doubly periodic domain with aspect ratio $\delta = 1.1$. Both the components relax toward zero, showing the asymptotic stability of the Euler equations (colors in the .pdf document).

Figure 34 page 128. The time series of perturbation velocity components $|v_{\delta,x}(y,t)|$ (a) and $|v_{\delta,y}(y,t)|$ (b) at three locations, $y = 0$ (vicinity of the stationary streamline) (red), $y = \pi/4$ (green), and $y = \pi/2$ (blue), for the initial perturbation profile $A(y) = 1$ and the aspect ratio $\delta = 1.1$. We observe the asymptotic forms $|v_{\delta,x}(y,t)| \sim t^{-\alpha}$, with $\alpha = 1$, and $|v_{\delta,y}(y,t)| \sim t^{-\beta}$, with $\beta = 2$, in accordance with the theory for the asymptotic behavior of the velocity (equations (113) and (114)). The initial perturbation profile is $\cos(x/\delta)$ in a doubly periodic domain with aspect ratio $\delta = 1.1$ (colors in the .pdf document).

Figure 35 page 129. The space-time series of the x-averaged perturbation vorticity, $\omega_0(y,t) = \omega(y,t)$-$\Omega_0(y,0)$. The initial condition is $\omega(y,t) = \Omega_0(y,0) + \varepsilon\cos(x)$, in a doubly periodic domain with aspect ratio $\delta = 1.1$ (colors in the .pdf document).

Figure 1: Observation of the Jovian atmosphere from Cassini (Courtesy of NASA/JPL-Caltech). See figure 12 page 71 for more detailed legends.

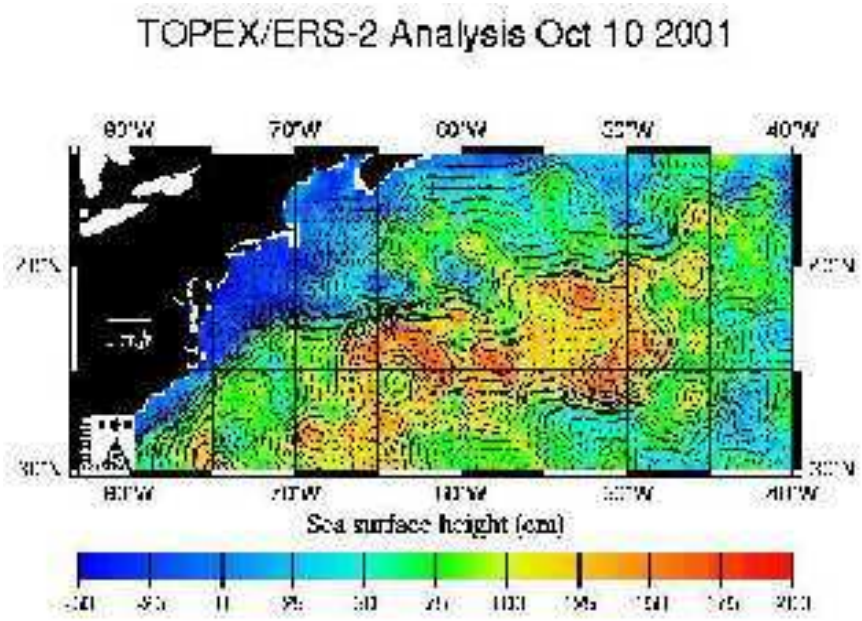

Figure 2: Observation of the north Atlantic ocean from altimetry. See figure 19 page 79 for more detailed legends.

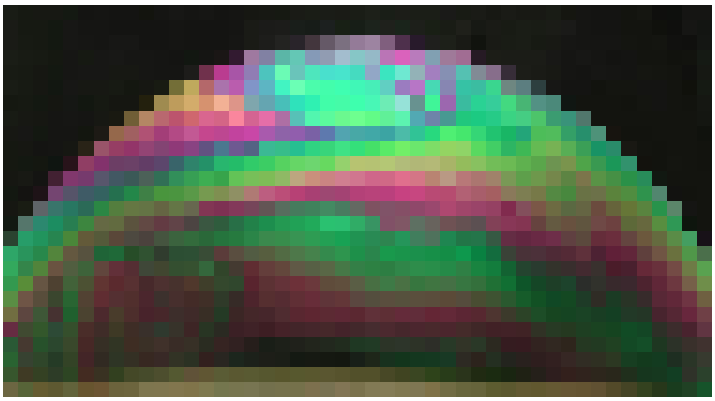

Figure 3: Example of an experimental realization of a 2D flow in a soap bubble, courtesy of American Physical Society. See [177] and [107] for further details.

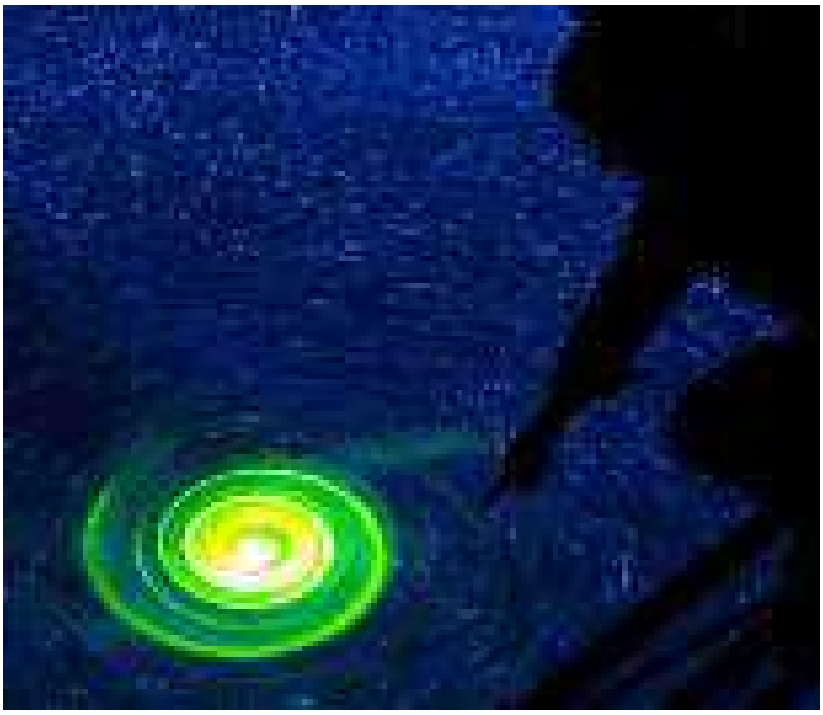

Figure 4: Experimental observation of a 2D long lived coherent vortex on the 14m diameter Coriolis turntable (photo gamma production).

1. Introduction

1.1. Two-dimensional and geostrophic turbulence

For many decades, two-dimensional turbulence has been a very active subject for theoretical investigations, motivated not only by the conceptual interest in understanding atmosphere and ocean turbulence, but also by the beauty and precision of the theoretical and mathematical achievements obtained thereby. For over two decades, two-dimensional flows have been studied experimentally in many different laboratory setups, as for instance illustrated in figures 4, 6, 23, and 27 (see also [107, 180] and references therein for further details).

Although they both involve a huge range of temporal and spatial scales, two-dimensional and three-dimensional turbulent flows are very different in nature.

The first difference is that whereas in three-dimensional turbulence energy flows forward (from the largest towards the smallest scales), it flows backward (from the smallest towards the largest scales) in two-dimensional turbulence. Three-dimensional turbulence transfers energy towards the viscous scale where it is dissipated into heat at a finite rate, no matter how small the viscosity. By contrast, in the absence of any strong dissipation mechanism at the largest scales, the dissipation of energy remains weak in two-dimensional turbulence. As a consequence, the flow dynamics is dominated by large scale coherent structures, such as vortices or jets. This review is devoted to the understanding and prediction of these stable and quasi-steady structures in two-dimensional turbulent flows.

The second fundamental difference between 2D and 3D turbulence is that the level of fluctuations in two-dimensional turbulence is very small. The largest scales of three-dimensional turbulent flows are the place of incessant instabilities, whereas the largest scales of two-dimensional turbulence are often quasi-stationary and evolve over a very long time scale, compared for instance to the turnover time of the large scale coherent structures.

As explained in this review, the above-mentioned peculiarities of two-dimensional turbulent flows are theoretically understood as the consequences of dynamical invariants of two-dimensional perfect flows, which are not invariants of perfect three-dimensional flows. These invariants, including the enstrophy, make the forward energy cascade impossible in two-dimensional flows, and explain the existence of an extremely large number of stable stationary solutions of the 2D Euler equations, playing a major role in the dynamics.

Atmospheric and oceanic flows are three-dimensional, but strongly dominated by the Coriolis force, mainly balanced by pressure gradients (geostrophic balance). The turbulence that develops in such flows is called geostrophic turbulence. Models describing it have the same type of additional invariants as two-dimensional turbulence has. As a consequence, energy flows backward and the main phenomenon is the formation of large scale coherent structures (jets, cyclones and anticyclones) (see figures 12 and 19). The analogy between two-dimensional turbulence and geophysical turbulence is further emphasized by the theoretical similarity between the 2D Euler equations – describing 2D flows – and the layered quasi-geostrophic or shallow-water models – describing the largest scales of geostrophic turbulence –: both are transport equations of a scalar quantity by a non-divergent flow, conserving an infinity of invariants.

The formation of large scale coherent structures is a fascinating problem and an essential part of the dynamics of Earth's atmosphere and oceans. This is the main motivation for setting up a theory for the formation of the largest scales of geostrophic and two-dimensional turbulence.

1.2. Turbulence and statistical mechanics

Any turbulence problem involves a huge number of degrees of freedom coupled via complex nonlinear interactions. The aim of any theory of turbulence is to understand the statistical properties of the velocity field. It is thus extremely tempting and interesting to attack these problems from a statistical mechanics point of view. Statistical mechanics is indeed a very powerful theory that allows us to reduce the complexity of a system down to a few thermodynamic parameters. As an example, the concept of phase transition allows us to describe drastic changes of the whole system when a few external parameters are changed. Statistical mechanics is the main theoretical approach that we develop in this review, and we show that it succeeds in explaining many of the phenomena associated with two-dimensional turbulence.

This may seem surprising at first, as it is a common belief that statistical mechanics is not successful in handling turbulence problems. The reason for this belief is that most turbulence problems are intrinsically far from equilibrium. For instance, the forward energy cascade in three-dimensional turbulence involves a finite energy dissipation flux no matter how small the viscosity (anomalous dissipation). Because of this flux, the flow cannot be considered close to some equilibrium distribution. By contrast, two-dimensional turbulence does not suffer from this problem (there is no anomalous dissipation of the energy), so that equilibrium statistical mechanics, or close to equilibrium statistical mechanics makes sense when small fluxes are present.

The first attempt to use equilibrium statistical mechanics ideas to explain the self-organization of 2D turbulence comes from Onsager in 1949 [153] (see [76] for a review of Onsager's contributions to turbulence theory). Onsager worked with the point-vortex model, a model made of singular point vortices, first used by Lord Kelvin and which is a special class of solution of the 2D Euler equations. The equilibrium statistical mechanics of the point-vortex model has a long and very interesting history, with wonderful pieces of mathematical achievements [153, 103, 33, 109, 66, 43, 75, 4]. In order to treat flows with continuous vorticity fields, another approach, taking account of the quadratic invariants only, was proposed by Kraichnan [113]. This last work has inspired a quadratic-invariant statistical theory for quasi-geostrophic flows over topography: the Salmon–Holloway–Hendershott theory [172, 171]. Another phenomenological approach based on a minimal enstrophy principle and leading to similar predictions for the large scale flow as the Salmon–Holloway–Hendershott theory has been independently proposed by Bretherton-Haidvogel [28]. The generalization of Onsager's ideas to the 2D Euler equation with continuous vorticity field, taking into account all invariants, has been proposed in the beginning of the 1990s [163, 139, 164, 168], leading to the Robert–Sommeria–Miller theory (RSM theory). The RSM theory includes the previous Onsager, Kraichnan, Salmon–Holloway–Hendershott and Bretherton-Haidvogel theories and determines the particular limits [1] within which those give relevant predictions and general results. The part of this review deal-

[1] Corresponding to special classes of initial conditions

ing with equilibrium statistical mechanics mainly falls within the framework of the RSM theory and presents its further developments.

Over the last fifteen years, the RSM equilibrium theory has been applied successfully to a large class of problems, for both the Euler and quasi-geostrophic equations. We cite and describe all relevant works and contributions to this subject. The aim of this review is also pedagogical, and as such we have chosen to emphasize on a class of problems that can be understood using analytical solutions. We give a comprehensive description only of those works. Nevertheless, this includes many interesting applications, such as predictions of phase transitions in different contexts, a model for the Great Red Spot and other Jovian vortices, and models of ocean vortices and jets.

Most turbulent flows are forced, and reach a statistically steady state where forcing is balanced on average by a dissipative mechanism. Such situations are referred to in statistical mechanics as Non-Equilibrium Steady States (NESS). One class of such problems in two-dimensional turbulence are the self-similar inertial cascades first described by Kraichnan [111]: the backward energy cascade and the forward enstrophy cascade. These are essential concepts of two-dimensional turbulence that will be briefly described. However, in the regime where the flow is dominated by large scale coherent structures, these self-similar cascades are no longer relevant and Kraichnan's theory provides no prediction. We will explain in this review how the vicinity to statistical equilibrium can be invoked in order to provide partial responses to the description of the non-equilibrium situations, for instance prediction of non-equilibrium phase transitions. We will also emphasize why and how such predictions based on equilibrium statistical mechanics are necessarily limited in scope, and explain how a non-equilibrium theory can be foreseen based on kinetic theory approaches.

1.3. About this review

The aim of this review is to give a self-contained description of statistical mechanics of two-dimensional and geophysical turbulence, and of its applications to real flows. For pedagogical purposes, we will emphasize analytically solvable cases, so the physics can be easily understood.

The typical audience should be graduate students and researchers from different fields. One of the difficulty with this review is that knowledge is required from statistical physics [117], thermodynamics [36], geophysical fluid dynamics [156, 195, 171, 85] and two-dimensional turbulence [113, 180, 186]. For each of these subjects, the notions needed will be briefly presented, in a self-contained way, but we refer to classical textbooks or review papers for more detailed presentations.

There already exist several presentations of the equilibrium statistical mechanics of two-dimensional and geostrophic turbulent flows [180, 129], some emphasizing kinetic approaches of the point-vortex model [43], other focusing on the legacy of Onsager [76]. Parts of the introductory sections of this review (two-dimensional fluid mechanics and the mean-field equilibrium statistical mechanics theory) are similar to those found in previous reviews or lectures (especially [180]). However, the statistical mechanics foundations of the theory is explained in further details and none of the applications discussed in this review, with emphasis on analytically solvable cases, were described in previous books or reviews. For instance, the present review gives i) a

precise explanation of the statistical mechanics basis of the theory, ii) a detailed discussion of the validity of the mean-field approximation, iii) an analytic treatment of phase diagrams for small energy and analytic models for the Great Red Spot as well as for ocean jets and vortices, iv) a detailed discussion of the irreversible behavior of the 2D Euler equations despite its being actually a time reversible equation. In addition, we present new results on non-equilibrium studies, on the different regime description, on non-equilibrium phase transitions and kinetic theories. Most of these new results have been derived over the last few years. Other important recent developments of the theory such as statistical ensemble inequivalence [69, 70] and related phase transitions [16] would be natural extensions of this review, but were considered too advanced for such a first introduction. We however always describe the main results and give the appropriate references to the appropriate papers, for an interested reader to be able to understand these more technical points.

We apologize that this review leaves little room for the description of experiments, for the cascade regimes of two dimensional turbulence or for the kinetic theory of the point-vortex model. For these we refer the reader to [180, 186], [113, 9, 74, 3] and [66, 43] respectively. Interesting related problems insufficiently covered in this review also include the mathematical works on the point-vortex model [33, 109, 75] or on the existence of invariant measures and their properties for the 2D stochastic Navier-Stokes equation [114, 115, 134], as well as studies of the self-organization of quasi-geostrophic jets on a beta-plane (see [91, 118, 188, 78, 65] and references therein).

1.4. Detailed outline

Section 2 is a general presentation of the equations and phenomenology of two-dimensional (2D Euler equations) and geophysical turbulence. One of the simplest possible models for geophysical flows, namely the 1.5-layer quasi-geostrophic model (also called Charney–Hasegawa–Mima model), is presented in section 2.1.

Section 2.2 deals with important properties of 2D Euler and quasi-geostrophic equations, and their physical consequences: the Hamiltonian structure (section 2.2.1), the existence of an infinite number of conserved quantities (section 2.2.2).

These conservation laws play a central part in the theory. They are for instance responsible for: i) the existence of multiple stationary solutions of the 2D Euler equations and the stability of some of these states (section 2.3.1), ii) the cascade phenomenology, with energy transferred upscale, and enstrophy downscale (section 2.3.2), iii) the most striking feature of 2D and geophysical flows: their self-organization into large scale coherent structures (section 2.3.3), iv) the non-trivial predictions of equilibrium statistical mechanics of two dimensional turbulence, compared to statistical mechanics of three-dimensional turbulence (sections 2.3.4 and 2.3.5). Sections 2.3.4 and 2.3.5 also explain in details the relations between the Kraichnan energy-enstrophy equilibrium theory and the Robert-Sommeria-Miller theory, and justify the validity of a mean field approach.

The self-organization of two-dimensional and geostrophic flows is the main motivation for a statistical mechanics approach of the problem. The presentation of the equilibrium theory is the aim of section 3. A reader more interested in applications than in the statistical mechanics basis of the theory can start her reading at the beginning of section 3.

Section 3.1 explains how the microcanonical mean field variational problem describes statistical equilibria. All equilibrium results presented afterwards rely on this variational problem. The ergodicity hypothesis is also discussed in section 3.1. Section 3.1.3 explains the practical and mathematical interest of canonical ensembles, even if they are not really relevant from a physical point of view. Section 3.3 explains the relations between the statistical mechanics of two dimensional flows and the statistical mechanics of other systems with long range interactions.

An analytically solvable case of phase transitions in a doubly periodic domain is presented section 3.5. This example chosen for its pedagogical interest, illustrate the scope and type of results one can expect from statistical theory of two-dimensional and geophysical flows. The concepts of bifurcations, phase transitions, and phase diagrams reducing the complexity of turbulent flows to a few parameters are emphasized.

Section 4 is an application of the equilibrium statistical mechanics theory to the explanation of the stability and formation, and precise modeling of large scale vortices in geophysical flows, such as Jupiter's celebrated Great Red Spot and the ubiquitous oceanic mesoscale rings. The analytical computations are carried out in the limit of a small Rossby radius (the typical length scale characterizing geostrophic flows) compared to the domain size, through an analogy with phase coexistence in classical thermodynamics (for instance the equilibrium of a gas bubble in a liquid).

Section 4.1 gives an account of the Van der Waals–Cahn–Hilliard model of first order transitions, which is the relevant theoretical framework for this problem. The link between Van der Waals–Cahn–Hilliard model and the statistical equilibria of the 1.5-layer quasi-geostrophic model is clarified in subsection 4.2. This analogy explains the formation of strong jets in geostrophic turbulence. All the geophysical applications presented in this review come from this result.

Subsection 4.4 deals with the application to mesoscale ocean vortices. Their self-organization into circular rings and their observed westward drift are explained as a result of equilibrium statistical mechanics.

Subsection 4.3 deals with the application to Jovian vortices. The stability and shapes of the Red Great Spot, white ovals and brown barges are explained by equilibrium statistical mechanics. A detailed comparison of statistical equilibrium predictions with the observed velocity field is provided. These detailed quantitative results are one of the main achievements of the application of the statistical equilibrium theory.

Section 5 gives another application of the statistical theory, now to the self-organization of ocean currents. By considering the same analytical limit and theoretical framework as in the previous section, we investigate the applicability of the equilibrium statistical theory to the description of strong mid-latitude eastward jets, such as the Gulf Stream or the Kuroshio (north Pacific Ocean). These jets are found to be marginally stable. The variations of the Coriolis parameter (beta effect) or a possible zonal deep current are found to be key parameters for the stability of these flows.

Section 6 deals with non-equilibrium situations: Non-Equilibrium Steady States (NESS), where an average balance between forces and dissipation imposes fluxes of conserved quantity (sections 6.1 to 6.5) and relaxation towards equilibrium (section 6.6). Section 6.1 is a general discussion about the 2D Navier-Stokes equations and conservation laws. The two regimes of two-dimensional turbulence, the inverse energy cascade and direct enstrophy cascade on one hand, and the regime dominated by large scale coherent structures on the other hand, are clearly delimited in sections 6.2 and 6.3. Section 6.4 delineates what can be learned from equilibrium statistical mechanics, and what cannot, in a non-equilibrium context. We also present predictions of non-equilibrium phase transitions using equilibrium phase diagrams and compare these predictions with direct numerical simulations. Section 6.5 comments progresses and challenges for a non-equilibrium theory based on kinetic theory approach. Section 6.6 presents recent results on the asymptotic behavior of the linearized 2D Euler equations and relaxation towards equilibrium of the 2D Euler equations.

2. Two-dimensional and geostrophic turbulence

In this section, we present the 2D Euler equations and the quasi-geostrophic equations, the simplest model of geophysical flows such as ocean or atmosphere flows. We also describe the Hamiltonian structure of these equations, the related dynamical invariants. The consequences of these invariants are explained: i) for the inverse energy cascade, ii) for the existence of multiple (stable and unstable) steady states for the equations.

2.1. 2D Euler and quasi-geostrophic equations

2.1.1. 2D Euler equations

The incompressible 3D Euler equations describe the momentum transport of a perfect and non-divergent flow. They read

$$\partial_t \mathbf{u} + \mathbf{u}\cdot\nabla\mathbf{u} = -\frac{1}{\rho}\nabla P \quad \text{with} \quad \nabla\cdot\mathbf{u} = 0\,. \tag{1}$$

where $\mathbf{u} = (\mathbf{v}, w) = \mathbf{v} + w\mathbf{e}_z$ ($\mathbf{v}$ is the projection of $\mathbf{u}$ in the plane ($\mathbf{e}_x$,$\mathbf{e}_y$)). The density ρ is assumed to be constant. If we assume the flow to be two-dimensional ($w = 0$ and $\mathbf{v} = \mathbf{v}(\mathbf{r})$ with $\mathbf{r} = (x,y)$), then it is easily verified that the vorticity is a scalar quantity: $\nabla\times\mathbf{v}$ is along $\mathbf{e}_z$. Defining the vorticity as $\omega = (\nabla\times\mathbf{v})\,.\,\mathbf{e}_z$, the 2D Euler equations take the simple form of a conservation law for the vorticity. Indeed, taking the curl of (1) gives

$$\partial_t\omega + \mathbf{v}\,.\nabla\omega = 0\;;\; \mathbf{v} = \mathbf{e}_z\times\nabla\psi\;;\; \omega = \Delta\psi, \tag{2}$$

where we have expressed the non divergent velocity as the curl of a streamfunction ψ. We complement the equation $\omega = \Delta\psi$ with boundary conditions: if the flow takes place in a simply connected domain $\mathscr{D}$, then the condition that $\mathbf{v}$ has no component along the normal to the interface (impenetrability condition) imposes ψ to be constant on the interface. This constant being arbitrary, we impose $\psi = 0$ on the interface. We may also consider flows on a doubly periodic domain $(0,\ 2\pi\delta)\times(0,\ 2\pi)$ of aspect ratio δ, in which case $\psi(x+2\pi\delta,y) = \psi(x,y)$ and $\psi(x,y+2\pi) = \psi(x,y)$.

The (purely kinetic) energy of the flow reads

$$\mathscr{E}[\omega] = \frac{1}{2}\int_{\mathscr{D}} \mathrm{d}\mathbf{r}\,\mathbf{v}^2 = \frac{1}{2}\int_{\mathscr{D}} \mathrm{d}\mathbf{r}\,(\nabla\psi)^2 = -\frac{1}{2}\int_{\mathscr{D}} \mathrm{d}\mathbf{r}\,\omega\psi, \tag{3}$$

where the last equality has been obtained with an integration by parts. This quantity is conserved by the dynamics ($d_t\mathscr{E} = 0$). As will be seen in section 2.2, the 2D Euler equations have an infinity of other conserved quantities.

Given the strong analogies between the 2D Euler and quasi-geostrophic equations, we further present the theoretical properties of both equations in section 2.2.

In the preceding paragraph, we started from the 3D Euler equation and assumed that the flow is two-dimensional. A natural question to raise is whether such two-dimensional flows actually exist. Over the last decades, a number of experimental realizations of two-dimensional flows

have been performed. Two-dimensionality can be achieved using strong geometrical constraints, for instance soap film flows [32, 107] (see figure 3, page 12) or very thin fluid layers over denser fluids [133, 155] (figure 24 page 93). Another way to achieve two-dimensionality is to use a very strong transverse ordering field: a strong transverse magnetic field in a metal liquid setup [179] (see figure 23, page 92), or the Coriolis force on a rapidly rotating fluids (see figure 4, page 12). Another original way to mimic the 2D Euler equations (2) is to look at the dynamics of electrons in a Penning trap [174, 173] (see figure 6, page 33).

2.1.2. Large scale geophysical flows: the geostrophic balance

The quasi-geostrophic equations are the simplest relevant model to describe mid- and high-latitude atmosphere and ocean flows. The model itself will be presented in section 2.1.3. To understand its physics, we need to introduce four fundamental concepts of geophysical fluid dynamics: beta-plane approximation, hydrostatic balance, geostrophic balance and Rossby radius of deformation. This section gives a basic introduction to these concepts, that is sufficient for understanding the discussions in the following sections ; a more precise and detailed presentation can be found in geophysical fluid dynamics textbooks [156, 195, 171, 85].

To begin with, we write the momentum equations in a rotating frame ($\boldsymbol{\Omega}$ being the Earth's rotation vector), with gravity $\mathbf{g}$, in Cartesian coordinates, calling $\mathbf{e}_z$ the vertical direction (upward) along $\mathbf{g}$, $\mathbf{e}_y$ the meridional direction (northward), and $\mathbf{e}_x$ the zonal direction (eastward)

$$\partial_t \mathbf{u} + \mathbf{u}\cdot\nabla\mathbf{u} + 2\boldsymbol{\Omega}\times\mathbf{u} = -\frac{1}{\rho}\nabla P + \mathbf{g}. \tag{4}$$

Beta-plane approximation. One can show that for mid-latitude oceanic basin of typical meridional extension $L \sim 5000\ km$, the lowest order effect of Earth's sphericity appears only through the projection of Earth's rotation vector on the local vertical axis: $f = 2\boldsymbol{\Omega}\cdot\mathbf{e}_z = f_0 + \beta_c y$, with $f_0 = 2\Omega\sin\theta_0$, where θ_0 is the mean latitude where the flow takes place, and $\beta_c = 2\Omega\cos\theta_0/r_e$, where r_e is the Earth's radius [195, 156]. At mid latitudes $\theta_0 \sim 45^0$, so that $f_0 \sim 10^{-4}\ s^{-1}$ and $\beta_c \sim 10^{-11}\ m^{-1}s^{-1}$.

Hydrostatic balance. Recalling $\mathbf{u} = (\mathbf{v}, w)$, the momentum equations (4) along the vertical axis read

$$\partial_t w + \mathbf{u}\cdot\nabla w + 2\,(\boldsymbol{\Omega}\times\mathbf{u})\cdot\mathbf{e}_z = -\frac{1}{\rho}\partial_z P + g.$$

In the ocean or atmosphere context, an estimation of the order of magnitude of each term [195, 156] lead to the conclusion that the dominant terms are the vertical pressure gradients and gravitation. Neglecting the others gives the hydrostatic balance:

$$\partial_z P = -\rho g\,. \tag{5}$$

Geostrophic balance. In the plane (x,y) perpendicular to the gravity direction, the momentum equations read

$$\partial_t \mathbf{v} + \mathbf{v}\cdot\nabla\mathbf{v} + w\partial_z\mathbf{v} + f\mathbf{e}_z\times\mathbf{v} = -\frac{1}{\rho}\nabla_h P, \tag{6}$$

where $\nabla_h P$ denotes the horizontal pressure gradient.

The Rossby number ε is defined by the ratio of the order of magnitude of the advection term $\mathbf{v}\cdot\nabla\mathbf{v}$ over that of the Coriolis term $f\mathbf{e}_z\times\mathbf{v}$. Introducing typical velocity U and length L for the flow, $\varepsilon = U/fL$. In mid-latitude atmosphere, $L\sim 10^4$ km (size of cyclones and anticyclones), $U\sim 10$ $m.s^{-1}$, so that $\varepsilon\approx 0.01$. In the ocean $L\approx 10^2$ km (width of ocean currents), $U\approx 1$ $m.s^{-1}$, so that $\varepsilon\approx 0.1$. In both cases, this number is small: $\varepsilon\ll 1$. In the limit of small Rossby numbers, the advection term becomes negligible in (6), and at leading order there is a balance between the Coriolis term and pressure gradients. This is called the geostrophic balance:

$$f\mathbf{e}_z\times\mathbf{v}_g = -\frac{1}{\rho}\nabla_h P, \tag{7}$$

where $\mathbf{v}_g$ is the geostrophic velocity. From (7), we see that the geostrophic velocity is orthogonal to horizontal pressure gradients. Taking the curl of the geostrophic balance (7), and noting that horizontal variations of ρ and f are much weaker than variations of $\mathbf{v}_g$, we see that the two-dimensional velocity field $\mathbf{v}_g$ is at leading order non-divergent: $\nabla\cdot\mathbf{v}_g = 0$.

Let us consider the case of a flow with constant density $\rho=\rho_0$. Then the combination of the vertical derivative of (7) and of the hydrostatic equilibrium gives $f\mathbf{e}_z\times\partial_z\mathbf{v}_g = \frac{g}{\rho_0}\nabla_h P = 0$: the geostrophic flow does not vary with depth. This is the Taylor-Proudman theorem. However geophysical flows have slightly variable densities and display therefore vertical variations. But the Taylor-Proudman theorem shows that such vertical variations are strongly constrained and explain the tendency of geostrophic flows towards two-dimensionality. Please see [195, 156, 171] for further discussions of the geostrophic balance.

The Rossby radius of deformation. A consequence of the combined effects of geostrophic and hydrostatic balances is the existence of density and pressure fronts, whose typical width is called the Rossby radius of deformation. This length plays a central role in geostrophic dynamics. In order to give a physical understanding of the Rossby radius of deformation, we consider a situation where a light fluid of density ρ lies above a denser fluid of density $\rho+\Delta\rho$ with $\Delta\rho\ll\rho$. We also assume here that the bottom layer is much thicker than the upper one. Then, because of the inertia of the deep layer, the dynamics will be limited to the upper layer of depth H (see figure 5).

We consider an initial condition where the interface has a steep slope of amplitude η, and study the relaxation of the interface slope. This classical problem is called the Rossby adjustment problem [85, 195].

Without rotation, the only equilibrium is a horizontal interface. If the interface is not horizontal, pressure gradients induce dynamics, for instance gravity waves, that transport potential energy and mass in order to restore the horizontal equilibrium. A typical velocity for this dynamics is the velocity of gravity waves c. Recalling that the top layer has a thickness H much smaller than the other one, and considering waves with wavelengths much longer than H (this is

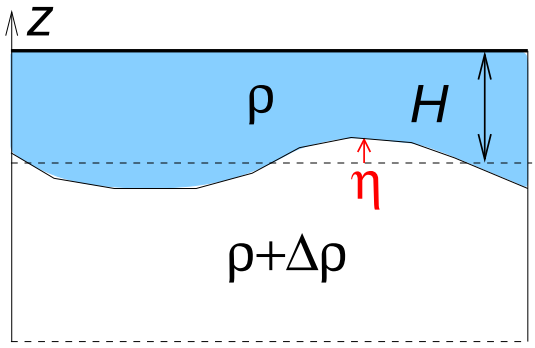

Figure 5: Vertical structure of the 1.5-layer quasi-geostrophic model: a deep layer of density $\rho+\Delta\rho$ and a lighter upper layer of thickness H and density ρ. Because of the inertia of the lower layer, the dynamics is limited to the upper layer.

the classic shallow-water approximation), the velocity of the gravity waves is $c=\sqrt{Hg'}$ $(m.s^{-1})$ where $g'=g\Delta\rho/\rho$ is called the reduced gravity.

With rotation, we see from (6) and (7) that horizontal pressure gradients can be balanced by the Coriolis force. It is then possible to maintain a stationary non-horizontal slope for the interface (or front) in this case.

The dynamical processes leading from an unstable front to a stable one is called the Rossby adjustment. Initially, the dynamics is dominated by gravity waves of typical velocity $c=\sqrt{Hg'}$. This initial process reduces the front slope until Coriolis forces become as important as pressure terms (related to gravity through hydrostatic balance). The typical time of the adjustment process is $\tau=f^{-1}$, where f is the planetary vorticity (also called Coriolis parameter). This time can be estimated by considering that it is the time scale at which velocity variations $\partial_t\mathbf{u}$ become of the order of the Coriolis force $-f\mathbf{e}_z\times\mathbf{u}$. These typical time τ and velocity c are the two important physical parameters of the adjustment. Then, the typical horizontal width of the front at geostrophic equilibrium can be estimated by a simple dimensional analysis: $R\sim c\tau$, which finally gives

$$R\sim\frac{\sqrt{g'H}}{f}\ .$$

This length is the Rossby radius of deformation. It depends on the stratification $\Delta\rho/\rho$, on g, on the Coriolis parameter f, and on a typical thickness of the fluid H. This is the typical length at which many fronts form in geophysical flows, resulting from a balance between Coriolis force and pressure gradients which are related to the stratification via the hydrostatic balance.

For the sake of simplicity, we have introduced the Rossby radius of deformation with a simple dimensional analysis. The Rossby adjustment is a very interesting physical problem in itself. Please see [85, 195] for more detailed analysis and discussions of this process.

In mid-latitude oceans, $\Delta\rho/\rho\sim 3\ 10^{-3}$ so $g'=0.03\ m.s^{-2}$ and $H=500\ m$, then the Rossby radius of deformation is $R\sim 60\ km$ and tends to a few kilometers closer to the poles. This length is easily observable on snapshots of oceanic currents, as shown in figures 16 and 19.

It corresponds for example to the jet width, either when jets are organized into either rings or zonal (eastward) flows. In the Earth's atmosphere $R \sim 1000\ km$, which is also the typical size of cyclones responsible for mid-latitude weather features. In the Jovian atmosphere $R \sim 2000\ km$, which corresponds to the typical width of the jet around the Great Red Spot. It is remarkable that in this latter case, the large scale flow, i.e. the Great Red Spot itself, has a much bigger length scale $\sim 20000\ km$.

2.1.3. The quasi-geostrophic model

We now present the quasi-geostrophic equations, a model for the dynamics of mid and high latitude flows, where the geostrophic balance (2.1.2) holds at leading order.

On the previous section 2.1.2, we have seen that for geophysical flows, the Rossby number $\varepsilon = U/fL$ is small, leading to the geostrophic balance (7) at leading order. In order to capture the dynamics, the quasi-geostrophic model is obtained through an asymptotic expansion of the Euler equations in the limit of small Rossby number ε, together with a Burger R/L of order one (where R is the Rossby radius of deformation introduced in the previous paragraph, and L a typical length for horizontal variations of the fields). We refer to [195] and [156] for a comprehensive derivation. Here we give only the resulting model and the physical interpretation.

We consider in this review the simplest possible model for the vertical structure of the ocean, that takes into account the stable stratification: an upper active layer where the flow takes place, and a lower denser layer either at rest or characterized by a prescribed stationary current (see figure 5). This is called the 1.5 layer quasi-geostrophic model. The full dynamical system reads

$$\partial_t q + \mathbf{v} \cdot \nabla q = 0, \tag{8}$$

$$\text{with } q = \Delta\psi - \frac{\psi}{R^2} + \eta_d(y), \tag{9}$$

$$\text{and } \mathbf{v} = \mathbf{e}_z \times \nabla\psi, \tag{10}$$

with the impenetrability boundary condition, equivalent to ψ being constant on the domain boundary $\partial\mathscr{D}$.

The complete derivation shows that the streamfunction gradient $\nabla\psi$ is proportional to the pressure gradient along the interface between the two layers; then relation (10) is actually the geostrophic balance (7). The dynamics (8) is a non-linear transport equation for a scalar quantity, the potential vorticity q given by (9). The potential vorticity is a central quantity for geostrophic flows [85, 195, 171, 156]. The term $\Delta\psi = \omega$ is the relative vorticity[2]. The term ψ/R^2 is related to the interface pressure gradient and thus to the interface height variations through the hydrostatic balance (see section 2.1.2). R is the Rossby radius of deformation introduced in section 2.1.2. Physically, an increase of $-\psi/R^2$ implies a stretching of the upper layer thickness. Since the potential vorticity is conserved, a stretching of the fluid column in the upper layer (i.e. an increase of $-\psi/R^2$) is associated with a decrease of the relative vorticity $\omega = \Delta\psi$, i.e. a tendency toward an anticyclonic rotation of the fluid column [171]. The term η_d represents the combined effects of the planetary vorticity gradient (remember that $f = f_0 + \beta y$) and of a given stationary

[2] The term "relative" refers to the vorticity ω in the rotating frame.

flow in the deep layer. We assume that this deep flow is known and unaffected by the dynamics of the upper layer. It is described by the streamfunction ψ_d which induces a permanent deformation of the interface with respect to its horizontal position at rest[3]. This is why the deep flow acts as a topography on the active layer. The detailed derivation gives

$$\eta_d = \beta_c y + \psi_d / R^2 \ .$$

Starting from (8) and (9) and assuming $\psi = 0$ at boundaries it is possible to prove that quasi-geostrophic flows conserve the energy:

$$\mathscr{E}[q] = \frac{1}{2}\int_{\mathscr{D}} \mathrm{d}\mathbf{r}\left[(\nabla\psi)^2 + \frac{\psi^2}{R^2}\right] = -\frac{1}{2}\int_{\mathscr{D}} \mathrm{d}\mathbf{r}\,(q-\eta_d)\,\psi. \tag{11}$$

Two contributions are distinguished in (11): a kinetic energy term $\frac{1}{2}\int_{\mathscr{D}} \mathrm{d}\mathbf{r}\,(\nabla\psi)^2$, as in the Euler equations, and a (gravitational) available potential energy term $\frac{1}{2}\int_{\mathscr{D}} \mathrm{d}\mathbf{r}\,\frac{\psi^2}{R^2}$.

2.2. Hamiltonian structure, Casimir's invariants and microcanonical measures

This subsection deals with theoretical properties of the 2D Euler and quasi-geostrophic equations. As already noticed, these properties are very similar because both dynamics are the nonlinear advection of a scalar quantity, the vorticity for the 2D Euler case or the potential vorticity for the quasi-geostrophic case. In the following, we discuss these properties in terms of the potential vorticity q, but they are also valid for the 2D Euler equation. Indeed the 2D Euler equation is included in the 1/2-layer quasi-geostrophic equation, as can be seen by considering the limit $R \to +\infty$, $\eta_d = 0$, in the expression (9) of the potential vorticity.

2.2.1. The theoretical foundations of equilibrium statistical mechanics

Let us consider a canonical Hamiltonian system: $\{q_i\}_{1\le i\le N}$ denote the generalized coordinates, $\{p_i\}_{1\le i\le N}$ their conjugate momenta, and $H(\{q_i,p_i\})$ the Hamiltonian. The variables $\{q_i,p_i\}_{1\le i\le N}$ belong to a $2N$-dimensional space Ω called the phase space. Each point $(\{q_i,p_i\})$ is called a microstate. The equilibrium statistical mechanics of such a canonical Hamiltonian system is based on the Liouville theorem, which states that the non-normalized measure

$$\mu = \prod_{i=1}^{N} \mathrm{d}p_i \mathrm{d}q_i$$

is dynamically invariant. The invariance of μ is equivalent to

$$\sum_i \left(\frac{\partial \dot{q}_i}{\partial q_i} + \frac{\partial \dot{p}_i}{\partial p_i}\right) = 0, \tag{12}$$

[3] A real topography $h(y)$ would correspond to $h(y) = -f_0\eta_d(y)/H$ where f_0 is the reference planetary vorticity at the latitude under consideration and H is the mean upper layer thickness. Due to the sign of f_0, the signs of h and η_d would be the same in the south hemisphere and opposite in the north hemisphere. As we will discuss extensively the Jovian south hemisphere vortices, we have chosen this sign convention for η_d.

which is a direct consequence of the Hamiltonian equations of motion

$$\begin{cases} \dot{q}_i = \dfrac{\partial H}{\partial p_i}, \\ \dot{p}_i = -\dfrac{\partial H}{\partial q_i}. \end{cases}$$

Note that the equations of motion can also be written in a Poisson bracket form:

$$\begin{cases} \dot{q}_i = \{q_i, H\}, \\ \dot{p}_i = \{p_i, H\}. \end{cases} \tag{13}$$

The terms in the sum (12) actually vanish independently:

$$\forall i, \quad \frac{\partial \dot{q}_i}{\partial q_i} + \frac{\partial \dot{p}_i}{\partial p_i} = 0.$$

This is called a detailed Liouville theorem.

For any conserved quantities $\{\mathscr{I}_1(p,q), ..., \mathscr{I}_n(p,q)\}$ of the Hamiltonian dynamics, the measures

$$\mu_F = \frac{1}{Z_F} \prod_i \mathrm{d}p_i \mathrm{d}q_i F(\mathscr{I}_1, ..., \mathscr{I}_n)$$

where Z_F is a normalization constant, are also invariant measures. An important question is to know which of these is relevant for describing the statistics of the physical system.

In the case of an isolated system, the dynamics is Hamiltonian and there is no exchange of energy or other conserved quantities with the environment. It is therefore natural to consider a measure that takes into account all these dynamical invariants as constraints. This justifies the definition of the microcanonical measure (for a given set of the values $\left\{I_1^0(q,p), \ldots, I_n^0(q,p)\right\}$ of the invariants $\{\mathscr{I}_1(q,p), \ldots, \mathscr{I}_n(q,p)\}$):

$$\mu_m\left(I_1^0, ..., I_n^0\right) = \frac{1}{\Omega\left(I_1^0, ..., I_n^0\right)} \prod_i \mathrm{d}p_i \mathrm{d}q_i \prod_{k=1,n} \delta\left(\mathscr{I}_k(p,q) - I_k^0\right), \tag{14}$$

where n is the number of constraints and $\Omega\left(I_1^0, ..., I_n^0\right)$ is a normalization constant [4]. For small variations of the constraints $\{\Delta\mathscr{I}_k\}_{1\leq k\leq n}$, the volume of the phase space with the constraint $I_k^0 \leq \mathscr{I}_k \leq I_k^0 + \Delta\mathscr{I}_k$ is given by $\Omega\left(I_1^0, ..., I_n^0\right) \prod_{k=1,n} \Delta\mathscr{I}_k$.

Then the Boltzmann entropy of the Hamiltonian system is

$$S = k_B \log \Omega.$$

[4] A more natural definition of the microcanonical measure would be as the uniform measure on the submanifold defined by $\mathscr{I}_k = I_k^0$ for all k. This would request adding determinants in the formula (14), and imply further technical difficulties. In most cases, however, in the limit of a large number of degrees of freedom N, these two definitions of the microcanonical measure become equivalent because the measures have large deviations properties (saddle points evaluations) where N is the large parameter, and such determinants become irrelevant. We note that in the original works of Boltzmann and Gibbs, the microcanonical measure refers to a measure where only the energy constraint is considered.

When the system considered is not isolated, but coupled with an external thermal bath of conserved quantities, other measures need to be used to describe properly the system by equilibrium statistical mechanics. Such measures are usually referred to as canonical or grand-canonical. A classical statistical mechanics result then proves that the relevant functions F are exponential (Boltzmann factors):

$$\mu_c = \frac{1}{Z_c} \prod_i \mathrm{d}p_i \mathrm{d}q_i exp\left(-\beta_1 I_1 - ... - \beta_n I_n\right) \tag{15}$$

where Z_c is a normalization constant. When coupled to a thermal bath, a system can receive from and give energy to the thermal bath, the resulting balance leading to the Boltzmann factor, as explained in statistical mechanics textbooks. Flows are forced and stirred by mechanisms that do not allow for this two-way exchange of energy characteristic of thermal baths. It is then hard to imagine the coupling of flows described by the Euler or quasi-geostrophic dynamics, with baths of energy, vorticity or potential vorticity. Then the relevant statistical ensemble for these models is the microcanonical one, and we will work in the following only starting from microcanonical measures. See subsection 3.2, page 49 on the physical interpretation of the microcanonical ensemble.

In statistical mechanics studies, it is sometimes argued that, in the limit of an infinite number of degrees of freedom, canonical and microcanonical measures are equivalent. Then as canonical measures are more easily handled, they are preferred in many works. However, whereas the equivalence of canonical and microcanonical ensembles is very natural and usually true in systems with short range interactions, common in condensed matter theory, it is often wrong in systems like the Euler equations. As a consequence, we will avoid the use of canonical measures in the following (see for instance [16, 59, 37, 22, 44, 15, 69] and references therein).

In statistical mechanics, a macrostate M is a set of microstates verifying some conditions. The conditions are usually chosen such that they describe conveniently the macroscopic behavior of the physical systems through a reduced number of variables. For instance, in a magnetic system, a macrostate M could be the ensemble of microstates with a given value of the total magnetization; in the case of a gas, a macrostate could be the ensemble of microstates corresponding to a given local density $f(\mathbf{x},\mathbf{p})$ in the six dimensional space $(\mathbf{x},\mathbf{p})$ (μ space), where f is defined for instance through some coarse-graining. In our fluid problem, an interesting macrostate will be the local probability distribution $\rho(\mathbf{x},\sigma)\,d\sigma$ to observe vorticity values $\omega(\mathbf{x}) = \sigma$ at $\mathbf{x}$ with precision $\mathrm{d}\sigma$.

If we identify the macrostate M with the values of the constraints that define it, we can define the probability of a macrostate $P(M)\,dM$. If the microstates are distributed according to the microcanonical measure, $P(M)$ is proportional to the volume of the subset Ω_M of phase space where microstates $\{q_i, p_i\}_{1\leq i\leq N}$ realize the state M. The Boltzmann entropy of a macrostate M is then defined to be proportional to the logarithm of the phase space volume of the subset Ω_M of all microstates $\{q_i, p_i\}_{1\leq i\leq N}$ that realize the state M.

In systems with a large number of degrees of freedom, it is customary to observe that the probability of some macrostates is concentrated close to a unique macrostate. There exist also cases where the probability of macrostates concentrates close to larger set of macrostates (see for instance [108]). Such a concentration is a very important information about the macroscopic

behavior of the system. The aim of statistical physics is then to identify the physically relevant macrostates, and to determine their probability and where this probability is concentrated. This is the program we will follow in the next sections, for the 2D Euler equations.

In the preceding discussion, we have explained that the microcanonical measure is a natural invariant measure with given values of the invariants. An important issue is to know if this measure describes also the statistics of the temporal averages of the Hamiltonian system. This issue, called ergodicity will be discussed in section 3.1.2.

The first step to define the microcanonical measure is to identify the equivalent of a Liouville theorem and the invariants. The Euler and quasi-geostrophic equations describe a conservative dynamics. They can be derived from a least action principle [171, 96], like canonical Hamiltonian systems. It is thus natural to expect Hamiltonian structure. There are however fundamental differences between infinite dimensional systems like the Euler equations and canonical Hamiltonian systems:

1. The Euler equation is a dynamical system of infinite dimension. The notion of the volume of an infinite dimensional space is meaningless. Then the microcanonical measure can not be defined straightforwardly.
2. For such infinite dimensional systems, we can not in general find a canonical structure (pair of canonically conjugated variables $\{q_i, p_i\}$ describing all degrees of freedom). There exists however a Poisson structure: one can define a Poisson bracket $\{.,.\}$, like in canonical Hamiltonian systems (13) and the dynamics reads

$$\partial_t q = \{q, \mathscr{H}[q]\}, \tag{16}$$

where $\mathscr{H}$ is the Hamiltonian.

For infinite dimensional Hamiltonian systems like the 2D Euler equations or quasi-geostrophic model, the Poisson bracket in (16) is degenerate [95, 144], leading to the existence of an infinite number of conserved quantities, the Casimir's functionals. These conservations laws have very important dynamical consequences, as explained in the next section. A detailed description of the Hamiltonian structure of infinite dimensional systems is beyond the scope of this review. We refer to [95, 144] for the description of the Poisson structure for many fluid systems. The conservation laws and the Liouville theorem are however essential consequences and we discuss them in the next two sections.

2.2.2. Casimir's conservation laws

Both Euler (2) and quasi-geostrophic (8) equations conserve an infinite number of functionals, named Casimirs. They are all functional of the form:

$$\mathscr{C}_s[q] = \int_{\mathscr{D}} \mathrm{d}\mathbf{r}\, s(q), \tag{17}$$

where s is any function sufficiently smooth. Here and in the following, q is the transported field, either the potential vorticity (9) for the quasi-geostrophic model or the vorticity in the case of the Euler equations for which $q = \omega$. As said in section 2.2.1, Casimir conserved quantities are related to the degenerate structure of infinite dimensional Hamiltonian systems. They can be

also understood as the invariants arising from the Noether's theorem, as a consequence of the relabeling symmetry of fluid mechanics (see for instance [171]).

Let us define $A(\sigma)$ the area of $\mathscr{D}$ with potential vorticity values lower than σ, and $\gamma(\sigma)$ the potential vorticity distribution

$$\gamma(\sigma) = \frac{1}{|\mathscr{D}|}\frac{dA}{d\sigma} \text{ with } A(\sigma) = \int_{\mathscr{D}} \mathrm{d}\mathbf{r}\, \chi_{\{q(\mathbf{x})\leq\sigma\}}, \tag{18}$$

where $\chi_{\mathscr{B}}$ is the characteristic function of the set $\mathscr{B} \subset \mathscr{D}$ ($\chi_{\mathscr{B}}(x) = 1$ for $x \in \mathscr{B}$), and $|\mathscr{D}|$ is the area of $\mathscr{D}$. As quasi-geostrophic (8) and 2D Euler equations (2) are transport equations by an incompressible flow, the area $\gamma(\sigma)$ occupied by a given vorticity level σ (or equivalently $A(\sigma)$) is a dynamical invariant.

The conservation of the distribution $\gamma(\sigma)$ is equivalent to the conservation of all Casimir's functionals (17). The domain averaged potential vorticity Γ, the enstrophy $\mathscr{G}_2$ and the other moments of the potential vorticity $\mathscr{G}_n$ are Casimirs of a particular interest

$$\mathscr{G}[q] = \mathscr{G}_1[q] = \int_{\mathscr{D}} \mathrm{d}\mathbf{r}\, q \quad \text{and } \mathscr{G}_n[q] = \int_{\mathscr{D}} \mathrm{d}\mathbf{r}\, q^n. \tag{19}$$

For the 2D Euler equations in a bounded domain, $\mathscr{G}$ is also the circulation $\mathscr{G} = \int_{\partial\mathscr{D}} \mathbf{v}\cdot\, d\mathbf{l}$.

In any Hamiltonian systems, symmetries are associated with conservation laws, as a consequence of Noether's theorem (see e.g. [171] and references therein). Then if the flow domain $\mathscr{D}$ is invariant under rotations or translations, it will be associated with angular momentum and momentum conservation. For domains with symmetries, these conservation laws have to be taken into account in a statistical mechanics analysis.

2.2.3. *Detailed Liouville theorem and microcanonical measure for the dynamics of conservative flows*

In order to discuss the detailed Liouville theorem, and build microcanonical measure, in the following we decompose the potential vorticity field on the eigenmodes of the Laplacian on $\mathscr{D}$; where $\mathscr{D}$ is the domain on which the flow takes place. We could have decomposed the field on any other orthogonal basis. Whereas the Laplacian and Fourier basis are simpler for the following discussion, finite elements basis are much more natural to justify mean field approximation and to obtain large deviation results for the measures, as discussed in section 2.3.5.

We call $\{e_i\}_{i\geq 1}$ the orthonormal family of eigenfunctions of the Laplacian on the domain $\mathscr{D}$, with Dirichlet boundary conditions (see subsection 2.1, page 19):

$$-\Delta e_i = \lambda_i e_i, \quad \int_{\mathscr{D}} \mathrm{d}\mathbf{r}\, e_i e_j = \delta_{ij}. \tag{20}$$

The eigenvalues λ_i are arranged in increasing order. For instance for a doubly periodic domain or infinite domain, $e_i(\mathbf{r})$ are Fourier modes. Any function g defined on the domain can be decomposed into $g = \sum_k g_k(t) e_k(\mathbf{r})$ with $g_k = \int d\mathbf{r}\, g e_k$. Then

$$q(\mathbf{r},t) = \sum_{i=1}^{+\infty} q_i(t)\, e_i(\mathbf{r}).$$

From (8), the quasi-geostrophic equations are

$$\dot{q}_i = \sum_{j=1}^{+\infty} \sum_{k=1}^{+\infty} A_{ijk} q_j q_k, \tag{21}$$

where the explicit expression for A_{ijk} will not be needed in the following discussion. For (21), a detailed Liouville theorem holds:

$$\forall i, \quad \frac{\partial \dot{q}_i}{\partial q_i} = 0, \tag{22}$$

see [120], [113]. Note that while we have discussed here the detailed Liouville theorem in the context of mode decomposition, more general results exist [165, 207] [5].

From the detailed Liouville theorem, we can define the microcanonical measure. First the n moment microcanonical measure (which, by including the energy, makes $n+1$ constraints) is defined as

$$\mu_{m,n}(E, \Gamma_1, ..., \Gamma_n) = \frac{1}{\Omega_n(E, \Gamma_1, ..., \Gamma_n)} \prod_i \mathrm{d}q_i \; \delta(\mathscr{E}[q] - E) \prod_{k=1,n} \delta(\mathscr{G}_k[q] - \Gamma_k), \tag{23}$$

where $\mathscr{E}$ (11) is the energy, Γ_n (19) the vorticity moments and $\delta(\cdot)$ the Dirac delta function. A precise definition of $\mu_{m,n}$ goes through the definition of approximate finite dimensional measures: for any observable ϕ_K depending on K components $\{q_i\}_{1 \leq i \leq K}$ of q , we define

$$< \mu^N_{m,n}, \phi_K > = \frac{\int \prod_{i=1,N} \mathrm{d}q_i \; \delta(\mathscr{E}_N[q] - E) \prod_{k=1,n} \delta(\mathscr{G}_{N,k}[q] - \Gamma_k) \phi_K}{\Omega_{n,N}(E, \Gamma_1, ..., \Gamma_n)},$$

where $\mathscr{E}_N$ and $\mathscr{G}_{N,n}$ are finite dimensional approximations of $\mathscr{E}$ (11) and $\mathscr{G}_n$ (19), and Ω_N is a normalization factor. Then we define $< \mu_{m,n}, \phi_K > = \lim_{N \to \infty} < \mu^N_{m,n}, \phi_K >$. Usually $\Omega_{n,N}$ has no finite limit when N goes to infinity, and the definition of $\Omega_n(E, \Gamma_1, ..., \Gamma_n)$ in the formal notation (23) implies a proper rescaling.

$\mu_{m,n}$ are ensembles of invariant measures. The microcanonical measure corresponding to the infinite set of invariants $\{\Gamma_i\}$ is then defined as

$$\mu_m(E, \{\Gamma_i\}) = \lim_{n \to \infty} \mu_{m,n}(E, \Gamma_1, ..., \Gamma_n),$$

and is denoted

$$\mu_m(E, \{\Gamma_i\}) = \frac{1}{\Omega(E, \{\Gamma_i\})} \prod_{i=1..\infty} \mathrm{d}q_i \; \delta(\mathscr{E}[q] - E) \prod_{k=1..\infty} \delta(\mathscr{G}_k[q] - \Gamma_k). \tag{24}$$

[5] A direct consequence of the detailed Liouville theorem (22) is that any truncation of the 2D Euler or quasi-geostrophic equations also verifies a Liouville theorem [113]. This result is actually much more general: any approximation of the Euler equation obtained by an L_2 projection on a finite dimensional basis verify a Liouville theorem, see [165]). For truncations preserving the Hamiltonian structure and a finite number of Casimir invariants, see [207].

2.3. Specificity of 2D and geostrophic turbulence as a consequence of Casimir's invariants

We discuss in this section the consequences of the conservation laws presented above. These consequences are important physical properties: i) the existence of an infinite number of stationary solutions to the 2D Euler equations, and the stability of some of these flows (section 2.3.1), ii) the existence of an inverse (or upscale) energy cascade and of a direct (or downscale) cascade of enstrophy (section 2.3.2), iii) the self organization of the large scale flow (section 2.3.3), iv) non-trivial results from the equilibrium statistical mechanics of two-dimensional flows by contrast with three dimensional flows (section 2.3.4), and v) the validity of a mean-field treatment of equilibrium statistical mechanics (section 2.3.5).

2.3.1. First physical consequence of 2D invariants: multiple stationary flows

Let us consider a dynamical system $\mathscr{G}$: $\dot{x} = G(x)$, where $\dot{x}$ is the temporal derivative of x, with conserved quantity $F(x)$ ($\dot{F}(x) = 0$). It can be proved easily that any non-degenerate extrema x_0 of F ($F'(x_0) = 0$) is a stationary solution ($\dot{x} = 0$) of $\mathscr{G}$ ($G(x_0) = 0$) and if, in addition, the second variations of G are either positive-definite or negative-definite, then this stationary solution is stable [95]. This general result seems natural when one considers the examples of energy and angular momentum extrema encountered in classical mechanics. This simple idea, coupled to convexity estimates, was used for instance by Arnold [5] to prove the stability of stationary solutions of the 2D Euler equations. Generalizations of these ideas to larger classes of stationary flows of the 2D Euler equations can be found in [205, 70, 35]. Generalizations of these ideas to many other fluid mechanics equations can be found in [95].

If we apply this idea to the 2D Euler and quasi-geostrophic equations, as a consequence of the infinite number of Casimir's invariants (2.2.2), there exists an infinite number of stationary flows, a large number of them being stable. In any dynamical system, fixed points play a major role. In the case of the 2D Euler equations, moreover they turn out to be attractive, as discussed in section 106.

We discuss now the case of the quasi-geostrophic equations, but the case of the 2D Euler equations is exactly similar. The conserved quantities we use are the so called Energy-Casimir functionals

$$\mathscr{F} = \mathscr{E}[q] + \mathscr{C}_s[q] = -\frac{1}{2}\int_{\mathscr{D}} \mathrm{d}\mathbf{r}\, q\psi + \int_{\mathscr{D}} \mathrm{d}\mathbf{r}\, s(q)\,, \tag{25}$$

where s is an arbitrary function. They are the sum of the energy (11) and a Casimir invariant (17). The critical points q_e of this functional (satisfying $\delta\mathscr{F} = \int_{\mathscr{D}} \mathrm{d}\mathbf{r}\,(\psi_e - s'(q_e))\,\delta q = 0$ for any perturbation δq) verify the equation

$$\psi = s'(q)\,. \tag{26}$$

As expected from the general argument above, these critical points should be stationary solutions of the quasi-geostrophic equation (8). From (8), we see that any dynamical invariant verifies $\nabla\psi \times \nabla q = 0$ (we recall that q, ψ and the velocity $\mathbf{v}$ are related by (9-10)). Then the dynamical invariants of the quasi-geostrophic equation (8), are all potential vorticity fields q, such that the isocontour lines for q and for ψ are the same. A special class of dynamical invariant are the

potential functional vorticity fields q, such that a relation $q = g(\psi)$ between q and ψ exist, with g an arbitrary function. Then solutions to (26) are indeed stationary flows.

The case when s is either strictly convex or concave is very interesting. Indeed, then s' is monotonous and (26) can be inverted: $q = (s')^{-1}(\psi)$. Moreover if the functional (25) is either strictly convex or concave, then we expect the critical points to exist and to be unique, and we expect them to be non degenerate (the second variations are either positive-definite or negative-definite). Then according to the general argument above, in this case we expect the stationary flows (25) to be dynamically stable.

In the case of fluid dynamics, there are further difficulties with the general argument above, because the potential vorticity field q lies in an infinite dimensional space variable. Roughly speaking, these difficulties are related to continuity properties of the functionals, which may depend on the chosen norm for the potential vorticity field. One then has to defines carefully the norm for the perturbation and a norm with respect to which the dynamics is stable. In the case of the Euler equations, these difficulties have first been dealt by Arnold [5], proving that when $\mathscr{F}$ is either strictly convex or strictly concave, the stationary flows (25) are indeed stable. Among Arnold's results, we learn that a sufficient condition for $\mathscr{F}$ to be strictly convex is s convex and a sufficient condition for $\mathscr{F}$ to be strictly concave is s concave with $s''(q_e) \geq c > \lambda_1$, where λ_1 is the smallest eigenvalue of the Laplacian on the domain $\mathscr{D}$, with Dirichlet boundary conditions (these two condition can be easily worked out). These results have found to be valid for weaker hypothesis and generalized to the quasi-geostrophic model and a number of other models in fluid dynamics and plasma physics (see for instance [95, 205, 70]).

In the preceding paragraphs, we have applied the property that nondegenerate extremum of conserved quantities are stable equilibria, to the minimization of Energy-Casimir functionals (25), following Arnold [5]. The same idea and property could be applied to other conserved functionals or conserved functionals with constrains. For instance, we may use that the dynamics conserve all Casimirs (17). Then the extremum of the energy (11) for fixed values of the Casimirs (17) (a constrained variational problem) should be a stable equilibria[6]. Such an extremization is called a Kelvin energy principle as Lord Kelvin was the first to realize this property [189]. We note that critical points of a Kelvin energy principle, like critical points of Energy-Casimir functionals (25), are stationary solutions of the quasi-geostrophic (or 2D Euler) equations. On the one hand, the class of stable solutions obtained through Kelvin energy principle is larger than the class obtained from Energy-Casimir variational problem, and in this sense, the Kelvin energy principle is less restrictive. On the other hand the stability of Kelvin energy minimizers is expected to be weaker compared to the stability of Energy-Casimir minimizer, as perturbations modifying the value of the Casimirs may destabilize the flow (for instance we know no counterparts of the Arnold theorems for Kelvin energy minimizers). We refer to [45] for a recent comprehensive review of these different variational problems and other related ones, and for a discussion of the conditions for second variations of these variational problems to be definite positive or definite negative.

[6] See [196, 191, 192] for interesting algorithms that allow to compute energy maxima while preserving the Casimir functionals.

We conclude that due to the infinite number of their invariants, the 2D Euler and quasi-geostrophic equations have an infinite number of stationary flows. Moreover an infinite class of these stationary flows can be proved to be stable. As in any dynamical system, we expect these stationary flows to play a very important role in the dynamics. We will see in section 3.1 that the microcanonical measure of statistical mechanics is concentrated close to some of these stationary flows. Moreover, the arguments of this section, or some generalizations, can be used to prove the dynamical stability of classes of statistical equilibria [138, 70].

2.3.2. Second physical consequence of 2D invariants: the inverse energy cascade

We saw that the infinite number of steady states of the 2D Euler and quasi-geostrophic equations, and the stability of some of these states, can be understood as a consequence of the conservation of Casimir invariants. We now look at another consequence of these conservation laws: the direction of the energy fluxes in spectral space is upscale. The argument developed in this section is a very classical one for physical systems with multiple invariants.

We treat here the case of decaying two-dimensional turbulence (for which the potential vorticity q is simply the relative vorticity ω), following [151]. A discussion of the direction of the energy and enstrophy fluxes was originally given by Fjortoft [79]. The case of statistically stationary cascade [112] is treated in section 6.2. Let us consider an infinite 2D domain and decompose the vorticity into Fourier eigenmodes. The energy spectrum $E(k)$ is defined such that $E(k)\,\mathrm{d}k$ is the energy contained in modes with wave numbers $\mathbf{k}'$ with $k \leq k' \leq k+\Delta k$, and such that the total energy is $E = \int \mathrm{d}k\, E(k)$. We define similarly the enstrophy spectrum $\Gamma_2(k)$: $\Gamma_2 = \int \mathrm{d}k\, \Gamma_2(k)$ (see 19 for Γ_2). It is easy to show that $\Gamma_2(k) = 2k^2 E(k)$.

A question of interest is to determine whether the energy goes towards large scales or small scales. To answer this, we look at rigorous bounds on the k-centroids k_E (and l-centroids l_E) for the energy:

$$k_E = \frac{1}{E}\int \mathrm{d}k\, kE(k) \;\text{ and }\; l_E = \frac{1}{E}\int \mathrm{d}k\, k^{-1}E(k),$$

and for the enstrophy

$$k_{\Gamma_2} = \frac{1}{\Gamma_2}\int \mathrm{d}k\, k\Gamma_2(k)\,dk \;\text{ and }\; l_{\Gamma_2} = \frac{1}{\Gamma_2}\int \mathrm{d}k\, k^{-1}\Gamma_2(k).$$

A transfer of energy toward large scales during the flow evolution is equivalent to an increase of the k- or the l-centroid.

Using Cauchy-Schwartz inequalities $\left(\int \mathrm{d}k\, f(k)g(k) \leq \sqrt{\int \mathrm{d}k\, f^2(k)\int \mathrm{d}k\, g^2(k)}\right)$, one can easily show that

$$k_E \leq \sqrt{\frac{\Gamma_2}{2E}}, \qquad k_{\Gamma_2} \geq \sqrt{\frac{\Gamma_2}{2E}}, \qquad k_E k_{\Gamma_2} \geq \frac{\Gamma_2}{2E}, \tag{27}$$

$$l_E \geq \sqrt{\frac{2E}{\Gamma_2}}, \qquad l_{\Gamma_2} \leq \sqrt{\frac{E}{\Gamma_2}}, \qquad l_E l_{\Gamma_2} \geq \frac{2E}{\Gamma_2}\,. \tag{28}$$

The first inequalities of (27) and (28) imply that the energy cannot be transferred to scales smaller than $\sqrt{2E/\Gamma_2}$, and enstrophy cannot be transferred to scales larger than $\sqrt{2E/\Gamma_2}$.

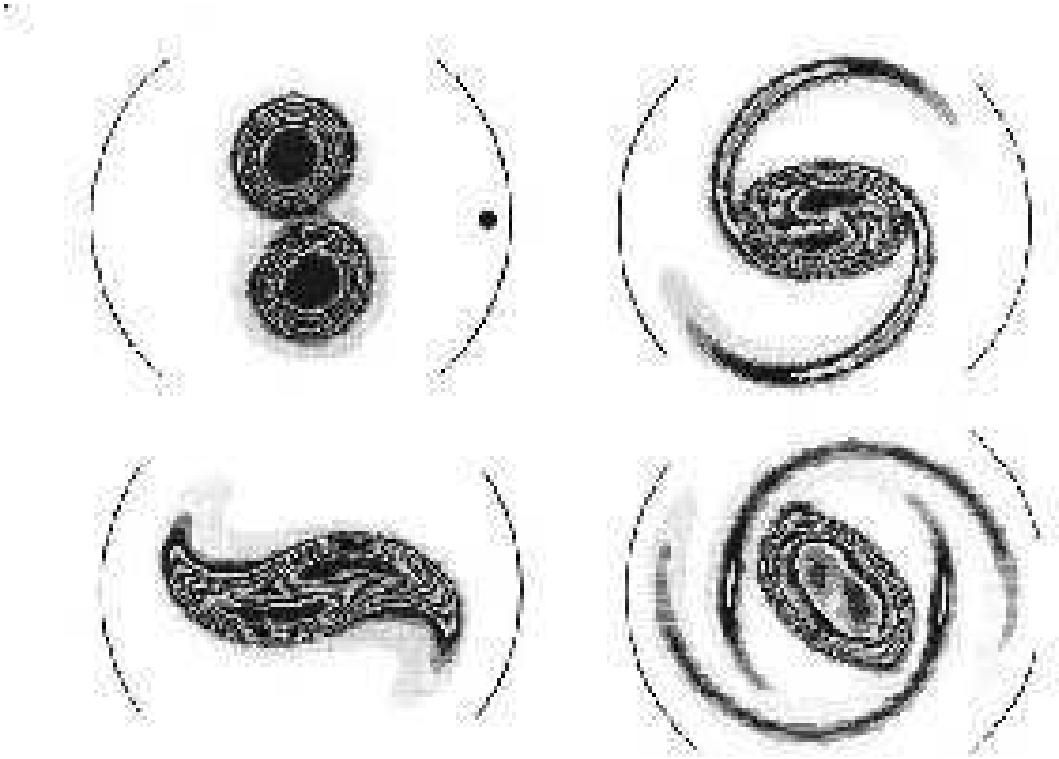

Figure 6: Snapshot of electron density (analogous to vorticity field) at successive time from an initial condition with two vortices to a single large scale coherent structure via turbulent mixing (see [173, 174]). The best experimental realization of inviscid 2D Euler equations is probably so far achieved in those magnetized electron plasma experiments where the electrons are confined in a Penning trap. The dynamics of both systems are indeed isomorphic, where the electron density plays the role of vorticity. The major drawback of this experimental setting comes from its observation, since any measurement requires the destruction of the plasma itself.

The last inequality of (27) implies that if the energy goes to larger and larger scales ($k_E \to 0$), then the enstrophy goes to smaller and smaller scales ($k_{\Gamma_2} \to +\infty$): an evolving state presenting an inverse flux of energy implies a simultaneous direct flux of enstrophy. Similarly, the last inequality of (28) implies than if the enstrophy goes to smaller and smaller scales ($l_{\Gamma_2} \to 0$) , then the energy goes to larger and larger scales ($l_E \to +\infty$): a direct flux of enstrophy implies an inverse flux of energy. A sufficient and necessary condition for the existence of a forward enstrophy flux is then the existence of an inverse energy flux.

2.3.3. Third physical consequence: the phenomenon of large scale self-organization of the flow

The most striking feature of 2D and geostrophic flows, and by far the most important phenomenon for applications, is their tendency to organize into large scale coherent structures. Be it in laboratory experiments (with the formation of long lived and robust 2D vortices, see for instance figure 6), in the ocean (with the formation of jets and rings), in the Jovian atmo-

sphere (with the Great Red Spot and other vortices), or in numerical simulations, these coherent structures are yet ubiquitous, and represent the main qualitative feature of turbulent 2D flows. Understanding their formation is thus a major challenge in geophysical fluid dynamics.

In the previous section, we proved that an upscale energy flux is always accompanied by a downscale enstrophy flux, and that there is a lower bound for the energy centroid. Using heuristic statistical mechanics arguments, we know that the dynamics will tend to partition as much as possible energy and enstrophy among the modes. The combination of these two arguments and the preceding are sufficient to conclude that the complex non-linear dynamics of the flow will tend to a transfer of energy toward largest scales and a transfer of enstrophy towards smallest scales.

We also explained in section 2.3.1 why the equations have infinitely many multiple stable stationary flows. This, together with the energy fluxes towards the largest scales is already sufficient to explain qualitatively the self-organization of the flow. On an inertial time scale (given for instance by the turnover time of the large scales of the turbulent flow), these large scale structures can be considered stationary solutions, in contrast to the complicated dynamics of the small scale turbulent flow.

The aim of this review is to present predictive theories for these large scale structures. We need to explain the physical mechanism at work and describe theoretically the dynamical mechanisms that will select some states among all the possible stationary flows. This is is where statistical mechanics will be very useful. The equilibrium theory predicts that turbulent mixing[7] will drive the flow toward a stationary state that maximizes a Boltzmann-Gibbs entropy formulae, while satisfying all the constraints of the dynamics presented in the previous subsections. This mixing entropy, derived from the Liouville theorem, will allow us to build theoretically natural invariant measures for the dynamics. We will also consider non-equilibrium theories for forced and dissipated flows.

Statistical mechanics is an extremely powerful tool that allows to reduce a complicated problem (the description of a fine-grained turbulent flow, our microscopic state with a huge number of degrees of freedom) to the study of a few parameters, which describes the large scale structures of the flow, our macroscopic state.

2.3.4. Fourth consequence: about Jeans paradox, why can we get a non-trivial equilibrium statistical mechanics for 2D flows by contrast with the 3D Euler ultraviolet divergence

In this section, for pedagogical reasons, we try to apply equilibrium statistical mechanics ideas to the three-dimensional Euler equations. This very simple discussion illustrates, with the example of the 3D Euler equations, that in most of Hamiltonian field equation a straight application of equilibrium statistical mechanics fails because of the so called Jeans paradox [159]. The reason is that in the simplest cases, for instance when energy is the only conserved quantity, at the statistical equilibria each degree of freedom has on average the same energy. Then because there are infinitely many degrees of freedom for a field, either the total energy is infinite, or if the energy is kept constant the average energy per modes is zero.

Then equilibrium statistical mechanics predicts that all the energy flows towards the smallest

[7] Here mixing does not refers to the effect of molecular viscosity, but rather to the stirring by the flow dynamics.

scales, for the three-dimensional Euler equations, in accordance with basic observations. But the microcanonical measure obtained in the limit of an infinite number of degrees of freedom is a trivial one, with no more energy in the largest scales. This argument proves that, because of Jeans paradox, three-dimensional turbulence is intrinsically a non-equilibrium process.

The main interest of this discussion is to show that, by contrast, two dimensional flows are different from this point of view and give non-trivial microcanonical measures. Basically thanks to the presence of more invariants, the Jeans paradox is avoided for the energy. Since the discussions of this section involves technical computations, it can be skipped at first reading. However, this discussion is essential for a physically relevant interpretation of the theory.

In section 2.2.3, we defined a microcanonical measure for the 2D Euler equations. We proceed here similarly. First, we note that for the three-dimensional Euler equations, for instance on a periodic cube, the velocity can be decomposed in Fourier modes $\mathbf{u}_\mathbf{k} = (u_{1,\mathbf{k}}, u_{2,\mathbf{k}}, u_{3,\mathbf{k}})$. The 3D Euler equations then read

$$\dot{u}_{i,\mathbf{k}} = \sum_{\mathbf{p},\mathbf{q};\, j,l=1,2,3} A_{j,l,\mathbf{k},\mathbf{p},\mathbf{q}} u_{j,\mathbf{p}} u_{l,\mathbf{q}}.$$

The explicit expression of A is not important for this discussion. The important point is that a detailed Liouville theorem holds:

$$\forall \mathbf{k}, \quad \sum_i \left(\frac{\partial \dot{u}_{i,\mathbf{k}}}{\partial u_{i,\mathbf{k}}} + \frac{\partial \dot{u}_{i,-\mathbf{k}}}{\partial u_{i,-\mathbf{k}}} \right) = 0,$$

see for instance [120] for more details. As the kinetic energy $\mathscr{E} = \frac{1}{2}\sum_\mathbf{k} |\mathbf{u}_\mathbf{k}|^2 = \frac{1}{2}\int d\mathbf{r}\, \mathbf{u}^2$ is the only invariant in this case, following discussion in section 2.2.3, the microcanonical measure is defined as

$$\mu_m = \lim_{K\to\infty} \mu_m^K \text{ with } \mu_m^K = \frac{1}{\Omega_K(E)} \prod_{|\mathbf{k}|\le K} \mathrm{d}\mathbf{v}_\mathbf{k}\, \delta(\mathscr{E}_K - E), \tag{29}$$

where $2\mathscr{E}_K = \sum_{|\mathbf{k}|\le K} |\mathbf{v}_\mathbf{k}|^2$ and m stand for "microcanonical".

Let us compute the average of $E_\mathbf{k} = |\mathbf{v}_\mathbf{k}|^2/2$, the energy of mode $\mathbf{k}$ for the measure μ_m^K. We note this average $\langle E_\mathbf{k}\rangle_{m,K} = \int \mu_m^K E_\mathbf{k}$. In (29), all degrees of freedoms $\mathbf{v}_{\mathbf{k}'}$ readily play a symmetric role. Henceforth we have energy equipartition $\langle E_\mathbf{k}\rangle_{m,K} = \langle E_{\mathbf{k}'}\rangle_{m,K}$ and $\langle E_\mathbf{k}\rangle_{m,K} = E/N(K)$ where $N(K)$ is the total number of modes such that $|\mathbf{k}| \le K$. This equipartition for the finite-dimensional measure μ_m^K leads to an energy spectrum $E(k)$ proportional to k^2 (see section 2.3.2 for definition of $E(k)$). This has been described by Kraichnan [111]. Recent applications to Galerkin truncations of the Euler equations and bottlenecks in turbulence can be found in Frisch *et al* [84].

We are now interested in invariant measures for the Euler equations themselves, not in invariant measures for truncated dynamics. We thus take the limit $K \to \infty$ (which then implies $N(K) \to +\infty$), with fixed energy because each trajectory has a finite energy. We obtain

$$\langle E_\mathbf{k}\rangle_m = \lim_{K\to\infty} \langle E_\mathbf{k}\rangle_{m,K} = 0.$$

Then, at statistical equilibrium, the average energy of each mode is exactly zero. Due to the infinite number of degrees of freedom, the tendency towards equipartition spreads energy on modes corresponding to smaller and smaller scales. This phenomenon associated with the existence of an infinite number of degrees of freedom is called the Jeans paradox [159]. It is a form of ultraviolet divergence.

We thus conclude that the equilibrium statistical mechanics of the 3D Euler equations explains the tendency for the energy to flow towards smaller and smaller scales. However, because in the microcanonical distribution, the energy per degree of freedom is zero, the microcanonical measure is trivial and thus useless. We see that for 3D turbulence, the statistically stationary flux of energy towards the smallest scales is intrinsically a far from equilibrium process. The equilibrium statistical mechanics is of no help to understand these fluxes, and the associated energy spectrum and velocity increment statistics.

Because of the additional Casimir invariants, the situation is quite different in 2D turbulence. All configurations of the microcanonical ensemble described in section 2.2.3 have the same energy E and enstrophy Γ_2. Then, for any configurations the l_E centroid inequality (28, page 32) holds: $l_E > \sqrt{\frac{2E}{\Gamma_2}}$. Henceforth, this is also true for the average over the microcanonical measure:

$$\langle l_E \rangle_m > \sqrt{\frac{2E}{\Gamma_2}}.$$

This simple argument shows that for the microcanonical measure, the energy cannot flow to the smallest scales. The microcanonical measure is thus non-trivial for two-dimensional conservative flows. It will describe large scale features that cannot be guessed straightforwardly. A detailed understanding of these equilibrium structures is the aim of the next sections.

The energy-enstrophy microcanonical measure of two dimensional flows. In order to illustrate that statistical mechanics gives non-trivial predictions for the 2D Euler case, we now consider the energy-enstrophy canonical measure

$$\mu_{m,2}(E,\Gamma_2) = \frac{1}{\Omega(E,\Gamma_2)} \prod_{i=1}^{\infty} \mathrm{d}\omega_i \, \delta(\mathscr{E}[\omega] - E) \, \delta(\mathscr{G}_2[\omega] - \Gamma_2)$$

This is the measure where we take into account only the quadratic invariants. There is no physical reason to exclude the other invariants; however the energy-enstrophy measure can be interesting because it may be in some cases a good approximation of the complete microcanonical measure. The interest and limitation of the energy-enstrophy measures are further discussed at the end of this section.

Our real motivation here is more pedagogical: it will be very useful to introduce mean-field treatment, and to explain on a simple example the relation between microcanonical measures defined on section 2.2.3 and mixing entropy used in section 3.1 and the following. The following discussion and the computation performed in the following paragraphs are adapted from the original presentation in [19].

An energy-enstrophy ensemble has been treated and discussed in length by many authors, including Kraichnan (see [113]), but in the canonical ensembles (that is using the canonical measure 15, page 26 rather than the microcanonical one). See also [129] for a precise discussion for the energy-enstrophy-circulation ensemble. It has also been proven, through computations of explicit inequalities, that the statistics of the small scales of the velocity field, in the energy-enstrophy ensemble, are incompatible with 2D Navier-Stokes invariant measures [11]).

The following discussion gives the first derivation of the microcanonical ensemble, its relation to the mean field variational problem, and the first observation of ensemble inequivalence for the energy-enstrophy ensemble. We come back to discuss Kraichnan type results in the end of this section.

Following the discussion in section 2.2.3, the microcanonical measure is defined through N dimensional approximations:

$$\mu_{m,2} = \lim_{N\to\infty} \mu_{m,2}^N \text{ with}$$

$$\mu_{m,2}^N = \frac{1}{\Omega_N(E,\Gamma_2)} \prod_{i=1..N} \mathrm{d}\omega_i \, \delta\left(\mathscr{E}_N[\omega] - E\right) \delta\left(\mathscr{G}_{2,N}[\omega] - \Gamma_2\right) \tag{30}$$

where, ω_i are components of ω on the base of eigenmodes e_i (see 20), $\mathscr{E}_N$ and $\Gamma_{2,N}$ are N dimensional approximations of the energy (3) and enstrophy (19): $2\mathscr{E}_N = \sum_{n=1..N} \omega_n^2/\lambda_n$ and $\mathscr{G}_{2,N}[\omega] = \sum_{n=1..N} \omega_n^2$. In the following, to simplify the argument, we assume that the first eigenvalue is non degenerate: $\lambda_1 \neq \lambda_2$, which is generically the case[8].

The main technical difficulty is to compute

$$\Omega_N(E,\Gamma_2) = \int \prod_{i=1..N} \mathrm{d}\omega_i \, \delta\left(\mathscr{E}_N[\omega] - E\right) \delta\left(\mathscr{G}_{2,N}[\omega] - \Gamma_2\right). \tag{31}$$

The computation of this result, using representation of the delta functions as integral in the complex plane, is given in [19], where it is shown that

$$\Omega_N(E,\mathscr{G}_2) \underset{N\to\infty}{=} C_3(N,\{\lambda_i\}) C_4(\{\lambda_i\},\Gamma_2,N) \frac{\exp\left[NS(E,\Gamma_2)\right]}{\sqrt{2E}} + o(N)$$

$$\text{with } S(E,\Gamma_2) = \frac{1}{2}\log\left(\Gamma_2 - 2\lambda_1 E\right) + \frac{\log 2}{2}, \tag{32}$$

where $C_3(N,\{\lambda_i\})$ depends only on N and $\{\lambda_i\}$ (i.e. does not depend on the physical parameters E and Γ_2) and C_4 has no exponentially large contribution ($\lim_{N\to\infty}(\log C_2)/N = 0$). The notation $o(N)$ refers to corrections that are negligible with respect to N when N becomes large enough. From (32) we have

$$S(E,\Gamma_2) = \lim_{N\to\infty} \frac{1}{N} \log\left(\Omega_N(E,\Gamma_2)\right) - C(N,\{\lambda_i\}), \tag{33}$$

[8] This is always true for simply connected bounded Lipshitz domains. An example of geometry for which the first eigenvalue is degenerate is a doubly periodic domain with aspect ratio $\delta = 1$.

where C can be computed from C_3, and depends only on N and on the geometric factors $\{\lambda_i\}$ (the entropy is defined up to an arbitrary constant).

We see that the quantity $S(E,\Gamma_2)$ is the Boltzmann entropy rescaled by $1/N$ with an unimportant additional constant. It counts the number of microstates Ω_N satisfying the constraints of the problem, i.e. characterized by energy E and enstrophy Γ_2.

From the entropy, we can compute the temperature $\beta = \partial S/\partial E = -\lambda_1/(\Gamma_2 - 2\lambda_1 E) \leq 0$ and chemical potential $\alpha = \partial S/\partial \Gamma_2 = 1/[2(\Gamma_2 - 2\lambda_1 E)]$. These thermodynamic potentials are related by $\beta = -2\lambda_1\alpha$. Then some couples of thermodynamic parameter are not obtained in the microcanonical ensemble, by contrast with what would be expected in the thermodynamics of classical condensed matter systems, which are most of the time short range interacting systems. Moreover the determinant of the Hessian of S $(\partial^2 S/\partial E^2.\partial^2 S/\partial \Gamma_2^2 - \left(\partial^2 S/\partial E \partial \Gamma_2\right)^2)$ is zero, showing that S is not strictly concave as one would expect for an entropy in the case of short range interacting systems. Both of these properties are signs of non-equivalence between the microcanonical and the canonical ensembles. (see for instance [16, 69, 59]). This case of the energy-enstrophy ensemble is actually a case of partial equivalence (see [69] for a definition).

From (30) we see that for the finite N dimensional measure μ_N, the distribution function for ω_n the amplitude of mode e_n is

$$P_{N,n}(\omega_n) = \frac{\Omega_{N-1;\lambda_n}\left(E - \omega_n^2/2\lambda_n, \Gamma_2 - \omega_n^2\right)}{\Omega_N(E,\Gamma_2)},$$

where $\Omega_{N-1;\lambda_n}$ is defined as Ω_N (equation. (31)), but with the integration over ω_n excluded, and with the constraint $\omega_n^2 \leq \max\{2\lambda_n E, \Gamma_2\}$. The distribution function for $E_n = \omega_n^2/2\lambda_n$, the energy of the mode e_n, is obtained by the change of variable $P_{N,n}(E_n)\,\mathrm{d}E_n = P_{N,n}(\omega_n)\,\mathrm{d}\omega_n$. Using result (32) for both $\Omega_{N-1;\lambda_1}$ (then λ_1 has to be replaced by λ_2) and Ω_N, we obtain

$$P_{N,1}(E_1) \underset{N\to\infty}{\sim} C\frac{\exp\left[N\log\left(\Gamma_2 - 2\lambda_2 E + 2(\lambda_2 - \lambda_1)E_1\right)/2\right]}{\sqrt{E_1(E - E_1)}}$$

$$\text{for } 0 \leq E_1 \leq E,$$

and $P_{N,1}(E_1) = 0$ otherwise, where C does not depend on E_1 (normalization constant). From this expression, we see that the most probable energy is $E_1 = E$. Moreover, the distribution is exponentially picked close to $E_1 = E$, such that in the infinite N limit (the microcanonical distribution) we have

$$P_1(E_1) = \delta(E - E_1).$$

All the energy condenses to the first mode.

If one disregards large deviations for $E - E_1$, a good approximation for large N of the finite N distribution is the exponential distribution

$$P_{N,1}(E_1) \underset{N\to\infty}{=} C\frac{\exp\left[-N\frac{\lambda_2-\lambda_1}{\Gamma_2 - 2\lambda_1 E}(E - E_1)\right]}{\sqrt{E - E_1}} \text{ for } 0 \leq E_1 \leq E$$

$$\text{and } N^{1/2}(E_1 - E) \ll 1; \tag{34}$$

the distribution for ω_1 being also exponential. The amplitude of the departure of E_1 from the value E is thus proportional to $1/N$ and to $(\Gamma_2 - 2\lambda_1 E)/(\lambda_2 - \lambda_1)$.

The distribution of the energy E_n of mode n is obtained similarly as

$$P_{N,n}(E_n) \underset{N\to\infty}{\sim} C\frac{\exp\left[N\log\left(\Gamma_2 - 2\lambda_1 E - 2(\lambda_n - \lambda_1)E_n\right)\right]}{\sqrt{E_n}} \tag{35}$$

$$\text{for } 0 \leq E_n \leq E. \tag{36}$$

For infinite N, the microcanonical distribution are thus a delta function with zero energy:

$$P_n(E_n) = \delta(E_n).$$

Disregarding large deviations, finite N distributions is also well approximated by an exponential distribution (a Gaussian distribution this time for ω_n) with typical energy departure from 0 of order $1/N$ for the energy and a variance of order $1/\sqrt{N}$ for ω_n. One may also check that for large n ($\lambda_n \gg \lambda_1$, the variance for the enstrophy becomes independent of n (asymptotic equipartition of the enstrophy).

Even if we have described finite N effects for finite N approximations of the microcanonical measure μ_m^N, the only invariant measure for the Euler equation is the limit one μ_m. From the preceding discussion we see that all the energy is concentrated on the first mode and that the excess enstrophy $\Gamma_2 - 2\lambda_1 E$ goes to smaller and smaller scales, leading to a zero energy or zero enstrophy per mode in the infinite N limit. This condensation of the energy in the first mode is the main physical result of this energy-enstrophy ensemble. This is a non trivial prediction of equilibrium statistical mechanics of two-dimensional flows, by contrast with the triviality of the results for three-dimensional flows.

The Kraichnan energy-enstrophy theory. The term of condensation has been proposed by Kraichnan from the analysis of the energy-enstrophy canonical ensembles [113]. As explained in section 2.2.1, canonical measure are not relevant for fluid systems and they may be useful only when given equivalent results to microcanonical measures. Kraichnan noticed this and worked nevertheless with the canonical ensemble, maybe because he didn't know how to make microcanonical computations, and most probably because at that time the possibilities of ensemble inequivalence were nearly unknown[9]. Unfortunately, as explained above the energy-enstrophy ensemble is an example of partial ensemble inequivalence. These remarks explain the difficulties encountered by Kraichnan by analyzing the canonical measure and why he wrongly concluded that a statistical mechanics approach would work only for truncated systems. Working in the microcanonical ensemble actually allows to build invariant measures of the real Euler equation. If one is however interested in truncated systems, then Kraichnan's work remains very useful.

[9]The first observation of ensemble inequivalence have been made in the astrophysical context [128, 92], and then observed for two dimensional flows [178, 109, 75, 69, 197]. Thorough study of ensemble inequivalence in the broad class of systems with long range interactions has been addressed during the last decade by many others, see for instance [59, 44, 38, 17, 37, 16] and references therein.

More importantly, when looking closely at Kraichnan's works (see for instance [113] page 565), one sees that in the canonical ensemble, a complete condensation of the energy on the gravest mode occurs only for specific values of the thermodynamical parameters. For most values of the thermodynamical parameters, an important part of the energy remains on the other modes. Still Kraichnan argued, probably from numerical observations available at the time and from physical insight, that these cases leading to a condensation were the most interesting ones. The microcanonical treatment we propose here proves that a complete condensation occurs whatever the values of the energy and of the enstrophy, in the microcanonical ensemble. A complete condensation is actually observed in many numerical simulations. We thus conclude that the physical insight of Kraichnan and his concept of condensation describes the relevant physical mechanism, but that a treatment in the microcanonical ensemble provides a much better understanding, and overcomes the preceding contradictions.

Limitations and interest of the energy-enstrophy approach. There is no reason to consider only the energy and enstrophy invariants, except for being able to solve easily the mathematics. Here we used this property for instance to illustrate the equivalence of the mean field variational problems with a direct definition of the microcanonical measure. Another class of statistical equilibria with easily solvable solutions is the one for which only energy, enstrophy and circulations are taken into account [197, 147] [10]. Moreover, several studies, among which [2, 67], have specifically addressed the importance of higher potential vorticity moments, showing that they may be indeed essential in some case.

From the following studies we will see that taking into account all invariants, it will be wrong that the energy is limited to the first mode e_1. However the energy-enstrophy measure may be in some cases a good approximation: for instance in the limit of small energy, most of the energy will remain in the first few modes. The notion of condensation will thus be valid only roughly speaking.

By contrast, in some cases like for instance for doubly periodic domains with aspect ratio close to one but not exactly one (see section 3.5), the notion of condensation would lead to completely wrong predictions.

2.3.5. Validity of a mean field approach to the microcanonical measures

For pedagogical reasons, we have considered in the previous section the energy-enstrophy microcanonical ensemble. It is shown in [19] that within this ensemble the correlation coefficient between vorticity at point $\mathbf{r}$ and vorticity at point $\mathbf{r}'$ is zero. It would be possible to prove without much difficulties that vorticity at points $\mathbf{r}$ and $\mathbf{r}'$ are actually independent variables. Such a result is extremely important and does apply to a much wider context than the energy-enstrophy measure, for instance it will remain true for all the microcanonical invariant measures, whatever the number of invariants. We will explain why vorticity fields are independent for microcanonical measures below. Let us first analyze an extremely important implication: the possibility to

[10] [197] proves relations between phase transitions on one hand, and ensemble equivalence and inequivalence results on the other hand. [147] proves specifically the equivalence between entropy maximization at fixed energy, circulation and enstrophy on one hand, and macroscopic enstrophy minimization at fixed energy and circulation on the other hand (see also [15] for equivalence results in a more general context)

quantify the volume of the phase space through the Boltzmann–Gibbs entropy formula.

A classical example where degrees of freedom can be considered independent is an ensemble of particles undergoing collisions (for instance hard spheres) in the dilute limit (the Boltzmann-Grad limit). Microscopically, particles travel at a typical velocity $\bar{v}$ and collide with each other after traveling a typical distance l called the mean free path. Let σ be the diffusion cross-section for these collisions. One has $\sigma = \pi a^2$ where the parameter a is of the order of the particle radius. The mean free path is defined as $l = 1/\left(\pi a^2 n\right)$, where n is the typical particle density. The Boltzmann equation applies when the ratio $\Gamma = a/l$ is small (the Boltzmann-Grad limit [184]). In the limit $\Gamma \to 0$, any two colliding particles can be considered as independent (uncorrelated) as they come from very distant areas. This is the basis of Boltzmann hypothesis of molecular chaos (Stosszahl Ansatz). It explains why the evolution of the μ-space distribution function $f(\mathbf{x},\mathbf{p},t)$ may be described by an autonomous equation, the Boltzmann equation ($\mathbf{x}$,$\mathbf{p}$ refers respectively to position and momentum, the μ-space is the six dimensional space of spatial variable $\mathbf{x}$ and momentum $\mathbf{p}$).

There is a classical argument by Boltzmann (that one can found in any good textbook in statistical mechanics) to prove that the Boltzmann entropy of the distribution f is, up to a multiplicative constant, given by the Boltzmann–Gibbs formula:

$$\mathscr{S} = -\int \mathrm{d}\mathbf{x}\mathrm{d}\mathbf{p}\, f \log f. \tag{37}$$

We stress that this formula for the Boltzmann entropy is not a Gibbs entropy [11]. The essential point is that this formula is a valid counting of the volume of the accessible part of the phase space only when particles can be considered as independent. For instance, for particles with short range interactions studied by Boltzmann, this is valid only in the Boltzmann-Grad limit.

As discussed above, in the energy-enstrophy ensemble, vorticity field values are independent. As we will explain bellow, the reason is completely different from the Boltzmann case, there is here no dilute-gas (Boltzmann-Grad) limit. However the consequences will be the same: if we define $\rho(\mathbf{r},\sigma)$ as $\rho(\mathbf{r},\sigma)\,\mathrm{d}\mathbf{r}\mathrm{d}\sigma$ being the probability to have values of the vorticity ω between σ and $\sigma + \mathrm{d}\sigma$ in the area element $\mathrm{d}\mathbf{r}$ around $\mathbf{r}$, then the entropy

$$\mathscr{S} = -\int_{\mathscr{D}} \mathrm{d}\mathbf{r} \int_{-\infty}^{+\infty} \mathrm{d}\sigma\, \rho \ln \rho, \tag{38}$$

actually quantifies the volume of the phase space. Let us explain the meaning of this last sentence, for instance in the case of the energy-enstrophy ensemble. The probability ρ is normalized ($N[\rho](\mathbf{r}) \equiv \int_{-\infty}^{+\infty} \mathrm{d}\sigma\, \rho(\sigma,\mathbf{r}) = 1$) and we define the average vorticity as $\bar{\omega}(\mathbf{r}) = \int_{-\infty}^{+\infty} \mathrm{d}\sigma\, \sigma\rho(\sigma,\mathbf{r})$.

[11] The Gibbs entropy $S = -k\int \rho(p_i,q_i)\log_2(\rho(p_i,q_i))\,dp_i dq_i$ is an ensemble entropy, a weight on the phase space, whereas the Boltzmann–Gibbs formula for the entropy is an integral over the μ-space. In the case of dilute gases, the Boltzmann–Gibbs formulae for the entropy is just the opposite of the H function of Boltzmann. We avoid this terminology here since our discussion is not related to relaxation towards equilibrium, and because the equivalent of an H theorem has never been proved for the 2D Euler equations.

Then the equilibrium entropy

$$S(E,\Gamma_2) = \sup_{\{\rho|N[\rho]=1\}} \left\{ \frac{1}{|\mathscr{D}|}\mathscr{S}[\rho] \mid \mathscr{E}[\overline{\omega}] = E \ , \int \mathrm{d}\mathbf{r}\mathrm{d}\sigma\, \sigma^2 \rho = \Gamma_2 \right\} \tag{39}$$

is exactly the same as the Boltzmann entropy defined from the rescaled logarithm of volume of the phase space defined by equation (33). This variational problem (39) means that the equilibrium entropy $S(E,\Gamma)$ is the supremum of the mixing entropy $\mathscr{S}[\rho]$ defined above, among all the normalized probability $\rho(\sigma,\mathbf{r})$ that are characterized by a given value of the energy E and enstrophy Γ_2.

The definition of the entropy (32-33) and the variational problem (39) are so different, that the fact that they express the same concept seems astonishing. These types of results are indeed one of the great achievements of statistical mechanics. It is shown in [19] that starting from (33) and computing $S(E,\Gamma_2)$ gives the same result as (32).

The deep reason why vorticity fields are independent for microcanonical measures, and henceforth why entropy can be expressed by (39) can be explained rather easily on a heuristic level. Correlations between variables could appear through the invariants constrains only. For instance the 2D Euler equation energy can be expressed in the form where interactions between vorticity appear explicitly, using the Laplacian Green function $H(\mathbf{r},\mathbf{r}')$ ($\Delta H(\mathbf{r},\mathbf{r}') = \delta(\mathbf{r},\mathbf{r}')$ with Dirichlet boundary conditions):

$$\mathscr{E}[\omega] = -\frac{1}{2}\int_{\mathscr{D}} \mathrm{d}\mathbf{r}\, \omega\Delta^{-1}\omega = -\frac{1}{2}\int_{\mathscr{D}}\int_{\mathscr{D}} \mathrm{d}\mathbf{r}\mathrm{d}\mathbf{r}'\, \omega(\mathbf{r}) H(\mathbf{r},\mathbf{r}')\omega(\mathbf{r}') \, . \tag{40}$$

In the formula above, $H(\mathbf{r},\mathbf{r}')$ appears as the coupling between vorticity at point $\mathbf{r}$ and vorticity at point $\mathbf{r}'$. The Green function of the Laplacian in a two-dimensional space is logarithmic, which is not integrable in the whole plane, hence lead to a non-local interaction. Then the vorticity at point $\mathbf{r}$ is coupled to the vorticity at any other points of the domains and not only close ones.

For people trained in statistical mechanics, it is natural that in systems where degrees of freedom are coupled to many other, these degrees of freedom can be considered as statistically independent and a mean-field approach will be valid. For instance in systems with nearest neighbor interactions, a mean field approach becomes exact for large dimensions, when the effective number of degrees of freedom to which one degree of freedom is coupled becomes infinite. For people not trained in statistical mechanics, this can be understood simply, as one increases the number of coupling, the interaction felt by one degree of freedom is no more sensitive to the fluctuations of the others but just to their average value, due to an effect similar to what happens for the law of large numbers. Then a mean field treatment becomes exact, which is equivalent to saying that different degrees of freedom can be considered as statistically independent.

Because of the non locality of the Green function, the vorticity field is virtually coupled to an infinite number of degrees of freedom, so that a mean-field is actually exact. This also explains why the energy computed from the average vorticity field appears in the variational problem (39).

To formalize the preceding heuristic explanation, in order to prove that the mean-field approximation is exact and to prove that the Boltzmann–Gibbs formulae for the entropy (37) is

relevant, we need a rather technical discussion. We will not explain this in details. This has been for instance justified by theoretical physicists for the point vortex model in the 1970s (assumed to be valid by Joyce and Montgomery [103] and then proved to be self-consistent, for instance in a Cramer Moyal expansions). In the 1980s, rigorous mathematical proofs have been given also for the point vortex model (see [75, 109, 33] and references therein). In the modern formulation of statistical mechanics, the entropy appears as a large deviation rate function for an ensemble of measures, justifying (37) and the variational problem (39). The proof of such large deviation results leading to the microcanonical measures for the Euler and quasi-geostrophic equations, justifying the mean field approach, can be found in [137] (see also [12] and references therein).

We thus conclude that a mean field approach to the microcanonical measures of the Euler and quasi-geostrophic equations is valid. This justifies the use of the entropy (37) and of variational problems similar to (39) but with all invariants of the Euler equations. This is a drastic simplification compared to direct approaches as the one presented in section 2.3.4 for the energy-enstrophy statistical mechanics. The first presentation of the equilibrium statistical mechanics of the 2D Euler and quasi-geostrophic equations on this form dates from the the beginning of the 1990s with the works of Robert, Sommeria and Miller [163, 139, 164, 169]. We thus call this theory the Robert-Sommeria-Miller (RSM) theory.

3. Equilibrium statistical mechanics of two dimensional and geophysical flows

In sections 2.2.1 and 2.2.3 we have recalled the basis of equilibrium statistical mechanics of Hamiltonian systems: building invariant measures based on the Liouville theorem, especially the microcanonical measure that takes into account all of the dynamical invariants of the equations. We have explained in sections 2.3.4 how this program can be applied to fluid dynamics equations and in section 2.3.5 why for the 2D Euler and quasi-geostrophic equations the microcanonical measure is described by a mean field variational problem.

The aim of this section is to describe this mean field variational problem and the tools used to actually compute the equilibrium states. We consider the limit of small energy, as a simple example were an analytic treatment is possible in order to illustrate the theory and especially the notion of phase transition. Phase transition is a key concept of thermodynamics and statistical physics, where the physical system undergoes drastic qualitative changes as external parameters are tuned. In the statistical mechanics of hydrodynamic problems, the flow undergoes continuous or discontinuous transitions of the topology of the flow streamlines. We discuss applications of this equilibrium theory to real flows, for instance in the geophysical context, in sections 4 and 5 and discussion of out of equilibrium statistical mechanics in section 6.

3.1. Mixing entropy and equilibrium states

3.1.1. Equilibrium entropy and microcanonical equilibrium states

We describe in this section the microcanonical variational problem and microcanonical entropy, the Robert-Sommeria-Miller theory, following these first papers [163, 139, 164, 169].

We explained is section 2.3.5 that for the microcanonical measure, the vorticity field at different locations are statistically independent. We denote $\rho(\mathbf{r},\sigma)\,\mathrm{d}\mathbf{r}\mathrm{d}\sigma$ the probability for

the vorticity ω to take values between σ and $\sigma + \mathrm{d}\sigma$ in the area element $\mathrm{d}\mathbf{r}$ around $\mathbf{r}$. Then the Boltzmann-Gibbs entropy

$$\mathscr{S}[\rho] \equiv -\int_{\mathscr{D}} d^2\mathbf{r} \int_{-\infty}^{+\infty} d\sigma\, \rho \log \rho. \tag{41}$$

is a quantification of the number of microscopic states (vorticity fields) corresponding to a macroscopic states (probability density ρ). A more precise meaning of this will be given with the variational problem (46) below. The most probable state, close to which most of the other states will be concentrated, will thus be the maximizer of the entropy (41) with constraints associated with each dynamical invariant.

We now list the constraints. As ρ is a local probability, it satisfies a local normalization

$$N[\rho](\mathbf{r}) \equiv \int_{-\infty}^{+\infty} \mathrm{d}\sigma\, \rho(\sigma, \mathbf{r}) = 1. \tag{42}$$

The conservation of all the Casimir functionals (17), or equivalently the known potential vorticity distribution (18) imposes

$$D[\rho](\sigma) \equiv \int_{\mathscr{D}} d\mathbf{r}\, \rho(\sigma, \mathbf{r}) = \gamma(\sigma). \tag{43}$$

The averaged potential vorticity is

$$\overline{q}(\mathbf{r}) = \int_{-\infty}^{+\infty} \mathrm{d}\sigma\, \sigma\rho(\sigma, \mathbf{r}). \tag{44}$$

with the average streamfunction $\overline{\psi}$, defined by $\overline{q} = \Delta\overline{\psi} - \frac{\overline{\psi}}{R^2} + h(y)$. As explained in section 2.3.5, because the interactions are long range and the energy is a sum over infinite contributions, the energy of the mean field will be equal to the initial energy

$$\mathscr{E}[\overline{q}] \equiv -\frac{1}{2}\int_{\mathscr{D}} \mathrm{d}\mathbf{r}\, \overline{\psi}\overline{q} = E. \tag{45}$$

Then the entropy of the system is given by the variational problem

$$S(E, \gamma) = \sup_{\{\rho | N[\rho]=1\}} \{\mathscr{S}[\rho] \mid \mathscr{E}[\overline{q}] = E\ , D[\rho] = \gamma\} \text{ (MVP)}. \tag{46}$$

and, thanks to the large deviation property [137] (see section 2.3.5) an overwhelming number of potential vorticity fields of the microcanonical ensemble will be close to the maximizer ρ of the variational problem (46).

Here MPV refers to "microcanonical variational problem". It says that the equilibrium entropy $S(E, \gamma)$ is the supremum of the mixing entropy $\mathscr{S}[\rho]$ among all the normalized probability density field $\rho(\sigma, \mathbf{r})$ that are characterized by a given value of energy E and of the global potential vorticity distribution $\gamma(\sigma)$.

Two routes are now possible. The classical one is to look for the critical points of the variational problem (46). For this, we introduce Lagrange multipliers β, $\alpha(\sigma)$ and $\zeta(\mathbf{r})$ associated

with the conservation of energy $\mathscr{E}$ (45), vorticity distribution $D(\sigma)$ 43), and normalization constraint N (42), respectively. Then critical points ρ are solutions of

$$\forall\, \delta\rho \quad \delta\mathscr{S} - \beta\delta\mathscr{E} - \int_{-\infty}^{+\infty} \mathrm{d}\sigma\ \alpha(\sigma)\delta D_\sigma - \int_{\mathscr{D}} \mathrm{d}\mathbf{r}\ \delta N = 0,$$

where the entropy is given by (41). Solving this equation for ρ and using the normalization constraint, we obtain that the critical points ρ verifies the Gibbs state equation [163, 139, 164, 168]:

$$\rho(\sigma,\mathbf{r}) = \frac{e^{\beta\sigma\psi(\mathbf{r})-\alpha(\sigma)}}{Z_\alpha(\beta\psi(\mathbf{r}))} \text{ with } Z_\alpha(u) = \int_{-\infty}^{\infty} \mathrm{d}\sigma \exp(\sigma u - \alpha(\sigma)), \tag{47}$$

We see that ρ depends on $\mathbf{r}$ through the average stream function $\bar{\psi}$. From (44) and (47) there is a functional relation between the equilibrium average potential vorticity and the stream functions

$$\bar{q} = g(\beta\bar{\psi}) \text{ with } g(u) = \frac{d}{du}\log Z_\alpha. \tag{48}$$

This last equation characterizes the statistical equilibrium. One can prove that g is a monotonously increasing function, such that the relation between potential vorticity $\overline{q}$ and streamfunction $\overline{\psi}$ is increasing for positive temperatures ($\beta > 0$), and decreasing for negative temperatures ($\beta < 0$). This equation has to be solved for any values of the Lagrange parameters β and $\alpha(\sigma)$. Then one has to compute the energy E and potential vorticity distribution $\gamma(\sigma)$ as a function of β and α.

For a given energy E and distribution $\gamma(\sigma)$, among all the possible values of β, α and distribution ρ solving (47-48), the one actually maximizing the entropy (46) is selected. In the general case, this program is not an easy one, and the aim of part of the following discussion will be to solve this in simple cases and to describe methods that will possibly make this program simpler.

The second route is to try to work directly with the variational problem (46) and to simplify it. In review we will try to rely as much as possible on variational problems only. This route will prove to be often physically more enlightening, at least for the specific examples treated in this review.

In his original papers, in the beginning of the 1990s, Miller [139, 140] justified formally the mean field variational problem from a formal discretization of the microcanonical measure and its solution through direct computations using the Hubbard-Stratonovich transformation. Robert and Sommeria [163, 164, 168] were assuming directly and phenomenologically the mean-field variational problem. Only latter on, did the work of Michel and Robert [138, 137] and Boucher, Ellis and Turkington [12] justify the mean-field variational problem more rigorously through expliciting the relation with large deviation theory.

We note that a similar mean field variational problem also describes the statistical mechanics of the violent relaxation of the Vlasov equation, both for self-gravitating systems and plasma physics. The mean field variational problem for the Vlasov equation has first been proposed on a phenomenological way by Lynden Bell in the end of the 1960s [128]. It can be justified following the same route as for the 2D Euler equations (see for instance [165]). There is indeed a deep

analogy, noticed from the 1950s, between the Vlasov and the 2D-Euler equation: both are nonlinear conservation laws with an infinite number of Casimir conservation laws, leading to similar properties and analogies, at the level of both dynamics and statistical mechanics. This analogy and its consequences from a statistical mechanics point of view have been used and described in details for instance in [51]. A larger class of systems have the same properties: systems with long range interactions. The analogies between the dynamics and statistical mechanics of these systems have been systematically studied during the last decade, see for instance [59, 44, 37, 38, 22].

3.1.2. Ergodicity

Section 3 describes the statistical equilibria through the variational problem (46). The solution of this variational problem is the most probable state and also, thanks to the large-deviation property, the state around which an overwhelming majority of states do concentrate, for the microcanonical measure. Besides, the microcanonical measure is the most natural invariant measure of the 2D Euler equations with the dynamical constraints.

Having described a natural invariant measure of the equations is an important theoretical step. Another important point would be to know if this invariant measure is the only one having the right values for the dynamical invariants. The evolution of one trajectory of the dynamical system also defines a measure (through time averaging). If we knew the invariant measure were unique, then it would mean that averaging over the microcanonical measure is equivalent to averaging over time. When this uniqueness property holds, we call the dynamical system ergodic.

Generally speaking, the ergodicity of a dynamical system is a property that is usually extremely difficult to prove. Such proofs exist only for very few extremely simple systems. Ergodicity is actually thought to be wrong in general. For instance, in Hamiltonian systems with a finite number of degrees of freedom, there often exist islands in phase space in which trajectories are trapped. The common belief in the statistical mechanics community is that those parts of phase space where the motion is trapped exist, but occupy an extremely small relative volume of the phase space, for generic systems with a large number of degrees of freedom. Apart from a few systems which were proved to be integrable, this common wisdom has successfully passed empirical tests of a century of statistical mechanics studies.

There is no reason to suspect that this general picture should be different in the case of the 2D Euler equations, in general. It is thus thought that an overwhelming number of initial conditions will have a dynamics consistent with the microcanonical measure predictions. However, similarly to most other Hamiltonian systems, the 2D Euler equations are actually non-ergodic. The proof is quite simple.

Indeed, it is proved in [19] that any Young measure for which $\bar{\omega}(\mathbf{r})$ is a stationary solution of the 2D Euler equations is either an invariant or a quasi-invariant measure. The class of invariant measures corresponding to ensemble of trajectories with given values of the invariants, is then much, much larger than the class of statistical equilibrium invariant measures with the same invariants. This proves that nontrivial sets of vorticity fields are dynamically invariant. In this restricted sense, this proves that the 2D Euler equations are not ergodic.

This theoretical argument proving non-ergodicity is in accordance with previous remarks about the phenomenology of the 2D Euler or quasi-geostrophic equations. For instance, it was observed numerically that initial conditions with localized vorticity, in large domains, remain localized (see [49] and references therein; [49] actually proposes an interesting phenomenological modification of the microcanonical measure approach to cope with this localized dynamics problem). Another example of possible non-ergodicity is the dynamics close to stable dynamical equilibria of the equations. When trajectories come close to such equilibria, they can be trapped (frozen) as was seen in some numerical simulations. A classical argument by Isichenko [98] is that for initial conditions close to parallel flows, "displacement in certain directions is uniformly small, implying that decaying Vlasov and 2D fluid turbulence are not ergodic". Even if the predicted algebraic laws by Isichenko are most probably wrong, the fact that displacement in directions normal to the streamlines is uniformly small is probably right, thus being another argument for non-ergodicity.

An important point to be noted, is that the Navier-Stokes equation with stochastic forces can be proved to be ergodic [29]. This ergodicity refers to invariant measures of the Navier-Stokes equations, which are non-equilibrium invariant measures with fluxes of conserved quantity. A very important point is to understand the limit of weak forces and dissipation for such invariant measures and to study their relations with the invariant measures of the 2D Euler equations. Some very interesting results can be found in [116].

3.1.3. Canonical and Grand Canonical ensembles

The microcanonical equilibrium describes the most probable state, resulting from the microcanonical measure with a given potential vorticity distribution and energy. From a mathematical point of view, we have to solve the variational problem (46). This is a tricky task, one of the main difficulty being due to the vorticity distribution and energy constraints. We here define canonical, grand canonical ensembles, and corresponding equilibrium, that will help us a lot in simplifying the description of the equilibrium states.

It is customary in statistical mechanics to consider statistical ensembles where the constraints coming from the dynamical invariants are relaxed (a phrase that will be clarified soon). For instance, in classical statistical mechanics, the canonical ensemble is obtained by relaxing the energy constraint, and the grand canonical ensemble by relaxing the constraint corresponding to the number of particles. We follow the same paths here. We call grand canonical ensemble, any ensemble where some or all of the constraints related to the potential vorticity distribution are relaxed. The meaning of this procedure is discussed in section 3.2.

Whereas the microcanonical ensemble is built on the assumption that all microstates with a given energy are equiprobable (microcanonical distribution), the canonical ensemble assumes a Boltzmann distribution of the microstates (distribution weighted by the Boltzmann factor $\exp(-\beta E)$). In section 2.3.5, we explained why a mean field description of the microcanonical measure is valid, and why it leads to the microcanonical variational problem (46). The same arguments allow to conclude that, for the canonical distribution, the most probable state and the Helmholtz free energy can be computed from the canonical variational problem

$$F(\beta,\gamma) = \inf_{\{\rho|N[\rho]=1\}} \{\mathscr{F}[\rho] = -\mathscr{S}[\rho] + \beta\, \mathscr{E}[\overline{q}] \;|D[\rho] = \gamma\,\} \text{ (CVP)}, \tag{49}$$

Here CVP refers to "canonical variational problem". The equilibrium free energy $F(\beta,\gamma)$ is the infimum of the free energy functional $\mathscr{F}[\rho]$ for any normalized field of probability density $\rho(\sigma,\mathbf{r})$ that are characterized by a given global potential vorticity distribution $\gamma(\sigma)$.

The canonical equilibrium states $\overline{q} = \int d\sigma\sigma\rho$ are the average potential vorticity fields where the free energy minima are achieved. Comparing (46) and (49), the canonical variational problem (49) appears to be similar to the variational problem associated with the microcanonical one, but with the energy constraint relaxed. This explains the expression “relaxation”. Thanks to the Lagrange multiplier rule, the canonical and microcanonical variational problems have the same critical points (47-48), but the stability properties of the two variational problems may be different (free energy minima and entropy maxima may be different). We discuss this last point in more detail in sections 3.2 and 3.3.

A similar relaxation, this time of the potential vorticity constraint, leads to fixed-energy grand canonical ensembles. This gives a new class of variational problems: the minimization of Casimir functionals

$$C(E_0,s) = \inf_q \left\{ \mathscr{C}_s[q] = \int_{\mathscr{D}} d^2\mathbf{r}\, s(q) \mid \mathscr{E}[q] = E_0 \right\} \text{ (EC-VP)}, \tag{50}$$

where $\mathscr{C}_s$ is a Casimir functionals, and s a convex function. Here EC-VP refers to "energy-Casimir variational problem". The fixed-energy grand canonical equilibria are the minimizers of this variational problem. The relation of this last variational problem to the microcanonical one is not obvious at a first sight. The mathematics of such a relation can be skipped, at first reading. For a detailed account of the derivation of (50) from the grand canonical distribution, we refer to [15]. The convex function s is related to the Lagrange parameters associated with the conservation of the vorticity distribution (the grand canonical thermodynamic variables)[12].

Critical points of (50) are solutions of

$$\forall\, \delta q \;\; \delta\mathscr{C}_s - \beta\delta\mathscr{E} = 0,$$

where β is the Lagrange parameter associated with the energy constraint. This yields to the following relation for the critical points:

$$q = \left(s'\right)^{-1}(-\beta\psi).$$

We conclude that if

$$\left(s'\right)^{-1}(-u) = g(u), \tag{51}$$

where $g(u)$ is defined by equation (48), then the microcanonical variational problem (46) and canonical one (50) have the same critical points. Moreover, it is proven in [15] that if (51) holds, then any stable canonical equilibrium (50) is a stable microcanonical equilibrium (46).

[12] These relations are given by formulas (12) and (16) of [15]

Notice that the variational problem EC-VP (50) was classically used before this statistical mechanics theory, and independently of it. It is called the Energy-Casimir variational problem, and was used in classical works on nonlinear stability of Euler stationary flows [5, 95], also allowing to prove the nonlinear stability of some of the statistical equilibrium states [168, 138]), as discussed in section 2.3.1. In addition, a minimum enstrophy principle has been previously proposed by Bretherton–Haidvogel [28] to predict the large scale organization of freely evolving 2D and geophysical flows. This approach led to the resolution of the variational problem (50) in the particular case $s(q) = -q^2$ (then the enstrophy of the flow is minimized at fixed energy). Although there is *a priori* no clear physical reason to motivate such a choice on a general context, the results of this subsection show that the Bretherton–Haidvogel theory is a particular case of the RSM statistical theory, since any solution of (50) is an RSM statistical equilibrium state.

3.2. Physical interpretation of the canonical and grand canonical ensembles

We have just presented canonical and grand canonical ensembles, and the relaxed variational problems. It is essential to understand their physical interpretation.

In classical statistical mechanics, two types of interpretations of canonical ensembles may be relevant, depending on the physical problem under consideration. The first physical interpretation is that the statistics of a system in contact with a thermal bath is actually described by the canonical distribution. The canonical distribution is thus the natural distribution in many cases, in condensed matter for instance. But when the physical system can be considered isolated (this is usually a matter of comparing the characteristic time for energy exchanges with the environment with the characteristic time for relaxation toward equilibrium), then the microcanonical distribution and ensemble are the relevant ones. In this case of an isolated system, the canonical distribution can still be considered, based on the fact that microcanonical and canonical distributions are usually equivalent in the thermodynamic limit: they give the same predictions for the average of macroscopic variables. In this second interpretation, the canonical distribution and ensemble appears as a very useful mathematical way to avoid some tricky technical difficulties related to the energy constraint in the microcanonical distribution.

Let us discuss more specifically the case of fluid dynamics, and the 2D Euler and quasi-geostrophic equations. First, there seems to be no way so far to couple such flows with a thermal bath. Also, for the grand canonical ensemble, it is hard to imagine what a potential vorticity bath could be. Then, only the second interpretation of the canonical ensemble can be a relevant interpretation of the relaxed ensembles: it is a very useful mathematical trick, nothing more. We are thus led to follow this second interpretation only. CVP (49) and EC-VP (50) are far more simple variational problems than the microcanonical ones MVP (46). Besides all solutions of CVP and EC-VP are solutions of MVP for some energies and some potential vorticity distributions (see [15] for a proof). The relaxed ensembles are thus very useful.

There is still a crucial difference between usual statistical mechanics and the statistical mechanics of two-dimensional and geophysical flows: microcanonical and relaxed ensembles are often non-equivalent. This is reflected by the fact that there may exist microcanonical equilibria that are not equilibria of the relaxed ensemble (the converse is not possible, as just stated above). An affirmative point however, is that such a situation of ensemble inequivalence can be detected

from the analysis of relaxed ensembles only (see [16] for a thorough discussion). Therefore, it is always a good choice to begin with the study of the least constrained ensemble. We show in section 3.5 how to use this general idea in specific examples.

3.3. Long range interactions and possible statistical ensemble non-equivalence

We explained in section 2.3.5 that the energy of the 2D Euler equations can be expressed in a form where interactions between vorticity values appear explicitly, using the Laplacian's Green function

$$\mathscr{E}[\omega] = -\frac{1}{2}\int_{\mathscr{D}} \mathrm{d}\mathbf{r}\, \omega\Delta^{-1}\omega = -\frac{1}{2}\int_{\mathscr{D}}\int_{\mathscr{D}} \mathrm{d}\mathbf{r}\mathrm{d}\mathbf{r}'\, \omega(\mathbf{r}) H(\mathbf{r},\mathbf{r}')\omega(\mathbf{r}')\,. \tag{52}$$

In formula (52), $H(\mathbf{r},\mathbf{r}')$ appears as the coupling between vorticity at point $\mathbf{r}$ and vorticity at point $\mathbf{r}'$. The Green function of the Laplacian in a two-dimensional space is logarithmic, which is not integrable over the whole plane. The interaction between vorticity at different points is thus a long-range interaction. This is the main reason why for statistical equilibria, the vorticity values at different points can be considered uncorrelated, and why mean-field variational problems (46) describe the statistical equilibria.

In physics, there is a large set of systems with long-range interactions (in the sense of a non-integrable potential). Self-gravitating stars [10, 183], plasma [152, 123], particles in accelerators, free-electron lasers, magnetic systems are examples among others of systems with long range interactions. For the same reasons as the ones presented in section 2.3.5, the equilibrium statistical mechanics of these systems will be described by mean-field variational problems similar to (46) or (49). Moreover, unlike systems with short range interactions, systems with long range interactions are not additive (in the limit of a large number of degrees of freedom, if the system is divided into two macroscopic sub-parts, the total energy is not approximately equal to the sum of the energies of the two sub-parts). This non-additivity has drastic physical consequences. For instance, the usual proof for the concavity of the entropy (in the context of short range interacting systems) relies on the additivity of the energy. It is then possible to observe non-concave entropies, and henceforth negative heat capacities (temperature decreases when energy increases!) for systems with long-range interactions, as first observed in self-gravitating systems [128].

The study of the statistical mechanics of systems with long-range interactions has been a very active branch of statistical mechanics over the past ten years (see articles in proceedings and reviews [59, 44, 38, 17, 37], among others). In two-dimensional and geophysical flows, unusual thermodynamic properties related to long range interactions have also been observed [178, 109, 33, 69, 70, 197] and their consequence for the stability theory [70] and related phase transitions [16] has been discussed.

The study of these thermodynamic peculiarities would be a natural extension of this review. Beyond their theoretical interest, these studies give important practical outcomes, such as simple characterization of equivalence between the variational problems (46) and (49) from the entropy curve [69], or actually from the free energy curve [16, 197], classification of all possible phase transitions [16], which is a very useful guide in any particular study, or new proofs of flow stability [70]. A detailed presentation of these results is however beyond the scope of this review.

3.4. *Statistical equilibria in the limit of affine relations between (potential) vorticity and streamfunction*

In section 3.1 we have described the variational problem which describe statistical equilibria (46). We have seen that the critical points of this variational problems give a nonlinear relation between (potential) vorticity and streamfunction (Eq. (48)), which we write again using the relation between streamfunction and potential vorticity (9)

$$q = \Delta\psi - \frac{\psi}{R^2} = g(\beta\psi) \tag{53}$$

(in order to simplify the discussion of this section we assume $\eta_d = 0$, the generalization to the case $\eta_d \neq 0$ would be easy). Equation (53) is a nonlinear elliptic partial differential equation whose general solution is not easily found. Some algorithms to solve numerically such an equation (or directly the variational problem (46)) will be described in section 3.6. Explicit analytic solution can be found only in some specific limit. A first limit, for which solutions are known is the limit when g is an affine function ($g(x) = ax + b$), called affine $q - \psi$ limit, that we describe in this section. This limit and normal forms due to small non-linear effects close phase transitions will also be used in the treatment of the example discussed in section 3.5. Another limit which can be treated analytically is a limit of very strong non-linearity which will be the method used in sections 4 and 5.

Chavanis and Sommeria first solved statistical equilibria for an affine g [47]. This work describe for instance phase transitions related to the domain geometry; for instance in a rectangular box a phase transition occurs between monopoles and dipoles when the aspect ratio is changed. We refer to [47] for a more detailed discussion. Subsequent works [197, 199], taking a different perspective by solving directly the variational problems, and describing wider classes of solutions have shown that the affine limit give examples of statistical ensemble inequivalence (see section 3.3) and of bicritical points and second order azeotropy, two phase transition types that were not observed before as statistical equilibria for turbulence problems. Applications to ocean model flows, like Fofonoff flows have also been discussed recently [197, 199, 147, 146]. All these results show that the affine $q - \psi$ limit is extremely rich from a physical point of view. The reference cited above contain much more results. The affine $q - \psi$ limit is also extremely interesting from a pedagogical point of view.

An essential point is to understand the physical circumstances for which the affine $q - \psi$ limit is relevant. Two different and complementary types of justification exist. In section 2.3.4, studying the energy-enstrophy ensemble, we have seen that taking into account enstrophy only as a Casimir invariant leads to an affine $q - \psi$ relation. We however stressed that there is no a priori reason to take into account only quadratic invariants. As first noticed in [47], when β is very small (very large temperatures) the energy constraint has less effect than in other situations and the system has a nearly homogenized potential vorticity [13]. Such states correspond to peculiar

[13] For a given global distribution $\gamma(\sigma)$, the macroscopic field ρ (47) does not depend on the spatial coordinates $\mathbf{r}$ when $\beta = 0$ (infinite temperatures). The corresponding potential vorticity field $\bar{q}$, given by equation (48), is therefore fully homogenized.

values of the energy. In this "strong mixing" limit $\beta \to 0$, an asymptotic expansion of (47) can be performed, by considering $\sigma\beta\psi$ as the small parameter. In this limit, statistical equilibrium states are characterized by a affine $q-\psi$ relations, whose properties depend on the energy and the circulation only, even if the infinite number of constraints are *a priori* considered (see [47, 147] for further discussions). This strong mixing limit is the first type of justification of the affine $q-\psi$ limit.

A second type of justification for the affine $q-\psi$ limit relies on the general results about equivalence between variational problems discussed in section 3.1.3 (please see also [15, 197]). We explained in the last paragraph of section 3.1.3 that the resolution of the variational problem (50) in the particular case $s(q) = -q^2$, leading to affine $q-\psi$ relation give access to an admissible class of statistical equilibria. We note, that actual potential vorticity distribution leading to affine or close to affine relations may be different in the two cases of the strong mixing limit, or using the mathematical properties of ensemble between variational problems. However, the coarse-grained potential vorticity fields will be the same as they are both described by the same class of affine $q-\psi$ relations. The phase diagram structure and phase transitions will also be the same in the two cases

3.5. Example of doubly-periodic flows

As an example of application of the equilibrium theory, we treat the case of the 2D Euler equations ($q=\omega$) on a doubly-periodic domain (torus) $(x,y) \in \mathscr{D} = (0, 2\pi\delta) \times (0, 2\pi)$; where δ is the aspect ratio. We believe this is a very good pedagogical example because of its simplicity. We will easily solve the problem analytically in the linearized limit, and make a nonlinear bifurcation analysis, leading to an interesting phase transition diagram.

This problem is also an interesting one from an academic point of view, as many direct numerical simulations (DNS) of the Euler or Navier–Stokes equations are performed in this geometry. The reason is that Fourier pseudo-spectral codes in periodic domains allow for much more efficient simulations than any other methods in bounded domains. This geometry is also advantageous because it does not involve the physics associated to boundary layers that make the situation more complex. This can also be considered a drawback, as it is hardly conceivable to make experimental realizations of this geometry in the lab.

Several generic properties of the theory should emerge through the study of this example. The first essential point is that the domain geometry always plays a crucial role. The second point is that the energy constraint is the one that prevents a complete mixing of the potential vorticity, it is thus also a key parameter. The last thing is that, like in usual thermodynamics, phase transitions also play an essential role for fluid dynamics applications. Indeed, they correspond to specific values of the physical parameters where drastic changes to the system occur. As such, these points are particularly interesting and any theoretical study should emphasize phase transitions.

This study in doubly periodic domains describes phase transitions between dipoles and parallel flows. The existence of these two types of statistical equilibria (dipole and parallel flows) were observed in direct numerical computations and numerical computations of statistical equilibria in [206]. The bifurcation theory we present here, predicting the phase diagram, the type of phase transitions, and the relevant physical control parameter (a balance between nonlinearity a_4 and domain geometry g) was first presented in [24, 143].

3.5.1. Variational problem

We consider the solutions of the variational problem:

$$C(E,s) = \inf_{\omega} \left\{ \mathscr{C}_s[\omega] = \int_{\mathscr{D}} d^2\mathbf{r}\, s(\omega) \mid \mathscr{E}[\omega] = E \right\} \text{ (EC-VP)} \tag{54}$$

where E is the energy and s a convex function of the vorticity ω (the second derivative of s with respect to ω are positive). This variational problem is the grand canonical variational problem (50) of section 3.1.3, in the case of the 2D Euler equations. We recall that any solution to (54) is a microcanonical statistical equilibrium, but that all microcanonical equilibria may not be solutions to (54), as discussed in section 3.2. We also recall (see equation (51) page 48) that the relation between s and the function g appearing in the solution of the microcanonical variational problem (48), is given by

$$\overline{\omega} = g(\overline{\psi}) = \left(s'\right)^{-1}(-\beta\overline{\psi}), \tag{55}$$

where β is the Lagrange parameter associated with the energy constraint.

3.5.2. Quadratic Casimir functionals

We first study the case of a quadratic Casimir functional $s(\omega) = \omega^2/2$. This leads to a linear relation between ω and ψ (see (55)). As discussed in section 3.4, a detailed study of microcanonical equilibria with linear $\omega - \psi$ relation was carried out in [47] (see also subsection 3.4), and a detailed study of variational problems with quadratic functional in relation with ensemble inequivalence is presented in [197, 199]. We note that in the case of the doubly periodic geometry, the strong mixing limit coincide with the weak energy limit.

We want to solve the variational problem

$$C_2(E) = \inf_{\omega} \left\{ \mathscr{C}_2[\omega] \equiv \frac{1}{2}\int_{\mathscr{D}} d^2\mathbf{r}\, \omega^2 \mid \mathscr{E}[\omega] = E \right\}. \tag{56}$$

It is convenient to decompose the fields on the Laplacian eigenmodes. Let us call $\{e_i\}_{i\geq 1}$ the orthonormal family of eigenfunctions of the Laplacian on the domain $\mathscr{D}$:

$$-\Delta e_i = \lambda_i e_i, \text{ with } \int_{\mathscr{D}} \mathrm{d}\mathbf{r}\, e_i e_j = \delta_{ij}. \tag{57}$$

The eigenvalues λ_i are arranged in increasing order. For a doubly periodic domain $(x,y) \in (0,2\pi\delta)\times(0,2\pi)$, $e_i(x,y)$ are sines and cosines. For instance, for $\delta > 1$: $e_1(x,y) = \sin(x/\delta)/2\pi\sqrt{\delta}$, $\lambda_1 = 1/\delta^2$, $e_2(x,y) = \sin(y)/2\pi\sqrt{\delta}$ and $\lambda_2 = 1$. We note that cosines are also eigenmodes, with the same eigenvalues λ_1 and λ_2. This degeneracy is due to translational invariance. In the following, we do not take them into account: this amounts to fixing two arbitrary phases associated with the translational invariance in the directions of $\mathbf{e}_x$ and $\mathbf{e}_y$.

We decompose the vorticity on the eigenbasis: $\omega = \sum_{i\geq 1} \omega_i e_i$. The energy (3) is then

$$\mathscr{E}[\omega] = \frac{1}{2}\sum_{i\geq 1} \lambda_i^{-1}\omega_i^2. \tag{58}$$

The energy constraint is absorbed into ω_1, giving $\omega_1^2 = 2\lambda_1 E - \sum_{i\geq 2}(\lambda_1/\lambda_i)\omega_i^2$. The condition $\omega_1^2 \geq 0$ imposes that the vector $\sum_{i\geq 2}\omega_i e_i$ be inside a volume V_E defined by

$$V_E = \left\{ \sum_{i\geq 2} \omega_i e_i \mid \sum_{i\geq 2} \lambda_i^{-1}\omega_i^2 \leq 2E \right\}. \tag{59}$$

Substituting the expression for ω_1^2 in (56), the variational problem becomes

$$C_2(E) = \lambda_1 E + \inf_{\{\omega_i\}_{i\geq 2}\in V_E} \left\{ \frac{1}{2}\sum_{i\geq 2} \frac{\lambda_i - \lambda_1}{\lambda_i}\omega_i^2 \right\}. \tag{60}$$

Since for all $i \geq 2$, $\lambda_i - \lambda_1 > 0$, one concludes that the minimizer of (60) verifies $\omega_i = 0$ for all $i \geq 2$:

$$\omega = (2\lambda_1 E)^{1/2} e_1 \text{ and } C_2(E) = \lambda_1 E. \tag{61}$$

We thus conclude that the equilibrium for a quadratic Casimir functional with an energy constraint is proportional to the first eigenmode of the domain. From the relation between vorticity and streamfunction, we see that the vorticity field e_1 corresponds to a parallel flow along the direction of maximum elongation of the domain

$$\mathbf{v} = \frac{(2E)^{1/2}}{2\pi\delta^{1/2}} \cos(x + \phi\delta)\, \mathbf{e}_y. \tag{62}$$

This example illustrates general properties of statistical equilibria:

1. The equilibrium structure is most of the times at the largest scales of the domain. This result is in agreement with the widely accepted empirical rule that the energy piles up to the largest scales of the domain.
2. The geometry of the domain plays a crucial role for the structure of the equilibria (in this case, we observe a transition from flows along the x direction towards flows along the y direction, as the aspect ratio crosses through the critical value $\delta_c = 1$).

The degenerate case. . A very interesting case is that of the periodic square domain $\mathscr{D} = (0,2\pi)\times(0,2\pi)$. In this case, the first eigenvalue λ_1 is degenerate, i.e. $\lambda_1 = \lambda_2$ (this degeneracy is not the degeneracy due to the translational invariance: there are actually four eigenmodes for the Laplacian corresponding to eigenvalues $\lambda_1 = \lambda_2$). Then, for a quadratic functional, a whole family of extrema exists: $\omega = \omega_1 e_1 + \omega_2 e_2$ with $\omega_1^2 + \omega_2^2 = 2\lambda_1 E$, and with entropy $C_2(E) = \lambda_1 E$.

This family of flows includes the parallel flows described previously, but also dipole flows. For instance, the symmetric dipoles of vorticity

$$\omega(x,y) = \frac{(2E)^{1/2}}{2\pi}\left[\sin(x+\phi) + \sin\left(y+\phi'\right)\right]. \tag{63}$$

We thus conclude that the maximization of a quadratic Casimir functional with energy constraint does not select the flow topology in a square domain; because of the degeneracy, it can be the topology of either parallel flows or dipoles.

3.5.3. Weak-energy limit for the maximization of symmetric Casimir functionals

We now consider the more general case of a Casimir functional

$$C_s(E) = \inf_{\omega} \left\{ \mathscr{C}_s[\omega] \equiv \int_{\mathscr{D}} d^2\mathbf{r}\, s(\omega) \;\mid \mathscr{E}[\omega] = E \right\}, \tag{64}$$

where s is a convex function. We suppose that s is even: $s(-\omega) = s(\omega)$. This is the case for any even initial distribution of the vorticity (an extension of the following discussion to the more general case would be easy).

It is clear that the multiplication of s by a constant will not change the minimizers of (64). Then we can assume, without loss of generality that $s''(0) = 1$.

We consider the weak-energy limit of the variational problem (64). Because the energy is positive-definite, it is clear that for weak energies, ω is small. Then $s(\omega) \sim \omega^2/2$. Then at leading order, in the weak-energy limit, the equilibrium structures are given by the minimization of a quadratic functional. They are thus close to the first eigenmodes of the Laplacian of the domain.

In the previous section, we saw that in a doubly periodic square domain, the minimization of a quadratic functional does not determine the flow topology, due to the degeneracy of the first Laplacian eigenvalues. An interesting issue is to understand how this degeneracy is removed by the next order contribution of a non quadratic functional. We thus consider

$$s(\omega) = \frac{1}{2}\omega^2 - \frac{a_4}{4}\omega^4 + o\left(\omega^4\right). \tag{65}$$

Parameter a_4. The parameter a_4 appearing in (65) plays a crucial role. It determines the first correction to a quadratic entropy. Moreover, it is intimately related to the shape of the relation $\omega = f(\psi) = (s')^{-1}(\beta\psi)$. Indeed, $s'(x) = x - a_4x^3 + o(x^3)$ and thus $(s')^{-1}(x) = x + a_4x^3 + o(x^3)$. For instance, when $a_4 > 0$, the curve $(s')^{-1}(x)$ bends upward for positive x, similarly to an hyperbolic sine; recalling that $\beta < 0$, the curve $f(\psi)$ is decreasing and similar to the opposite of an hyperbolic sine. When $a_4 < 0$, $(s')^{-1}(x)$ will bend downward, similar to an hyperbolic tangent. We will refer later on the case $a_4 > 0$ as the sinh-like case and the case $a_4 < 0$ as the tanh-like case.

3.5.4. Normal forms and selection between degenerate states in the weak energy limit

We now study how the degeneracy between eigenstates for a doubly periodic square is lifted. We saw in section 3.5.2 that the modification of the domain geometry (aspect ratio) removes the degeneracy. We suggested in the previous section that the contribution $a_4\omega^4$ of the Casimir functional may also remove the degeneracy. We study how these two effects compete, by making a quasi-linear study of the variational problem (64) in the weak energy limit.

We first evaluate the range of parameters for these two effects to be of the same order. We have seen that at leading order (maximization of a quadratic Casimir), the vorticity scales like $(\lambda_1 E)^{1/2}$. The fourth order term $a_4\omega^4$ is thus of order $a_4\lambda_1^2E^2$. The leading order correction due to the geometry in (56) is of order $(\lambda_2 - \lambda_1)E$. Therefore, one may omit non-quadratic corrections provided $a_4\lambda_1^2E^2 \ll (\lambda_2 - \lambda_1)E$ (case dominated by the geometry), and one could omit geometry effect for $a_4\lambda_1^2E^2 \gg (\lambda_2 - \lambda_1)E$ (case dominated by non quadratic contributions to the

Casimir functional). This suggests that interesting phenomena may occur in the weak-energy limit when $\lambda_2 - \lambda_1 = O(a_4 E)$ (we assume λ_1 of order one, which is the case if the domain area is of order one).

Given the preceding discussion, it is natural to define a geometry parameter g by

$$g = \frac{\lambda_2 - \lambda_1}{E}. \tag{66}$$

$g > 0$ is a measure of the degeneracy removal by the domain geometry ($\lambda_2 - \lambda_1$), scaled by E, the scale of relative non quadratic corrections in the small energy limit[14]. For a doubly periodic rectangular domain $(x,y) \in (0, 2\pi\delta)X(0, 2\pi)$, with aspect ratio δ, we have $\lambda_1 = 1/\delta^2$ and $\lambda_2 = 1$ (see section 3.5.2). Then $g = (\delta^2 - 1)/(\delta^2 E)$.

We now maximize the Casimir (54) using (66) and consider the limit $a_4 E \to 0$ for fixed values of g.

At leading order, the flow is dominated by the degenerate eigenmodes of the Laplacian. We thus have

$$\omega = (\omega_1 e_1 + \omega_2 e_2)\,(1 + o\,(a_4 E))\,, \tag{67}$$

The energy constraint (58) can be expressed as

$$\omega_2^2 = 2E\lambda_2 X + o\,(a_4 E) \;\text{ and }\; \omega_1^2 = 2\lambda_1 E(1-X) + o\,(a_4 E) \tag{68}$$

with $0 \le X \le 1$. The expression for the quadratic part (60) of the Casimir functional is

$$C_2(E) = E\,(\lambda_1 + gXE + o\,(gE))\,. \tag{69}$$

Similarly, we compute the fourth-order contribution to the entropy. Let define the structure coefficients by

$$\gamma_{n,k} = \int_{\mathscr{D}} d^2\mathbf{r}\, e_1^k e_2^{n-k}. \tag{70}$$

Given the symmetric role played by x and y, we have $\gamma_{4,0} = \gamma_{4,4}$ and $\gamma_{4,1} = \gamma_{4,3} = 0$ for the doubly-periodic square domain. These equalities will be used in the following for slightly rectangular domains, which is correct at leading order in $\lambda_2 - \lambda_1$ (or $\delta - 1$). We also define $\gamma = 3\gamma_{2,2} - \gamma_{4,0}$. We note that $\gamma = 3/8\pi^2 > 0$, which can be verified by a direct computation.

Straightforward computations then give

$$a_4 \int_{\mathscr{D}} d^2\mathbf{r}\, \frac{\omega^4}{4} = E\left[\left(\lambda_1^2\gamma_{4,0} + 2\gamma\lambda_1^2 X(1-X)\right) a_4 E + o\,(a_4 E)\right]. \tag{71}$$

From (64), (65), (69) and (71) we conclude, that at leading order, the minimum of the Casimir functional (64) is given by

$$C(E) = \lambda_1 E - \gamma_{4,0}\lambda_1^2 a_4 E^2 + E^2 \max_{0\le X\le 1} h(X), \tag{72}$$

[14] As may be noticed, the actual small parameter in the low energy expansion is $a_4 E$. One could have defined g by rescaling $\lambda_2 - \lambda_1$ by $a_4 E$ rather than by E only. This would however be inconvenient in the following discussion, as the sign of a_4 plays an essential role.

with

$$h(X) = -gX + 2\gamma\lambda_1^2 a_4 X(1-X). \tag{73}$$

Square geometry.. In order to understand the effects of the non-quadratic part only, let us first consider the case of the doubly periodic square domain, where the geometry parameter $g = 0$. The function $X(1-X)$ in h has a single maximum at $X = 1/2$. This solution where both eigenmodes e_1 and e_2 coexist equally is called a *mixed state*. From (67-68), we see that this mixed state is the vorticity of a symmetric dipole (see the description of (63)).

For the square geometry $g = 0$, there are also two global minima to $X(1-X)$: $X = 0$ ($\omega_2 = 0$ corresponding to e_1, see (67-68)), and $X = 1$ ($\omega_1 = 0$, corresponding to e_2). We call e_1 and e_2 *pure states*; we recall that e_1 and e_2 corresponds to parallel flows (see (62)).

From (73), we see that the maximization of the Casimir functional (72) depends crucially on the sign of a_4. For the square geometry $g = 0$, for the sinh-like case $a_4 > 0$, the non quadratic contribution selects the dipole (mixed state), whereas for the tanh-like case $a_4 < 0$, the non quadratic contribution selects the parallel flows (pure states).

Equilibria in the sinh*-like case ($a_4 > 0$) in a rectangular geometry.*. In a rectangular doubly periodic geometry $g \neq 0$, when $a_4 > 0$, the function $h(X)$ is a concave parabola. It thus has a single maximum for

$$X^\star = \frac{1}{2} - \frac{g}{4\gamma\lambda_1^2 a_4}. \tag{74}$$

Clearly $X^\star \leq 1/2$: the dipole is stretched in the same direction as the domain. The constraint $X^\star \geq 0$ must be verified (see 68). This is the case only if $g \leq g^\star$ with

$$g^\star = 2\gamma\lambda_1^2 a_4. \tag{75}$$

The discussion follows:

1. For $g > g^\star$ the effect of the geometry dominates and only the parallel flow associated with e_1 ($X = 0$) is observed. The Casimir minima is

$$C_s(E) = \lambda_1 E - \gamma_{4,0} a_4 \lambda_1^2 E^2 + o\left(a_4 E^2\right). \tag{76}$$

2. For $g < g^\star$ the effect of the non-quadratic term dominates, we then observe a mixed state corresponding to $X = X^\star$. The entropy is

$$C_s(E) = \lambda_1 E + \left[-\gamma_{4,0}\lambda_1^2 a_4 + \frac{1}{8\gamma\lambda_1^2 a_4}\left(g - g^*\right)^2\right] E^2. \tag{77}$$

   The solution $X = 0$ is a local maximizer of (64) (unstable state).

We thus conclude that in the sinh-like case ($a_4 > 0$), there exists a second order phase transition (i.e. a discontinuity in the second order derivative of the equilibrium entropy with respect to the energy) where the flow bifurcates from a dipole when the non quadratic part dominates ($g < 2\gamma\lambda_1^2 a_4$) to a parallel flow when the geometry dominates ($g > 2\gamma\lambda_1^2 a_4$).

Equilibria in the tanh*-like case ($a_4 < 0$) in a rectangular domain.*. In a rectangular doubly periodic geometry $g \neq 0$, when $a_4 > 0$, $h(X)$ is a convex parabola. Since $-gX$ favors the state e_1, the global statistical equilibrium is always the pure state e_1 ($X = 0$). The equilibrium value of the Casimir functional is

$$C_s(E) = \lambda_1 E - \gamma_{4,0}\lambda_1^2 a_4 E^2. \tag{78}$$

We now study the metastable and unstable equilibria. The function $h(X)$ has a single minimum for $X = X^\star$ (see (74)), but because now $a_4 < 0$, $X^\star \geq 1/2$. Depending on the position of $X^\star$ with respect to 1, two cases occur:

1. For $g > -g^\star$, then $X^\star < 1$, the mixed state exists as an unstable state. The pure state e_2 ($X = 1$) is a local maximum (metastable state).

2. For $g < -g^\star$, then the mixed state is no more a critical point. The pure state e_2 corresponding to $X = 1$ is a local minimum (unstable).

The results for the equilibrium structures are summarized on figure 7. There is thus a second order phase transition along the line $g = g^\star = 2\gamma\lambda_1^2 a_4$

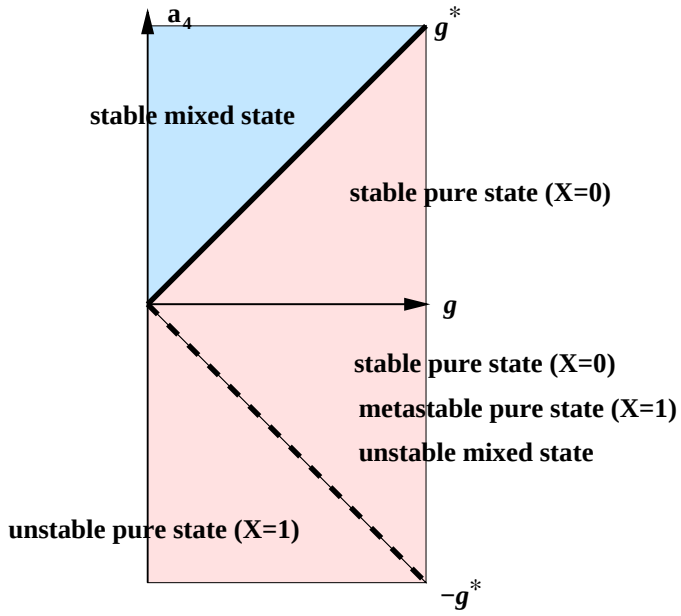

Figure 7: Bifurcation diagram for the statistical equilibria of the 2D Euler equations in a doubly periodic domain with aspect ratio δ, in the limit where the normal form treatment is valid, in the g-a_4 parameter plane. The geometry parameter g is inversely proportional to the energy and proportional to the difference between the two first eigenvalues of the Laplacian (or equivalently to $\delta - 1$ in the limit of small$\delta - 1$), the parameter a_4 measures the non-quadratic contributions to the Casimir functional. The solid line is a second order phase transition between a dipole (mixed state) and a parallel flow along the y direction (pure state $X = 0$). Along the dashed line, a metastable parallel flow (along the x direction, pure state $X = 1$) loses its stability.

The second order phase transition from the energy point of view.. In the preceding computations, we have worked with a rescaled geometry parameter g (66), because this is the correct scaling for studying the phase transition (balance between the effect of quartic part of the Casimir functional and the effect of the geometry). From a physical point of view, in many situations it is more natural to think in terms of energy, for a fixed geometry configurations.

We now consider fixed aspect ratio δ and a_4 parameters. Using (66), from the phase transition criteria (75), we deduce that a phase transition occurs for a critical energy E^* given by

$$E^* = \frac{4\pi^2\delta^2\left(\delta^2-1\right)}{3a_4}; \tag{79}$$

we have used $\gamma = 3/8\pi^2$, $\lambda_1 = \delta^{-2}$ and $\lambda_2 = 1$. The phase transition line is thus a hyperbola in the $(E - a_4$ plane). For energies $E < E^*$, we have $g > g^*$ and equilibria are dipoles, while for $E > E^*$ equilibria are parallel flows.

The computations of last sections are obtained as an expansion in powers of a_4E. The result (79) is thus valid for small a_4E^* or equivalently for small values of $\delta - 1$. The transition lines for larger values of the parameter $\delta - 1$ is discussed in next section.

3.5.5. Larger energy phase diagram

In order to look at the phase diagram for larger energies, we use a continuation algorithm to numerically compute solution to (55) corresponding to $f_{a_4}(x) = (1/3 - 2a_4)\tanh x + (2/3 + 2a_4)\sinh x$. Using $f = (s')^{-1}$, one can check that (65) is verified. The results are shown in figure 8. The inset of Fig 8 **a)** shows good agreement for transition lines obtained either with the continuation algorithm or the low-energy limit theoretical result, for $\delta = 1.01$. Figure 8 **b)** shows the bifurcation diagram for $\delta = 1.1$; in such a case the transition line is still very close to a hyperbola provided energy is small.

In this section, we have computed the phase diagrams for the statistical equilibria of the 2D Euler equations in a doubly periodic geometry. This is an illustration of the type of results provided by a statistical mechanics approach: prediction of large scale flow pattern, of phase transitions between these, explanation from statistical mechanics ideas the stability of these flows, and description of the few key parameters that characterize these flows.

We will come back to the doubly periodic geometry in section 6.4, and show how prediction of equilibrium phase transitions can be useful also for out of equilibrium situations, when dissipation and forcing are present.

3.6. Numerical methods to compute statistical equilibria

We have seen previously that it is possible to compute analytically equilibrium states of the RSM theory in some limit cases, and to get important insights on their physical properties through these computations. However, one might in practice want to be able to compute these equilibrium states for more general situations. One can distinguish three different numerical algorithms to find equilibrium states:

1. The use of an iterative algorithm proposed by Turkington and Whitaker, that computes local entropy maxima by linearizing the constraints of the variational problem [204, 194].

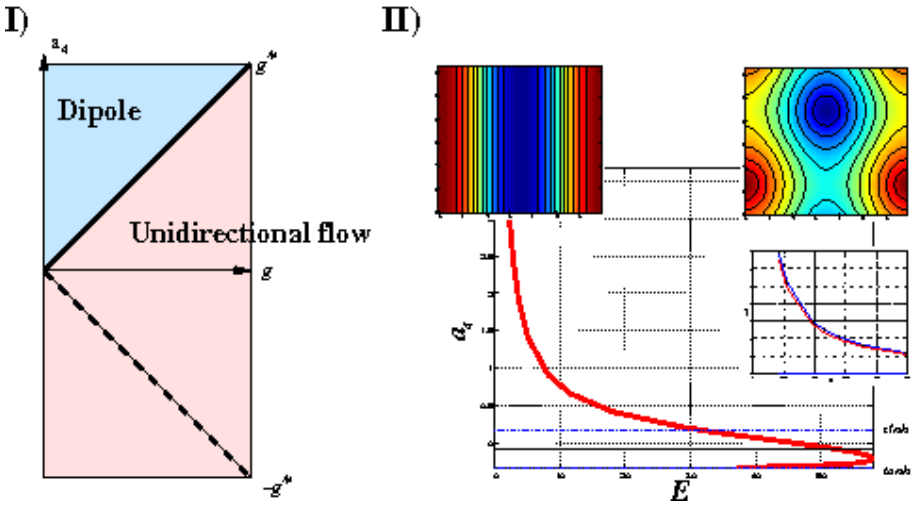

Figure 8: Bifurcation diagrams for statistical equilibria of the 2D Euler equations in a doubly periodic domain a) in the g-a_4 plane (see figure 7) b) obtained numerically in the $E - a_4$ plane, in the case of doubly periodic geometry with aspect ratio $\delta = 1.1$. The colored insets are streamfunction and the inset curve illustrates good agreement between numerical and theoretical results in the low energy limit.

2. The use of relaxation equations that maximize the entropy production of the system while keeping constant the constraints of the problem (potential vorticity distribution and energy) [169]. This method also drives the system toward a local entropy maximum. Generalization of relaxation equations to large classes of variational problems, with or without constrains have been devised, see for instance [45] for a recent review.
3. The use of continuation methods to compute the critical points of the variational problems (48). This method is very useful to follow a branch of stationary states by changing one parameter, and to detect bifurcations [187, 24].

One has to be aware that non-linear optimization, with or without constraint is not an easy task. One has to be able to follow several bifurcate branches of solutions, and actually be able to track the good one!

Each of these three methods have its own advantages and drawbacks. The advantage of methods 1 and 2 is that they actually deal with constrained variational problems. For instance if we speak about the energy constraint only, the control parameter of methods 1 and 2 will be the energy E of the flow and not the inverse temperature. The associated drawback is that they have to be initialized with fields having either the energy of interest (method 2) or an energy larger than the energy of interest (method 1, then one has to be able to compute energy extrema). Another advantage of methods 1 and 2 is that they actually compute local extrema. The associated drawback is that it is not possible to compute saddle or local minima, which is often necessary.

The advantage of method 3 is that it allows to actually follow branches of solution, whereas methods 1 and 2 lead to jump from one branch to an other in rather uncontrolled way. It also allows to precisely tracks bifurcations, and thus finds all the branches of solutions connected to the initial one. It thus gives a precise and complete view of the ensemble of critical points. It is

however more difficult to master.

The main drawback of all of these methods is that there is never any insurance to have caught the actual extrema.

3.7. Past studies of statistical equilibria and relaxation towards equilibrium

Most of theoretical contributions are described along this review. As far as applications are concerned, we have described only few examples of statistical equilibrium studies. Our choice was based on their pedagogical interest or on their interest for modeling natural phenomena. There have been however lots of other studies of statistical equilibria, comparisons with direct numerical simulations or experiments, see e.g. [180, 129] and references therein. We give in this section a brief overview of these works. We also discus briefly phenomenological approaches based on statistical mechanics ideas, discussing relaxation towards equilibrium, the closure problem in turbulence.

During the first stage following the appearance of RSM theory, there have been attempt to consider its application to classical fluid mechanics problems, like shear layer problems [182], or von-Karman vortex streets [187], and to check the prediction of statistical mechanics, as well as to describe symmetry breaking phenomena during the self-organization of initial conditions containing negative and positive vortex patches with equal strength and area, in various domain geometries [105]. Statistical equilibria computations were mainly done numerically. It was found that in any of these situation, statistical equilibrium predict that the most probable flow is a self organized large scale structure, qualitatively very similar to the numerically observed one. Quantitative agreement has to be discussed on a case by case basis [182, 187, 105]. Similarly, phase diagrams of statistical equilibrium states in a disk (for asymmetric vorticity distribution), and comparison with numerical simulations are provided in [54, 55, 53]. In the case of a doubly periodic domain, [206] found that freely evolving turbulent flow may for some classes of initial conditions be self-organized into "bar" (parallel flows) equilibrium states, different from the dipole associated with the gravest horizontal mode. An analytical understanding of this phenomenon is given in [24], see also section 3.5.

Note that they may also exist some class of initial conditions for which the final state may be unsteady (presenting quasi-periodic movements), which is not described by the statistical mechanics approach [176].

Some numerical studies of decaying 2D turbulence have specifically addressed the temporal evolution of the microscopic and macroscopic vorticity distribution [27, 39], or the effect of boundaries in closed domains [57].

The first analytical computations of RSM equilibrium states have been performed in the framework of the 2D Euler equations, for states characterized by a linear $q - \psi$ relation [47], which is justified in a strong mixing limit, see section 3.4. Generalization to a larger class of flow models (including quasi-geostrophic equations with topography), and relation with possible inequivalence between ensembles is given in [197, 199].

As explained in section 3.4, some of the states characterized by a linear $q - \psi$ relation had been previously described in the framework of the energy-enstrophy theory (and all are RSM

equilibrium states). This includes the original description of "Fofonoff flows" as statistical equilibria [172], see also [40] for further discussions and results, and [208, 200] for a comparison with direct numerical simulations. Generalization to continuously stratified quasi-geostrophic turbulence in doubly periodic domains (with bottom topography, but without beta effect) is discussed in [135]. Generalization to barotropic flows above finite topography is discussed in [136].

Energy enstrophy equilibrium states on a sphere have also been computed for a two-layers quasi-geostrophic model [81], and for a spin-lattice model of fluid vorticity [125, 126].

Because linear $q - \psi$ relations were also predicted by a phenomenological minimum enstrophy principle [28], the relation between such states and RSM theory has been widely discussed in earlier studies on the RSM theory, see e.g. [47, 26]. It is now understood that minimum enstrophy states are only a particular class of RSM equilibriums states [47, 15, 147].

In some cases, the final state flow organization observed in laboratory or numerical experiments is different from the one predicted by the RSM theory. This has lead to several phenomenological approaches inspired by the RSM theory. In most of these approaches, some additional constraints (different from the dynamical invariants) are imposed to the system.

In order to describe the self-organization of turbulent flow in unbounded domains, [49] proposed to impose an additional kinetic constraint of entropy maximization in a prescribed "bubble".

Another phenomenological approach, assuming *a priori* the existence of different "mixing regions" has been proposed to describe the self-organization following the equilibration of an unstable baroclinic jet in a two-layer quasi-geostrophic model in a channel [72].

It has been observed experimentally and numerically that in some cases, two slightly different initial conditions can lead to very different final states, one being predicted by the RSM theory, the other being a quasi-stationary state in which several vortex are organized into a long-lived crystal configuration, which persists during the time of the experiments, see e.g. [174], and [110] for an application to mesoscale vortices in cyclones. A phenomenological "regional entropy maximization" approach, assuming a priori the existence of several vortex, has been proposed to describe these vortex crystals [99, 100].

The idea of an application of equilibrium statistical mechanics to the description of Jovian vortices was mentioned in the early development of the theory (see for instance [181, 140, 138]). The fact that the ring shape of the Great Red Spot velocity field is related to the small value of the Rossby deformation radius in a Quasi-Geostrophic model has been understood in [181]. The first theoretical modeling and quantitative predictions are given in [25, 21] in the framework of 1.5 layer quasi-geostrophic equation. In particular, analytical result were obtained by considering the limit of small Rossby radius of deformation (and then strongly non-linear $q - \psi$ relations), see [25] and section 4. At the same time, the conditions for the appearance of the spot on the south hemisphere rather than on the south one, have been discussed in [193]. The small Rossby radius of deformation theory has been further developed in the oceanic context to describe rings and jets, see [202, 198] and sections 4 and 5.

Another attempt to apply equilibrium statistical mechanics to oceanic flows had been performed by [60, 61] in the framework of the Heton model of [93] for the self-organization phe-

nomena following deep convection events, by numerically computing statistical equilibrium states of a two-layer quasi-geostrophic model.

In the atmospheric context, the equilibrium statistical theory has been applied by [160] to predict final state organization of the stratospheric polar vortex.

In the ocean context, there has been many attempts to propose subgrid-scale parameterizations inspired by the equilibrium statistical mechanics[15], as first advocated by Holloway in the framework of the energy-enstrophy approach (see e.g. [94, 82] for a review and further references) , and further developed by [106] to take into account higher order invariants.

The parameterization of [106] is actually a direct application to the oceans of the relaxation equations proposed by Robert and Sommeria in the case of the Euler equations [169]. The relaxation equations are obtained through an interesting systematic approach based on a maximum entropy production principle (MEPP) in order to obtain equations, preserving the invariant structure of the initial equation but converging towards the equilibrium states. At a phenomenological level, they can be considered as a turbulent closure for the parameterization of small scale mixing. It has been shown empirically that they do not describe the actual turbulent fluxes [14]. This is however a drawback shared by most of existing parameterizations, and the essential fact that they preserve the mathematical properties (conservation laws, and so on) make relaxation equation better model candidates than most of other parameterizations. The relaxation equations were further developed in a number of works, see for instance [166, 167, 48, 14, 46] and references therein.

Other closures based on statistical mechanics ideas have been proposed by the group of Majda, sometime at a phenomenological level [89, 88], sometimes at a more fundamental level for specific problems [130].

4. Statistical equilibria and jet solutions, application to ocean rings and to the Great Red Spot of Jupiter

In section 3.5, we have described analytically the equilibrium flows with a normal form study close to a linear relation between potential vorticity and stream function (or equivalently in the limit of a quadratic Energy-Casimir functional). We have pointed out that more general solutions are very difficult to find analytically, and may require numerical computations, for instance using continuation algorithms.

There are however other limits where an analytical description becomes possible. This is for instance the case in the limit of large energies [191]. This is a very interesting, nontrivial and subtle limit; we do not describe it this review. The second interesting limit applies to the quasi-geostrophic model with 1.5 layers. It is the limit of Rossby deformation radius R much smaller than the size of the domain[16] ($R \ll L$), where the nonlinearity of the vorticity-stream

[15] We emphasize that such parameterization are phenomenological approaches, contrary to the equilibrium statistical mechanics.

[16] The study of equilibria of the quasi-geostrophic model is a first step before studying equilibria of the shallow water model, for which taking the limit $R \ll L$ give similar results.

function relation becomes essential. This limit case and its applications to the description of coherent structures in geostrophic turbulence is the subject of this section.

In the limit $R \ll L$, the variational problems of the statistical theory are analogous to the Van-Der-Waals Cahn Hilliard model that describes phase separation and phase coexistence in usual thermodynamics. The Van-Der-Waals Cahn Hilliard model describes for instance the equilibrium of a bubble of a gas phase in a liquid phase, or the equilibria of soap films in air. For these classical problems, the essential concepts are the free energy per unit area, the related spherical shape of the bubbles, the Laplace equation relating the radius of curvature of the bubble with the difference in pressure inside and outside the bubble (see section 4.1), or properties of minimal surfaces (the Plateau problem). We will present an analogy between those concepts and the structures of quasi-geostrophic statistical equilibrium flows.

For these flows, the limit $R \ll L$ leads to interfaces separating phases of different free energies. In our case, each phase is characterized by a different value of average potential vorticity, and corresponds to sub-domains in which the potential vorticity is homogenized. The interfaces correspond to strong localized jets of typical width R. This limit is relevant for applications showing such strong jet structures.

From a geophysical point of view, this limit $R \ll L$ is relevant for describing some of Jupiter's features, like for instance the Great Red Spot of Jupiter (a giant anticyclone) (here $R \simeq 500 - 2000\,km$ and the length of the spot is $L \simeq 20,000\,km$) (see section 4.3).

This limit is also relevant to ocean applications, where R is the internal Rossby deformation radius ($R \simeq 50\,km$ at mid-latitude). We will apply the results of statistical mechanics to the description of robust (over months or years) vortices such as ocean rings, which are observed around mid-latitude jets such as the Kuroshio or the Gulf Stream, and more generally in any eddying regions (mostly localized near western boundary currents) as the Aghulas current, the confluence region in the Argentinian basin or the Antarctic Circumpolar circulation (see section 4.4). The length L can be considered as the diameters of those rings ($L \simeq 200\,km$).

We will also apply statistical mechanics ideas in the limit $R \ll L$ to the description of the large scale organization of oceanic currents (in inertial region, dominated by turbulence), such as the eastward jets like the Gulf Stream or the Kuroshio extension (the analogue of the Gulf Stream in the Pacific ocean). In that case the length L could be thought as the ocean basin scale $L \simeq 5,000\,km$ (see section 5).

4.1. The Van der Waals–Cahn Hilliard model of first order phase transitions

We first describe the Van der Waals–Cahn Hilliard model. We give in the following subsections a heuristic description based on physical arguments. Some comments and references on the mathematics of the problem are provided in section 4.1.4.

This classical model of thermodynamics and statistical physics describes the coexistence of phase in usual thermodynamics. It involves the minimization of a free energy with a linear constraint:

$$\left\{ \begin{array}{c} F = \min\{\mathscr{F}[\phi] \mid \mathscr{A}[\phi] = -B\} \\ \text{with } \mathscr{F} = \int_{\mathscr{D}} \mathrm{d}\mathbf{r} \left[\frac{R^2(\nabla\phi)^2}{2} + f(\phi)\right] \text{ and } \mathscr{A}[\phi] = \int_{\mathscr{D}} \mathrm{d}\mathbf{r}\,\phi \end{array} \right. \tag{80}$$

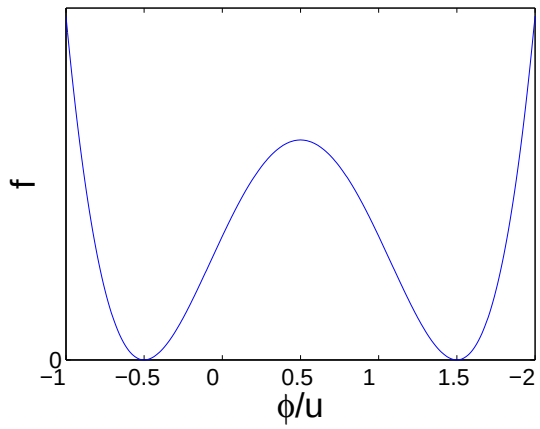

Figure 9: The double well shape of the specific free energy $f(\phi)$ (see equation (80)). The function $f(\phi)$ is even and possesses two minima at $\phi = \pm u$. At equilibrium, at zeroth order in R, the physical system will be described by two phases corresponding to each of these minima.

where ϕ is the non-dimensional order parameter (for instance the non-dimensionality local density), and $f(\phi)$ is the non-dimensional free energy per unit volume. We consider the limit $R \ll L$ where L is a typical size of the domain. We assume that the specific free energy f has a double well shape (see figure 9), characteristic of a phase coexistence related to a first order phase transition. For a simpler discussion, we also assume f to be even; this does not affect the properties of the solutions discussed bellow.

4.1.1. First order phase transition and phase separation

At equilibrium, in the limit of small R, the function $f(\phi)$ plays the dominant role. In order to minimize the free energy, the system will tend to reach one of its two minima (see figure 9). These two minima correspond to the value of the order parameters for the two coexisting phases, the two phases have thus the same free energy.

The constraint $\mathscr{A}$ (see equation. 80) is related to the total mass (due to the translation on ϕ to make f even, it can take both positive and negative values). Without the constraint $\mathscr{A}$, the two uniform solutions $\phi = u$ or $\phi = -u$ would clearly minimize $\mathscr{F}$: the system would have only one phase. Because of the constraint $\mathscr{A}$, the system has to split into sub-domains: part of it with phase $\phi = u$ and part of it with phase $\phi = -u$. In a two dimensional space, the area occupied by each of the phases are denoted A_+ and A_- respectively. They are fixed by the constraint $\mathscr{A}$ by the relations $uA_+ - uA_- = -B$ and by $A_+ + A_- = 1$ (where 1 is the total area). A sketch of a situation with two sub-domains each occupied by one of the two phases is provided in figure 10.

Up to now, we have neglected the term $R^2(\nabla\phi)^2$ in the functional (80). In classical thermodynamics, this term is related to non-local contributions to the free energy (proportional to the gradient rather than to only point-wise contributions). Moreover the microscopic interactions fix a length scale R above which such non-local interactions become negligible. Usually for a

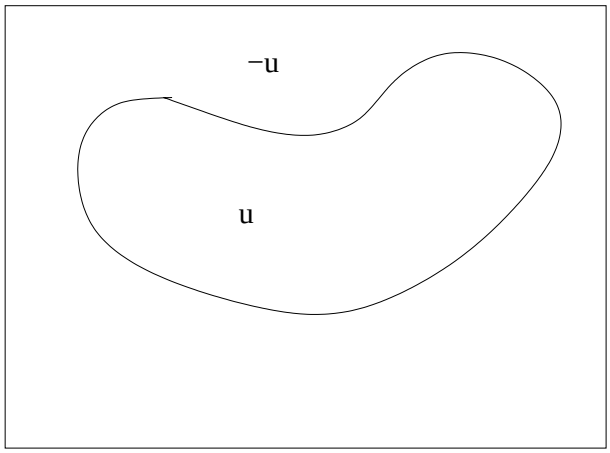

Figure 10: At zeroth order, ϕ takes the two values $\pm u$ on two sub-domains $A_{\pm}$. These sub-domains are separated by strong jets. The actual shape of the structure, or equivalently the position of the jets, is given by the first order analysis.

macroscopic system such non-local interactions become negligible in the thermodynamic limit. Indeed as will soon become clear, this term gives finite volume or interface effects.

We know from observations of the associated physical phenomena (coarsening, phase separations, and so on) that the system has a tendency to form larger and larger sub-domains. We thus assume that such sub-domains are delimited by interfaces, with typical radius of curvature r much larger than R[17]. Actually the term $R^2 (\nabla\phi)^2$ is negligible except on an interface of width R separating the sub-domains. The scale separation $r \gg R$ allows to consider independently what happens in the transverse direction to the interface on the one hand and in the along interface direction on the other hand. As described in next sections, this explains the interface structure and interface shape respectively.

4.1.2. The interface structure

At the interface, the value of ϕ changes rapidly, on a scale of order R, with $R \ll r$. What happens in the direction along the interface can thus be neglected at leading order. To minimize the free energy (80), the interface structure $\phi(\zeta)$ needs thus to minimize a one dimensional variational problem along the normal to the interface coordinate ζ

$$F_{int} = \min \left\{ \int \mathrm{d}\zeta \left[\frac{R^2}{2} \left(\frac{d\phi}{d\zeta} \right)^2 + f(\phi) \right] \right\}. \tag{81}$$

Dimensionally, F_{int} is a free energy F divided by a length. It is the free energy per unit length of the interface.

We see that the two terms in (81) are of the same order only if the interface has a typical width of order R. We rescale the length by R: $\zeta = R\tau$. The Euler-Lagrange equation of (81)

[17] This can indeed be proved mathematically, see section 4.1.4

gives

$$\frac{d^2\phi}{d\tau^2} = \frac{df}{d\phi}. \tag{82}$$

This equation is a very classical one. For instance making an analogy with mechanics, if ϕ would be a particle position, τ would be the time, equation (82) would describe the conservative motion of the particle in a potential $V = -f$. From the shape of f (see figure 9) we see that the potential has two bumps (two unstable fixed points) and decays to $-\infty$ for large distances. In order to connect the two different phases in the bulk, on each side of the interface, we are looking for solutions with boundary conditions $\phi \to \pm u$ for $\tau \to \pm\infty$. It exists a unique trajectory with such limit conditions: in the particle analogy, it is the trajectory connecting the two unstable fixed points (homoclinic orbit).

This analysis shows that the interface width scales like R. Moreover, after rescaling the length, one clearly sees that the free energy per length unit (81) is proportional to R: $F_{int} = eR$, where $e > 0$ could be computed as a function of f (see e.g. [25, 198]).

4.1.3. The interface shape: an isoperimetrical problem

In order to determine the interface shape, we come back to the free energy variational problem (80). In the previous section, we have determined the transverse structure of the interface, by maximizing the one dimensional variational problem (81). We have discussed the quantity $F_{int} = Re$, a free energy per unit length, which is the unit length contribution of the interface to the free energy. The total free energy is thus

$$\mathscr{F} = eRL, \tag{83}$$

where we have implicitly neglected contributions of relative order R/r, where r is the curvature radius of the interface.

In order to minimize the free energy (83), we thus have to minimize the length L. We must also take into account that the areas occupied by the two phases, A_+ and A_- are fixed, as discussed in section 4.1.1. We thus look for the curve with the minimal length, that bounds a surface with area A_+

$$\min\{eRL \,|\, \text{Area} = A_+\}. \tag{84}$$

This type of problem is called an isoperimetrical problem. In three dimensions, the minimization of the area for a fixed volume leads to spherical bubbles or plane surface if the boundaries does not come into play. When boundaries are involved, the interface shape is more complex (it is a minimal surface -or Plateau- problem). This can be illustrated by nice soap films experiments, as may be seen in very simple experiments or in many science museums. Here, for our two dimensional problem, it leads to circle or straight lines, as we now prove.

It is a classical exercice of variational calculus to prove that the first variations of the length of a curve is proportional to the inverse of its curvature radius r. The solution of the problem (84) then leads to

$$\frac{eR}{r} = \alpha, \tag{85}$$

Figure 11: Illustration of the Plateau problem (or minimal area problem) with soap films: the spherical bubble minimizes its area for a given volume (Jean Simeon Chardin, *Les bulles de savon*, 1734)

where α is a Lagrange parameter associated with the conservation of the area. This proves that r is constant along the interface: solutions are either circles or straight lines. The law (85) is the equivalent of the Laplace law in classical thermodynamics, relating the radius of curvature of the interface to the difference of pressure inside and outside of the bubble[18].

We have thus shown that the minimization of the Van-Der-Waals Cahn Hilliard functional, aimed at describing statistical equilibria for first order phase transitions, predicts phase separation (formation of sub-domains with each of the two phases corresponding to the two minima of the free energy). It predicts the interface structure and that its shape is described by an isoperimetrical problem: the minimization of the length for a fixed enclosed area. Thus equilibrium structures are either bubbles (circles) or straight lines. In the following sections, we see how this applies to the description of statistical equilibria for quasi-geostrophic flows, describing vortices and jets.

4.1.4. The mathematics of the Van-Der-Waals Cahn Hilliard problem

The mathematical study of the Van-Der-Waals Cahn Hilliard functional (80) was a mathematical challenge during the 1980s. It's solution has followed from the analysis in the framework of spaces of functions with bounded variations, and on results from semi-local analysis. One of the main contributions to this problem was achieved by Modica, in 1987 [141]. This functional

[18] Indeed, at next order, the Lagrange parameter α leads to a slight imbalance between the two phase free energy, which is related to a pressure difference for the two phases. This thus gives the relation between pressure imbalance, radius of curvature and free energy per unit length (or unit surface in the 3D case).

analysis study proves the assumptions of the heuristic presentation given in the previous subsections: ϕ takes the two values $\pm u$ in sub-domains separated by transition area of width scaling with R.

As a complement to these mathematical works, a more precise asymptotic expansion based on the heuristic description above, generalizable at all order in R, with mathematical justification of the existence of the solutions for the interface equation at all order in R, is provided in [13]. Higher order effects are also discussed in this work.

4.2. Quasi-geostrophic statistical equilibria and first order phase transitions

The first discussion of the analogy between statistical equilibria in the limit $R \ll L$ and phase coexistence in usual thermodynamics, in relation with the Van-Der-Waals Cahn Hilliard model is given in [13, 25]. This analogy has been recently put on a more precise mathematical ground, by proving that the variational problems of the RSM statistical mechanics and the variational problem are indeed related [15]. More precisely, any solution to the variational problem:

$$\left\{ \begin{array}{c} F = \min\{\mathscr{F}[\phi] \mid \mathscr{A}[\phi] = -B\} \\ \text{with } \mathscr{F} = \int_{\mathscr{D}} \mathrm{d}\mathbf{r} \left[\frac{R^2(\nabla\phi)^2}{2} + f(\phi) - R\phi h\right] \text{ and } \mathscr{A}[\phi] = \int_{\mathscr{D}} \mathrm{d}\mathbf{r}\, \phi \end{array} \right. \tag{86}$$

where $\psi = R^2\phi$ (ψ is the stream function defined by equation (10) on page 23), is a RSM equilibria of the quasi-geostrophic equations (8 on page 23).

It is easy to prove that any critical point to (86) is a critical point to the grand canonical Energy-Casimir functional (50), and is a critical point of the entropy maximization. Considering the problem (86), using a part integration and the relation $q = R^2\Delta\phi - \phi + Rh$ yields

$$\delta\mathscr{F} = \int \mathrm{d}\mathbf{r}\ \left(f'(\phi) - \phi - q\right)\delta\phi \quad \text{and} \quad \delta\mathscr{A} = \int \mathrm{d}\mathbf{r}\ \delta\phi.$$

Critical points of (86) are therefore solutions of $\delta\mathscr{F} - \alpha\delta\mathscr{A} = 0$, for all $\delta\phi$, where α is the Lagrange multiplier associated with the constraint $\mathscr{A}$. These critical points satisfy

$$q = f'\left(\frac{\psi}{R^2}\right) - \frac{\psi}{R^2} - \alpha.$$

We conclude that this equation is the same as (48), on page 45, provided that $f'\left(\frac{\psi}{R^2}\right) = g(\beta\psi) + \frac{\psi}{R^2} - \alpha$.

The proof that any solution to (86) is a RSM equilibria involves more complicated mathematical considerations; we assume this in the following and refer the interested readers to [15] for more details.

In the case of an initial distribution γ (43) with only two values of the potential vorticity: $\gamma(\sigma) = |\mathscr{D}|\,(a\delta(\sigma_1) + (1-a)\delta(\sigma_2))$, only two Lagrange multipliers α_1 and α_2 are needed, associated with σ_1 and σ_2 respectively, in order to compute g, equation (48), on page 45)). In that case, the function g is exactly tanh function. There exists in practice a much larger class of initial conditions for which the function g would be an increasing function with a single inflexion point, similar to a tanh function, especially when one considers the limit of small Rossby radius

of deformation. The works [25, 198] give physical arguments to explain why it is the case for Jupiter's troposphere or oceanic rings and jets.

When g is a tanh-like function, the specific free energy f has a double well shape, provided that the inverse temperature β is negative, with sufficiently large values.

4.2.1. Topography and anisotropy

The topography term $\eta_d = Rh(y)$ in (86) is the main difference between the Van-Der-Waals Cahn Hilliard functional (80) and the quasi-geostrophic variational problem (86). We recall that this term is due to the beta plane approximation and a prescribed motion in a lower layer of fluid (see section 2.1.3). This topographic term provides an anisotropy in the free energy. Its effect will be the subject of most of the theoretical discussion in the following sections.

Since we suppose that this term scales with R, the topography term will not change the overall structure at leading order: there will still be phase separations in sub-domains, separated by an interface of typical width R, as discussed in section 4.1. We now discuss the dynamical meaning of this overall structure for the quasi-geostrophic model.

4.2.2. Potential vorticity mixing and phase separation

In the case of the quasi-geostrophic equations, the order parameter ϕ is proportional to the stream function ψ: $\psi = R^2\phi$. At equilibrium, there is also a functional relation between the stream function ψ and the coarse-grained potential vorticity q (48). Then the sub-domains of constant ϕ are domains where the (coarse grained) potential vorticity q is also constant. It means that the level of mixing of the different fine grained potential vorticity levels are constant in those sub-domains. We thus conclude that the coarse grained potential vorticity is homogenized in sub-domains that corresponds to different phases (with different values of potential vorticity), the equilibrium being controlled by an equality for the associated mixing free energy.

4.2.3. Strong jets and interfaces

In section 4.1.3, we have described the interface structure. The order parameter ϕ varies on a scale of order R mostly in the normal to the interface direction, reaching constant values far from the interface. Recalling that ϕ is proportional to ψ, and that $\mathbf{v} = \mathbf{e}_z \wedge \nabla\psi$ (10), we conclude that:

1. The velocity field is nearly zero far from the interface (at distances much larger than the Rossby deformation radius R). Non zero velocities are limited to the interface areas.
2. The velocity is mainly directed along the interface.

These two properties characterize strong jets. In the limit $R \ll L$, the velocity field is thus mainly composed of strong jets of width R, whose path is determined from an isoperimetrical variational problem.

4.3. Application to Jupiter's Great Red Spot and other Jovian features

Most of Jupiter's volume is gas. The visible features on this atmosphere, cyclones, anti-cyclones and jets, are concentrated on a thin outer shell, the troposphere, where the dynamics is described by similar equations to the ones describing the Earth atmosphere [62, 97]. The

Figure 12: Observation of the Jovian atmosphere from Cassini (Courtesy of NASA/JPL-Caltech). One of the most striking feature of the Jovian atmosphere is the self organization of the flow into alternating eastward and westward jets, producing the visible banded structure and the existence of a huge anticyclonic vortex $\sim 20,000$ *km* wide, located around 20 South: the Great Red Spot (GRS). The GRS has a ring structure: it is a hollow vortex surrounded by a jet of typical velocity ~ 100 $m.s^{\{-1\}}$ and width $\sim 1,000\,km$. Remarkably, the GRS has been observed to be stable and quasi-steady for many centuries despite the surrounding turbulent dynamics. The explanation of the detailed structure of the GRS velocity field and of its stability is one of the main achievement of the equilibrium statistical mechanics of two dimensional and geophysical flows (see figure 13 and section 4).

inner part of the atmosphere is a conducting fluid, and the dynamics is described by Magneto-hydrodynamics (MHD) equations.

The most simple model describing the troposphere is the 1-1/2 quasi-geostrophic model,

described in section 2.1.3. This simple model is a good one for localized mid latitude dynamics. Many classical work have used it to model Jupiter's features, taking into account the effect of a prescribed steady flow in a deep layer acting like an equivalent topography $h(y)$ (see section 2.1.3). We emphasize that there is no real bottom topography on Jupiter.

Some works based on soliton theory aimed at explaining the structure and stability of the Great Red Spot. However, none of these obtained a velocity field qualitatively similar to the observed one, which is actually a strongly non-linear structure. Structures similar to the Great Red Spot have been observed in a number of numerical simulations, but without reproducing in a convincing way both the characteristic annular jet structure of the velocity field and the shape of the spot. Detailed observations and fluid mechanics analysis described convincingly the potential vorticity structure and the dynamical aspects of the Great Red Spot (see [62, 97, 131] and references therein). The potential vorticity structure is a constant vorticity inside the spot surrounded by a gentle shear outside, which gives a good fluid mechanics theory [131]. In this section we explain this potential vorticity structure thanks to statistical mechanics. Statistical mechanics provides also more detailed, and analytical theory of the shape of Jupiter vortices.

The explanation of the stability of the Great Red Spot of Jupiter using the statistical mechanics of the quasi-geostrophic model is cited by nearly all the papers from the beginning of the Robert-Sommeria-Miller theory. Some equilibria having qualitative similarities with the observed velocity field have been computed in [181]. The theoretical study in the limit of small Rossby deformation radius, especially the analogy with first order phase transitions [25, 21] gave the theory presented below: an explanation of the detailed shape and structure and a quantitative model. These results have been extended to the shallow-water model [18]. The work [193] argued on the explanation of the position of the Great Red Spot based on statistical mechanics equilibria.

We describe in the following the prediction of equilibrium statistical mechanics for the quasi-geostrophic model with topography. The start from the Van-Der-Waals Cahn Hilliard variational problem in presence of small topography (86), recalling that its minima are statistical equilibria of the quasi-geostrophic model (see section 4.2).

The Rossby deformation radius at the Great Red Spot latitude is evaluated to be of order of $500-2000$ km, which has to be compared with the size of the spot: $10,000 X\, 20,000$ km. This is thus consistent with the limit $R \ll L$ considered in the description of phase coexistence within the Van-Der-Waals Cahn Hilliard model (section 4.1), even if the criteria $r \ll R$ is only marginally verified where the curvature radius r of the jet is the larger.

In the limit of small Rossby deformation radius, the entropy maxima for a given potential vorticity distribution and energy, are formed by strong jets, bounding areas where the velocity is much smaller. Figure 13 shows the observation of the Great Red Spot velocity field, analyzed from cloud tracking on spacecraft pictures. The strong jet structure (the interface) and phase separation (much smaller velocity inside and outside the interface) is readily visible. The main difference with the structure described in the previous section is the shape of the vortex: it is not circular as was predicted in the case without topography or with a linear topography. We consider the effect of a more general topography in the next section.

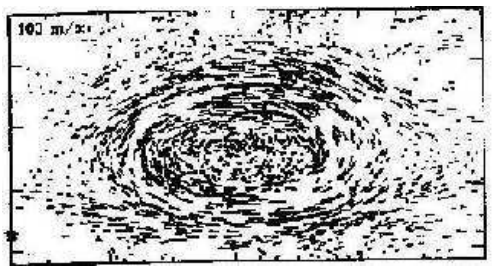

Observation (Voyager)

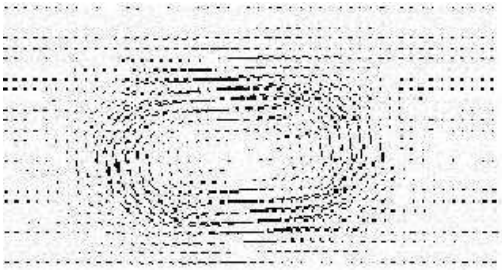

Statistical Equilibrium

Figure 13: Left: the observed velocity field is from Voyager spacecraft data, from Dowling and Ingersoll [63] ; the length of each line is proportional to the velocity at that point. Note the strong jet structure of width of order R, the Rossby deformation radius. Right: the velocity field for the statistical equilibrium model of the Great Red Spot. The actual values of the jet maximum velocity, jet width, vortex width and length fit with the observed ones. The jet is interpreted as the interface between two phases; each of them corresponds to a different mixing level of the potential vorticity. The jet shape obeys a minimal length variational problem (an isoperimetrical problem) balanced by the effect of the deep layer shear.

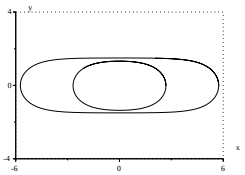

Statistical Equilibria

Great Red Spot and White Oval BC

A Brown Barge

Figure 14: Left panel: typical vortex shapes obtained from the isoperimetrical problem (curvature radius equation (85)), for two different values of the parameters (arbitrary units). The characteristic properties of Jupiter's vortex shapes (very elongated, reaching extremal latitude y_m where the curvature radius is extremely large) are well reproduced by these results. Central panel: the Great Red Spot and one of the White Ovals. Right panel: one of the Brown Barge cyclones of Jupiter's north atmosphere. Note the very peculiar cigar shape of this vortex, in agreement with statistical mechanics predictions (left panel)..

4.3.1. Determination of the vortex shape: the typical elongated shape of Jupiter's features

In order to determine the effect of topography on the jet shape, we consider again the variational problem (86). We note that the topography $\eta_d = Rh$ has been rescaled by R in the term $Rh(y)\phi$ appearing in the variational problem. This corresponds to a regime where the effect of the topography is of the same order as the effect of the jet free energy. Two other regimes exist: one for which topography would have a negligible impact (this would lead to circular vortices, as treated in section 4.2) and another regime where topography would play the dominant role. This last regime may be interesting in some cases, but we do not treat it in this review.

Due to the scaling $Rh\phi$, the topography does not play any role at zeroth order. We thus still conclude that phase separation occurs, with sub-domains of areas A_+ and A_- fixed by the potential vorticity constraint (see section 4.1.1), separated by jets whose transverse structure is described in section 4.1.3. The jet shape is however given by minimization of the free energy

contributions of order R. Let us thus compute the first order contribution of the topography term $RH = \int_{\mathscr{D}} \mathrm{d}\mathbf{r}\ (-R\phi h(y))$. For this we use the zeroth order result $\phi = \pm u$. We then obtain $H = -u\int_{A_+} \mathrm{d}\mathbf{r}\, h + u\int_{A_-} \mathrm{d}\mathbf{r}\, h = H_0 - 2u\int_{A_+} \mathrm{d}\mathbf{r}\, h$, where $H_0 \equiv u\int_{\mathscr{D}} \mathrm{d}\mathbf{r}\, h$. We note that H_0 does not depend on the jet shape.

Adding the contribution of the topography to the jet free energy (83), we obtain the first order expression for the modified free energy functional

$$\mathscr{F} = RH_0 + R\left(eL - 2u\int_{A_+} \mathrm{d}\mathbf{r}\, h(y)\right), \tag{87}$$

which is valid up to correction of order $e(R/r)$ and of order R^2H. We recall that the total area A_+ is fixed. We see that, in order to minimize the free energy, the new term tends to favor as much as possible the phase A_+ with positive values of stream function $\phi = u$ (and then negative values of potential vorticity $q = -u$) to be placed on topography maxima. This effect is balanced by the length minimization.

In order to study in more details the shape of the jet, we look at the critical points of the minimization of (87), with fixed area A_+. Recalling that first variations of the length are proportional to the inverse of the curvature radius, we obtain

$$2uRh(y) + \alpha = \frac{eR}{r}, \tag{88}$$

where α is a Lagrange parameter associated with the conservation of the area A_+. This relates the vortex shape to the topography and parameters u and e. From this equation, one can write the equations for X and Y, the coordinates of the jet curve. These equations derive from a Hamiltonian, and a detailed analysis allows to specify the initial conditions leading to closed curves and thus to numerically compute the vortex shape (see [25] for more details)

Figure 14 compares the numerically obtained vortex shapes, with the Jovian ones. This shows that the solution to equation (88) has the typical elongated shape of Jovian vortices, as clearly illustrated by the peculiar cigar shape of Brown Barges, which are cyclones of Jupiter's north troposphere. We thus conclude that statistical mechanics and the associated Van-Der-Waals Cahn Hilliard functional with topography explain well the shape of Jovian vortices.

Figure 15 shows a phase diagram for the statistical equilibria, with Jupiter like topography and Rossby deformation radius. This illustrates the power of statistical mechanics: with only few parameters characterizing statistical equilibria (here the energy E and a parameter related to the asymmetry between positive and negative potential vorticity B), we are able to reproduce all the features of Jupiter's troposphere, from circular white ovals, to the GRS and cigar shaped Brown Barges. The reduction of the complexity of turbulent flow to only a few order parameters is the main interest and achievement of a statistical mechanics theory.

Moreover, as seen on figure 15, statistical mechanics predicts a phase transition from vortices towards straight jets. The concept of phase transition is an essential one in complex systems, as the qualitative physical properties of the system drastically change at a given value of the control parameters. This is also an essential point, to be bring such a concept in turbulent problems. This will be further emphasized in section 6.4.3.

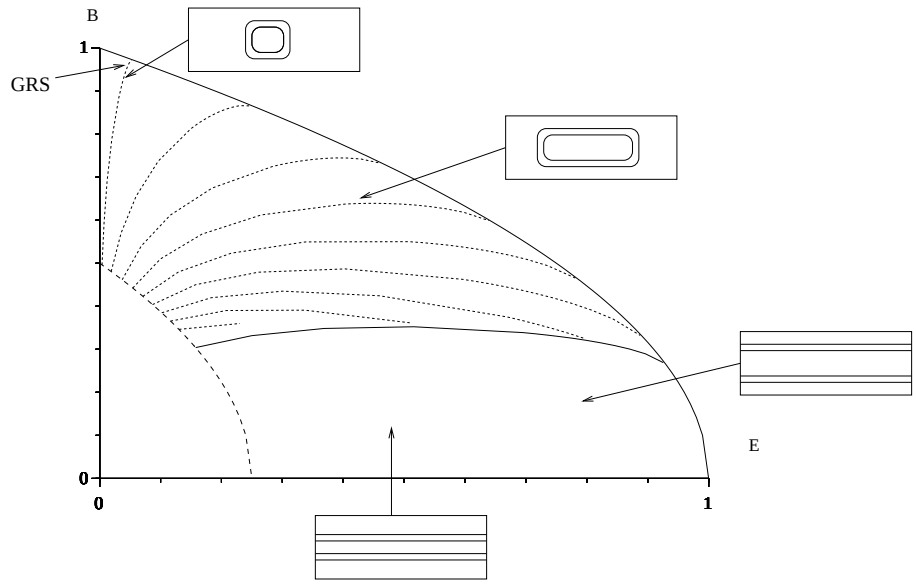

Figure 15: Phase diagram of the statistical equilibrium states versus the energy E and a parameter related to the asymmetry between positive and negative potential vorticity B, with a quadratic topography. The inner solid line corresponds to a phase transition, between vortex and straight jet solutions. The dash line corresponds to the limit of validity of the small deformation radius hypothesis. The dot lines are constant vortex aspect ratio lines with values 2,10,20,30,40,50,70,80 respectively. We have represented only solutions for which anticyclonic potential vorticity dominate ($B > 0$). The opposite situation may be recovered by symmetry. For a more detailed discussion of this figure, the precise relation between E, B and the results presented in this review, please see [21].

4.3.2. Quantitative comparisons with Jupiter's Great Red Spot

In the preceding section, we have made a rapid description of the effect of a topography to first order phase transitions. We have obtained and compared the vortex shape with Jupiter's vortices. A much more detailed treatment of the applications to Jupiter and to the Great Red Spot can be found in [25, 21]. The theory can be extended in order to describe the small shear outside of the spot (first order effect on ϕ outside of the interface), on the Great Red Spot zonal velocity with respect to the ambient shear, on the typical latitudinal extension of these vortices. A more detailed description of physical considerations on the relations between potential vorticity distribution and forcing is also provided in [25, 21].

4.4. Application to ocean rings

Application of equilibrium statistical mechanics to the description of oceanic flows is a long-standing problem, starting with the work of Salmon–Holloway–Hendershott [172] in the framework of energy-enstrophy theory.

Another attempt to apply equilibrium statistical mechanics to oceanic flows had been performed by [60, 61] in the framework of the Heton model of [93] for the self-organization phenomena following deep convection events, by numerically computing statistical equilibrium states of a two-layer quasi-geostrophic model.

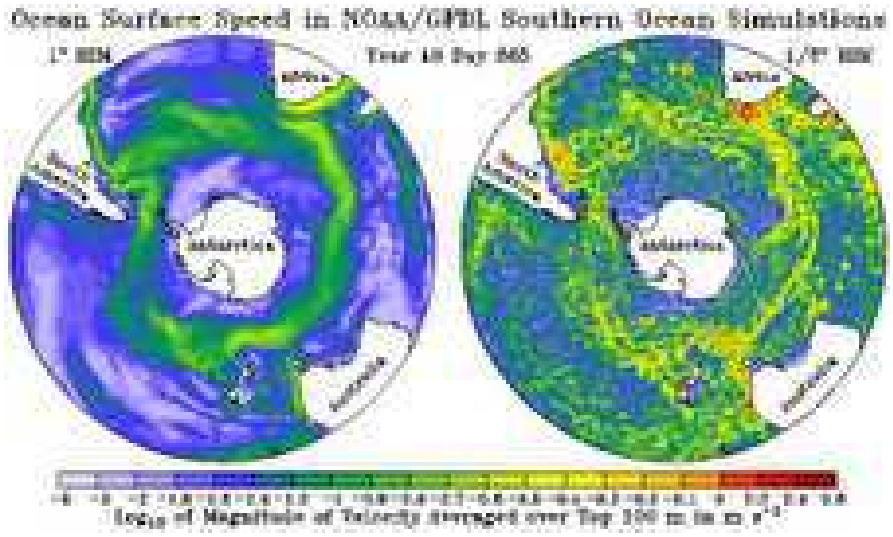

Figure 16: Snapshot of surface velocity field from a comprehensive numerical simulation of the southern Oceans [90]. Left: coarse resolution, the effect of mesoscale eddies ($\sim 100km$) is parameterized. Right: higher resolution, without parameterization of mesoscale eddies. Note the formation of large scale coherent structure in the high resolution simulation: there is either strong and thin eastward jets or rings of diameter ~ 200 *km*. Typical velocity and width of jets (be it eastward or around the rings) are respectively $\sim 1\ m.s^{-1}$ and ~ 20 *km*. The give a statistical mechanics explanation and model for these rings.

None of these previous approaches have explained the ubiquity of oceanic rings. We show in the following that such rings can actually be understood as statistical equilibria by similar arguments that explain the formation of Jovian vortices (see [198] for more details).

4.4.1. Rings in the oceans

The ocean has long been recognized as a sea of eddies. This has been first inferred from *in situ* data by Gill, Green and Simmons in the early 1970s [86]. During the last two decades, the concomitant development of altimetry [52, 185] and realistic ocean modeling [90, 6] has made possible a quantitative description of those eddies. The most striking observation is probably their organization into westward propagating rings of diameters $(L_e \sim 200\ km)$, as for instance seen in figure 16. In that respect, they look like small Jovian Great Red Spots.

Those eddies plays a crucial role for the general ocean circulation and its energy cycle, since their total energy is one order of magnitude above the kinetic energy of the mean flow.

Those rings are mostly located around western boundary currents, which are regions characterized by strong baroclinic instabilities[19], such as the Gulf Stream, the Kuroshio, the Aghulas

[19]When the mean flow present a sufficiently strong vertical shear, baroclinic instabilities [156, 195] release part of the available potential energy associated with this mean flow, which is generally assumed to be maintained by a large scale, low frequency forcing mechanism such as surface wind stress or heating [195]

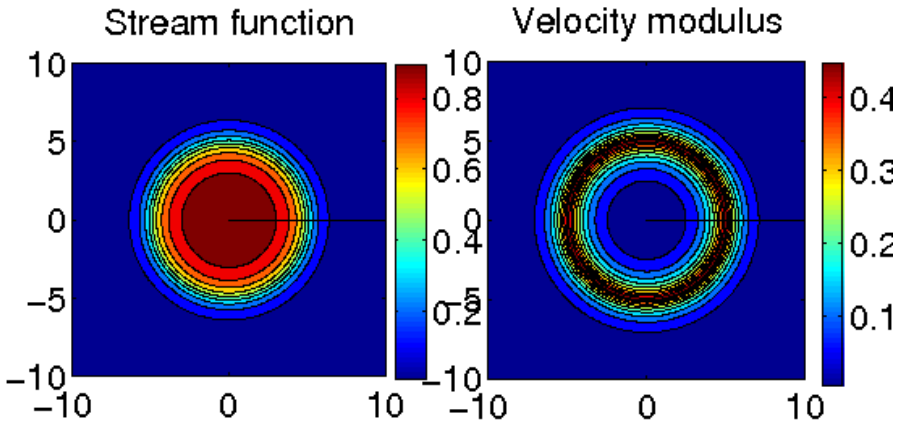

Figure 17: Vortex statistical equilibria in the quasi-geostrophic model. It is a circular patch of (homogenized) potential vorticity in a background of homogenized potential vorticity, with two different mixing values. The velocity field (right panel) has a very clear ring structure, similarly to the Gulf-Stream rings and to many other ocean vortices. The width of the jet surrounding the ring has the order of magnitude of the Rossby radius of deformation R.

currents below South Africa or the confluence region of the Argentinian basin, as seen on figures 16 and 19. The rings can also propagate far away from the regions where they are created.

Most of those rings have a baroclinic structure, i.e. a velocity field intensified in the upper layer ($H \sim 1\ km$) of the oceans. This baroclinic structure suggest that the 1.5 layer quasi-geostrophic model introduced in the previous sections is relevant to this problem. The horizontal scale of the rings $(L_e \sim 200\ km)$ are larger than the width $R \sim 50\ km$ of the surrounding jet, of typical velocities $U = 1\ m.s^{-1}$.

The organization of those eddies into coherent rings can be understood by the same statistical mechanics arguments that have just been presented in the case of Jupiter's Great Red Spot. The rings correspond to one phase containing most of the potential vorticity extracted from the mean flow by baroclinic instability, while the surrounding quiescent flow corresponds to the other phase. This statistical mechanics approach, the only one to our knowledge to describe the formation of large scale coherent structures, might then be extremely fruitful to account for the formation of such rings. It remains an important open question concerning the criteria that select the size of such coherent structures. This is an ongoing subject of investigation.

4.4.2. The westward drift of the rings

In this section, we consider the consequences of the beta effect (see section 2.1.3), which corresponds to linear topography $\eta_d = \beta_c y$ in (9). We prove that this term can be easily handled and that it actually explains the westward drift of oceanic rings with respect to the mean surrounding flow.

We consider the quasi-geostrophic equations on a domain which is invariant upon a translation along the x direction (either an infinite or a periodic channel, for instance). Then the quasi-geostrophic equations are invariant over a Galilean transformation in the x direction. We

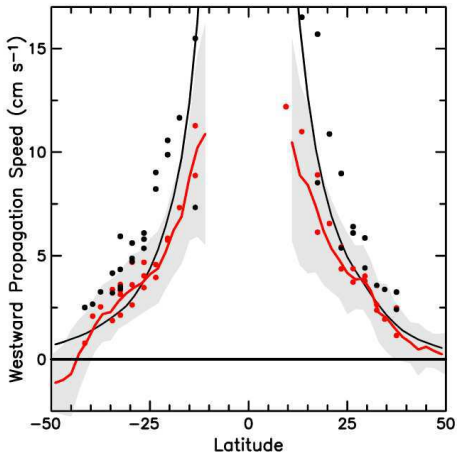

Figure 18: Altimetry observation of the westward drift of oceanic eddies (including rings) from [52], figure 4. The red line is the zonal average (along a latitude circle) of the propagation speeds of all eddies with life time greater than 12 weeks. The black line represents the velocity $\beta_c R^2$ where β_c is the meridional gradient of the Coriolis parameter and R the first baroclinic Rossby radius of deformation. This eddy propagation speed is a prediction of statistical mechanics (see section 4.4.2)

consider the transformation

$$\mathbf{v}' = \mathbf{v} + V\mathbf{e}_x,$$

where $\mathbf{v}$ is the velocity in the original frame of reference and $\mathbf{v}'$ is the velocity in the new Galilean frame of reference.

From the relation $\mathbf{v} = \mathbf{e}_z \wedge \nabla\psi$ (10), we obtain the transformation law for ψ: $\psi' = \psi - Vy$ and from the expression $q = \Delta\psi - \psi/R^2 + \beta_c y$ (9) we obtain the transformation law for q: $q' = q + Vy/R^2$. Thus the expression for the potential vorticity in the new reference frame is

$$q = \Delta\psi - \frac{\psi}{R^2} + \left(\beta_c + \frac{V}{R^2}\right) y.$$

From this last expression, we see that a change of Galilean reference frame translates as a beta effect in the potential vorticity. Moreover, in a reference frame moving at velocity $-\beta_c R^2 \mathbf{e}_x$, the β_c effect is exactly canceled out.

From this remark, we conclude that taking into account the beta effect, the equilibrium structures should be the one described by the minimization of the Van-Der-Waals Cahn Hilliard variational problem, but moving at a constant westward speed $V = \beta_c R^2$. A more rigorous treatment of the statistical mechanics for the quasi-geostrophic model with translational invariance would require to take into account an additional conserved quantity, the linear momentum, which would lead to the same conclusion: statistical equilibria are rings with a constant westward speed $V = \beta_c R^2$. See also [198] for more details and discussions on the physical consequences of this additional constraint.

This drift is actually observed for the oceanic rings, see for instance figure 18.

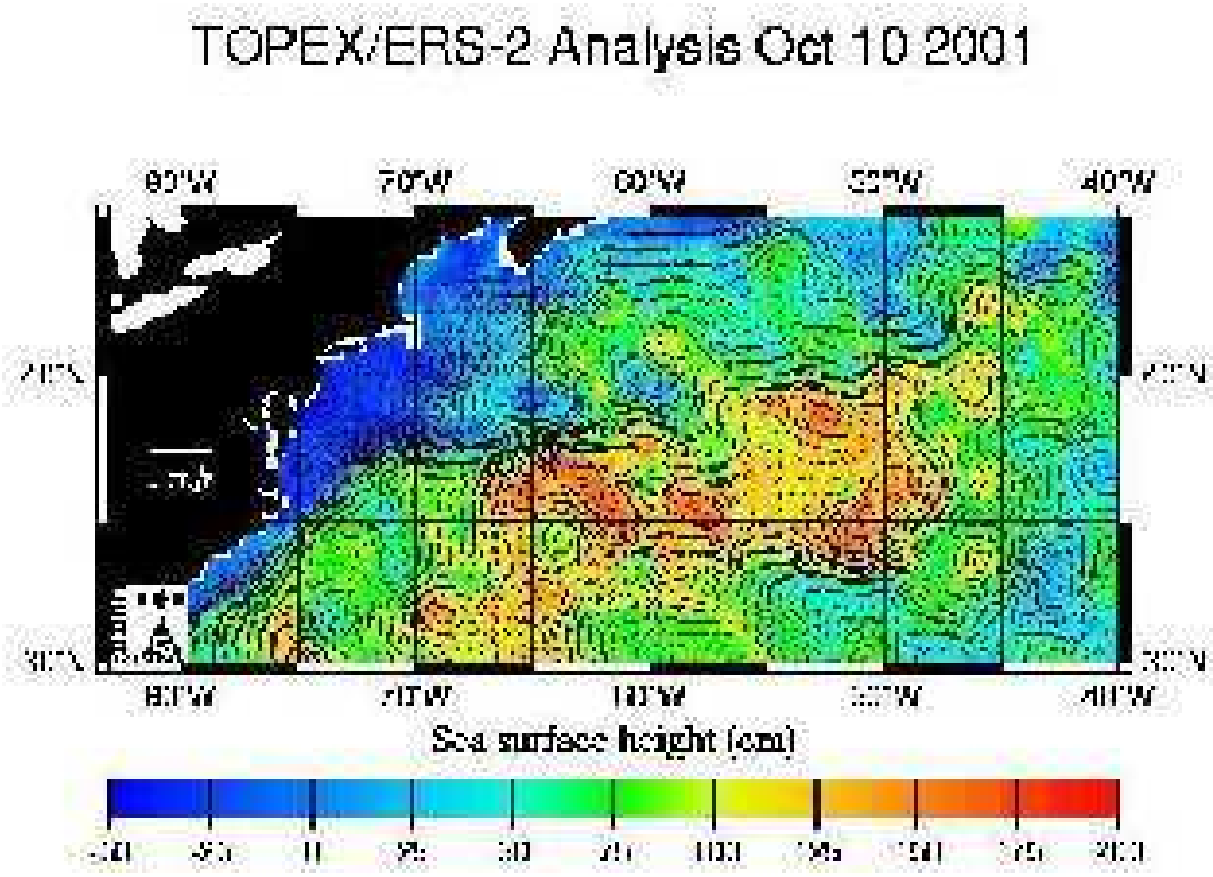

Figure 19: Observation of the sea surface height of the north Atlantic ocean (Gulf Stream area) from altimetry REF. As explained in section 2.1, for geophysical flows, the surface velocity field can be inferred from the see surface height (SSH): strong gradient of SSH are related to strong jets. The Gulf stream appears as a robust eastward jet (in presence of meanders), flowing along the east coast of north America and then detaching the coast to enter the Atlantic ocean, with an extension $L \sim 2000$ *km*. The jet is surrounded by numerous westward propagating rings of typical diameters $L \sim 200$ *km*. Typical velocities and widths of both the Gulf Stream and its rings jets are respectively 1 $m.s^{-1}$ and 50 *km*, corresponding to a Reynolds number $Re \sim 10^{11}$. Such rings can be understood as local statistical equilibria, and strong eastward jets like the Gulf Stream and obtained as marginally unstable statistical equilibria in simple academic models (see subsections 4.4-5).

5. Are the Gulf-Stream and the Kuroshio currents close to statistical equilibria?

In section 4.4, we have discussed applications of statistical mechanics ideas to the description of ocean vortices, like the Gulf-Stream rings. We have also mentioned that statistical equilibria, starting from the Van-Der-Waals Cahn Hilliard functional (86), may model physical situations where strong jets, with a width of order R, bound domains of nearly constant potential vorticity.

This is actually the case of the Gulf Stream in the North Atlantic ocean or of the Kuroshio extension in the North Pacific ocean. This can be inferred from observations, or this is observed

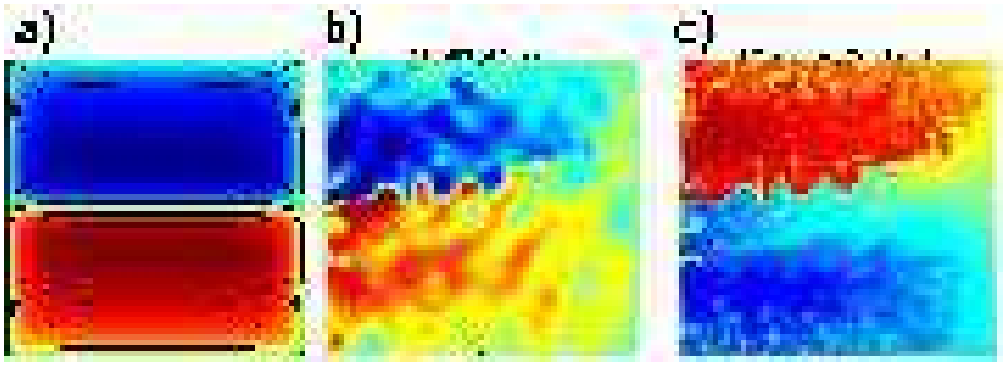

Figure 20: b) and c) represent respectively a snapshot of the streamfunction and potential vorticity (red: positive values; blue: negative values) in the upper layer of a three layers quasi-geostrophic model in a closed domain, representing a mid-latitude oceanic basin, in presence of wind forcing. Both figures are taken from numerical simulations [1], see also [7]. a) Streamfunction predicted by statistical mechanics, see section 5 on the preceding page for further details. Even in an out-equilibrium situation like this one, the equilibrium statistical mechanics predicts correctly the overall qualitative structure of the flow.

in high resolution numerical simulations of idealized wind driven mid-latitude ocean, see for instance figure 20 (and ref. [7] for more details).

It is thus very tempting to interpret the Gulf Stream and the Kuroshio as interfaces between two phases corresponding to different levels of potential vorticity mixing, just like the Great Red Spot and ocean rings in the previous section. The aim of this chapter is to answer this natural question: are the Gulf-Stream and Kuroshio currents close to statistical equilibria?

More precisely, we address the following problem: is it possible to find a class of statistical equilibria with a strong mid-basin eastward jet similar to the Gulf Stream of the Kuroshio, in a closed domain? The 1-1/2 layer quasi-geostrophic model (see section 2.1.3) is the simplest model taking into account density stratification for mid-latitude ocean circulation (in the upper first $1000\,m$) [157, 195]. We analyze therefore the class of statistical equilibria which are minima of the Van-Der-Waals Cahn Hilliard variational problem (86), as explained in section 4.2. We ask whether it exists solutions to

$$\left\{ \begin{array}{c} F = \min\{\mathscr{F}[\phi] \mid A[\phi] = -B\} \\ \text{with } \mathscr{F} = \int_{\mathscr{D}} d\mathbf{r} \left[\frac{R^2(\nabla\phi)^2}{2} + f(\phi) - R\tilde{\beta}_c y\phi \right] \text{ and } \mathscr{A}[\phi] = \int_{\mathscr{D}} d\mathbf{r}\,\phi \end{array} \right. \tag{89}$$

in a bounded domain (let say a rectangular basin) with strong mid-basin eastward jets. At the domain boundary, we fix $\phi = 0$ (which using $\phi = R^2\psi$, and (10) turns out to be an impermeability condition). We note that the understanding of the following discussion requires the reading of sections 4.1 to 4.3.

The term $R\tilde{\beta}_c y$ is an effective topography including the beta effect and the effect of a deep zonal flow (see section 2.1.3). Its significance and effects will be discussed in section 5.2. As in the previous section, we consider the limit $R \ll L$ and assume f be a double well function.

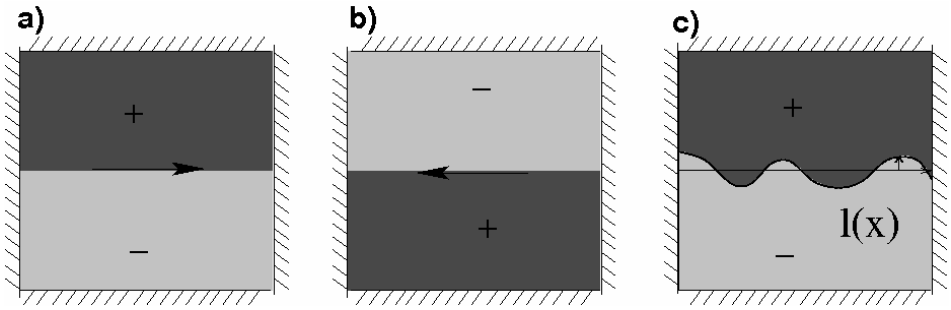

Figure 21: a) Eastward jet: the interface is zonal, with positive potential vorticity $q = u$ on the northern part of the domain. b) Westward jet: the interface is zonal, with negative potential vorticity $q = -u$ in the northern part of the domain. c) Perturbation of the interface for the eastward jet configuration, to determine when this solution is a local equilibrium (see subsection 5.2). Without topography, both (a) and (b) are entropy maxima. With positive beta effect (b) is the global entropy maximum; with negative beta effect (a) is the global entropy maximum.

As discussed in chapter 4.1, with these hypothesis, there is phase separation in two subdomains with two different levels of potential vorticity mixing. These domains are bounded by interfaces (jets) of width R. In view of the applications to mid-basin ocean jets, we assume that the area A_+ occupied by the value $\phi = u$ is half of the total area of the domain (this amounts to fix the total potential vorticity constraint Γ_1 (2.2.2)). The question is to determine the position and shape of this interface. The main difference with the cases treated in subsection 4.1 is due to the effect of boundaries and of the linear effective topography $R\tilde{\beta}_c y$.

5.1. Eastward jets are statistical equilibria of the quasi-geostrophic model without topography

The value $\phi = \pm u$ for the two coexisting phases is not compatible with the boundary condition $\phi = 0$. As a consequence, there exists a boundary jet (or boundary layer) in order to match a uniform phase $\phi = \pm u$ to the boundary conditions. Just like inner jets, treated in section 4, these jets contribute to the first order free energy, which gives the jet position and shape. We now treat the effect of boundary layer for the case $h = 0$ ($\widetilde{\beta}_c = 0$ in this case). As explained in section 4.1.3, the jet free energy is the only contribution to the total free energy.

We first quantify the unit length free energy, F_b, for the boundary jets. Following the reasoning of section 4.1.3, we have

$$F_b = \min \left\{ \int d\zeta \left[\frac{R^2}{2} \frac{d^2\phi}{d\zeta^2} + f(\phi) \right] \right\}.$$

This expression is the same as (81), the only difference is the different boundary conditions: it was $\phi \to_{\zeta \to +\infty} u$ and $\phi \to_{\zeta \to -\infty} -u$, it is now $\phi \to_{\zeta \to +\infty} u$ and $\phi(0) = 0$. Because f is even, one easily see that a boundary jet is nothing else than half of a interior domain jet. Then

$$F_b = \frac{1}{2} F_{int} = \frac{e}{2} R,$$

where F_{int} and e are the unit length free energies for the interior jets, as defined in section 4.1.3. By symmetry, a boundary jet matching the value $\phi = -u$ to $\phi = 0$ gives the same contribution[20]. Finally, the first order free energy is given by

$$\mathscr{F} = eR\left(L + \frac{L_b}{2}\right),$$

where L_b is the boundary length. Because the boundary length L_b is a fixed quantity, the free energy minimization amounts to the minimization of the interior jet length. The interior jet position and shape is thus given by the minimization of the interior jet length with fixed area A_+. We recall that the solutions to this variational problem are interior jets which are either straight lines or circles (see section 4.1.3).

In order to simplify the discussion, we consider the case of a rectangular domain of aspect ratio $\tau = L_x/L_y$. Generalization to an arbitrary closed domain could also be discussed. We recall that the two phases occupy the same area $A_+ = A_- = \frac{1}{2}L_xL_y$. We consider three possible interface configurations with straight or circular jets:

1. the zonal jet configuration (jet along the x axis) with $L = L_x$,
2. the meridional jet configuration (jet along the y axis with $L = L_y$,
3. and an interior circular vortex, with $L = 2\sqrt{\pi A_+} = \sqrt{2\pi L_xL_y}$.

The minimization of L for these three configurations shows that the zonal jet is a global minimum if and only if $\tau < 1$. The criterion for the zonal jet to be a global RSM equilibrium state is then $L_x < L_y$. We have thus found zonal jet as statistical equilibria in the case $h = 0$.

An essential point is that both the Kuroshio and the Gulf Stream are flowing eastward (from west to east). From the relation $\mathbf{v} = \mathbf{e}_z \times \nabla\psi$ (10), we see that the jet flows eastward ($v_x > 0$) when $\partial_y\psi < 0$. Recalling that $\phi = R^2\psi$, the previous condition means that the negative phase $\phi = -u$ has to be on the northern part of the domain, and the phase $\phi = u$ on the southern part. From (9), we see that this corresponds to a phase with positive potential vorticity $q = u$ on the northern sub-domains and negative potential vorticity $q = -u$ on the southern sub-domain, as illustrated in the panel (a) of figure (21).

Looking at the variational problems (89), it is clear that in the case $\widetilde{\beta}_c = 0$, the minimization of ϕ is invariant over the symmetry$\phi \to -\phi$. Then solutions with eastward or westward jets are completely equivalent. Actually there are two equivalent solutions for each of the case 1, 2 and 3 above. However, adding a beta effect $h = R\widetilde{\beta}_c y$ will break this symmetry. This is the subject of next section.

We conclude that in a closed domain with aspect ratio $L_x/L_y < 1$, without topography, equilibrium states exist with an eastward jet at the center of the domain, recirculating jets along the domain boundary and a quiescent interior. For $L_x/L_y > 1$, these solutions become metastable

[20] We have treated the symmetric case when f is even. The asymmetric case could be also easily treated

states (local entropy maximum). This equilibrium is degenerated, since the symmetric solution with a westward jet is always possible.

5.2. Addition of a topography

For ocean dynamics, the beta effect plays a crucial role. Let us now consider the case where the topography is $\eta_d = \beta_c y + \frac{\psi_d}{R^2}$. The first contribution comes from the beta-effect (the variation of the Coriolis parameter with latitude). The second contribution is a permanent deviation of the interface between the upper layer and the lower layer. For simplicity, we consider the case where this permanent interface elevation is driven by a constant zonal flow in the lower layer: $\psi_d = -U_d y$, which gives $\eta_d = \left(\beta_c - \frac{U_d}{R^2}\right) y = R\widetilde{\beta}_c y$. Then the combined effect of a deep constant zonal flow and of the variation of the Coriolis parameter with latitude is an effective linear beta effect.

In the definition of $\widetilde{\beta}_c$ above, we use a rescaling with R. This choice is considered in order to treat the case where the contribution of the effective beta effect appears at the same order as the jet length contribution. This allows to easily study how the beta effect breaks the symmetry $\phi \to -\phi$ between eastward and westward jets. Following the arguments of section 4.3.1, we minimize

$$\mathscr{F} = RH_0 + R\left(eL - 2u\int_{A_+} \mathrm{d}\mathbf{r}\,\tilde{\beta}_c y\right), \tag{90}$$

(see equation (87)), with a fixed area A_+. The jet position is a critical point of this functional: $e/r - 2u\tilde{\beta}_c y_{jet} = \alpha$ (see equation (88)), where α is a Lagrange parameter and y_{jet} the latitude of the jet. We conclude that zonal jets (curves with constant y_{jet} and $r = +\infty$) are solutions to this equation for $\alpha = -2uR\tilde{\beta}_c y_{jet}$. Eastward and westward jets described in the previous section are still critical points of entropy maximization.

5.2.1. With a negative effective beta effect, eastward jets are statistical equilibria

We first consider the case $\widetilde{\beta}_c < 0$. This occurs when the zonal flow in the lower layer is eastward and sufficiently strong ($U_d > R^2\beta_c$). If we compute the first order free energy (90) for both the eastward and the westward mid-latitude jet, it is easy to see that in order to minimize $\mathscr{F}$, the domain A_+ has to be located at the lower latitudes: taking $y = 0$ at the interface, the term $-2u\int_{A_+} d^2\mathbf{r}\,\tilde{\beta}_c y = u\tilde{\beta}_c L_x L_y/4$ gives a negative contribution when the phase with $\phi = u$ (and $q = -u$) is on the southern part of the domain ($A_+ = (0, L_x) \times (-\frac{L_y}{2}, 0)$). This term would give the opposite contribution if the phase $\phi = u$ would occupy the northern part of the domain. Thus the statistical equilibria is the one with negative streamfunction ϕ (corresponding to positive potential vorticity q) on the northern part of the domain. As discussed in the end of section 5.1 and illustrated on figure 21, panel (b), this is the case of an eastward jet.

Thus, we conclude that taking into account an effective negative beta-effect term at first order breaks the westward-eastward jet symmetry. When $\widetilde{\beta}_c < 0$, statistical equilibria are flows with mid-basin eastward jets.

5.2.2. With a positive effective beta effect, westward jets are statistical equilibria

Let us now assume that the effective beta coefficient is positive. This is the case when $U_d < R^2\beta_c$, i.e. when the lower layer is either flowing westward, or eastward with a sufficiently low velocity. The argument of the previous paragraph can then be used to show that the statistical equilibrium is the solution presenting a westward jet.

5.2.3. With a sufficiently small effective beta coefficient, eastward jets are local statistical equilibria

We have just proved that mid-basin eastward jets are not global equilibria in the case of positive effective beta effect. They are however critical points of entropy maximization. They still could be local entropy maxima. We now consider this question: are mid-basin strong eastward jets local equilibria for a positive effective beta coefficient? In order to answer, we perturb the interface between the two phases, while keeping constant the area they occupy, and compute the free energy perturbation.

The unperturbed interface equation is $y = 0$, the perturbed one is $y = l(x)$, see figure 21. Qualitatively, the contributions to the free energy $\mathscr{F}$ (90), of the jet on one hand and of the topography on the other hand, are competing with each other. Any perturbation increases the jet length $L = \int dx\ \sqrt{1+\left(\frac{dl}{dx}\right)^2}$ and then increases the second term in equation (90) by $\delta\mathscr{F}_1 = Re\int dx\,(dl/dx)^2$. Any perturbation decreases the third term in equation (90) by $\delta\mathscr{F}_2 = -2Ru\tilde{\beta}_c\int dx\ l^2$.

We suppose that $l = l_k \sin\frac{k\pi}{L_x}x$ where $k \geq 1$ is an integer. Then

$$\delta\mathscr{F} = \delta\mathscr{F}_1 + \delta\mathscr{F}_2 = -2u\tilde{\beta}_c + e\left(\frac{k\pi}{L_x}\right)^2.$$

Because we minimize $\mathscr{F}$, we want to know if any perturbation leads to positive variations of the free energy. The most unfavorable case is for the smallest value of k^2, i.e. $k^2 = 1$. Then we conclude that eastward jets are local entropy maxima when

$$\widetilde{\beta}_c < \widetilde{\beta}_{c,cr} = \frac{1}{2}\frac{e}{u}\frac{\pi^2}{L_x^2}\ .$$

We thus conclude that eastward zonal jets are local equilibria for sufficiently small values of $\widetilde{\beta}_c$.

The previous result can also be interpreted in terms of the domain geometry, for a fixed value of $\widetilde{\beta}_c$. Eastward jets are local entropy maxima if

$$L_x < L_{x,cr} = \pi\sqrt{\frac{e}{2u\widetilde{\beta}_{c,cr}}}.$$

Let us evaluate an order of magnitude for $L_{x,cr}$ for the ocean case, first assuming there is no deep flow ($U_d = 0$). Then $R\tilde{\beta}_c$ is the real coefficient of the beta plane approximation. Remembering that a typical velocity of the jet is $U \sim uR$, and using $e \sim u^2$ (see [198] for more details). Then

$L_{x,cr} \approx \pi\sqrt{\frac{U}{\beta_{c,cr}}}$. This length is proportional to the Rhine's' scale of geophysical fluid dynamics [195]. For jets like the Gulf Stream, typical jet velocity is 1 $m.s^{-1}$ and $\beta_c \sim 10^{-11}$ $m^{-1}.s^{-1}$ at mid-latitude. Then $L_{cr} \sim 300$ km. This length is much smaller than the typical zonal extension of the inertial part of the Kuroshio or Gulf Stream currents. We thus conclude that in a model with a quiescent lower layer and the beta plane approximation, currents like the Gulf Stream or the Kuroshio are not statistical equilibria, and they are not neither close to local statistical equilibria.

Taking the oceanic parameters ($\beta_c = 10^{-11}$ $m^{-1}s^{-1}$, $R \sim 50$ km), we can estimate the critical eastward velocity in the lower layer $U_{d,cr} = 5$ cm s^{-1} above which the strong eastward jet in the upper layer is a statistical equilibria. It is difficult to make further conclusions about real mid-latitude jets; we conjecture that their are marginally stable. This hypothesis of marginal stability is in agreement with the observed instabilities of the Gulf-Stream and Kuroshio current, but overall stability of the global structure of the flow. A further discussion of these points will be the object of future works.

In all of the preceding considerations, we have assumed that the term $R\widetilde{\beta}_c$ was of order R in dimensionless units. This is self-consistent to compute the unstable states. To show that a solution is effectively a statistical equilibria when $R\widetilde{\beta}_c$ in of order one, one has to use much less straightforward considerations than in the preceding paragraphs, but the conclusions would be exactly the same.

Notice that the description of an inertial solution presenting an eastward jet in a closed domain constitutes in itself an important step toward theoretical studies of oceanic mid-latitude jets, beside the application to statistical mechanics. It can be for instance the starting point of stability studies, by applying classical methods to describe the evolution of perturbations around this mean state.

5.3. Conclusion

We have shown that when there is a sufficiently strong eastward flow in the deep layer (i.e. when $U_d > U_{d,cr}$ with $U_{d,cr} = R^2\beta_{c,cr}$), ocean mid-latitude eastward jets are statistical equilibria, even in presence of a beta plane. When the flow in the deep layer is lower than the critical value $U_{d,cr}$ but still almost compensate the beta plane ($0 < \beta_c - \frac{U_d}{R^2} < \frac{1}{2}\frac{e}{u}\frac{\pi^2}{L_x^2}R$), the solutions with the eastward jets are local equilibria (metastable states). When $\beta_c - \frac{U_d}{R^2} > \frac{1}{2}\frac{e}{u}\frac{\pi^2}{L_x^2}R$ the solution with an eastward jet are unstable.

We have also concluded that the inertial part of the real Gulf-Stream or of the Kuroshio extension are likely to be marginally stable from a statistical mechanics point of view.

The statistical equilibria that we have described in this section have a flow structure that differs notably from the celebrated Fofonoff solution [80].

The Fofonoff solution is a stationary state of the quasi-geostrophic equations (8-9-10) on a beta plane ($\eta_d = \beta_c y$) obtained by assuming a linear relationship between potential vorticity and streamfunction ($q = a\psi$), in the limit $a + R^{-2} \gg L^{-2}$, where L is the domain size. In this limit,

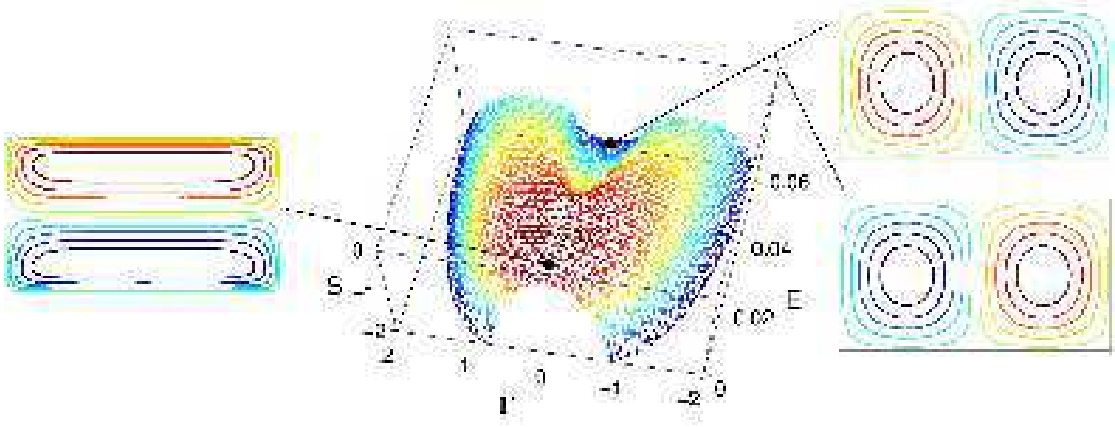

Figure 22: Phase diagrams of RSM statistical equilibrium states of the 1.5 layer quasi-geostrophic model, characterized by a linear $q-\psi$ relationship, in a rectangular domain elongated in the x direction. $S(E,\Gamma)$ is the equilibrium entropy, E is the energy and Γ the circulation. Low energy states are the celebrated Fofonoff solutions [80], presenting a weak westward flow in the domain bulk. High energy states have a very different structure (a dipole). Please note that at high energy the entropy is non-concave. This is related to ensemble inequivalence (see 3.3 page 50), which explain why such states were not computed in previous studies. The method to compute explicitly this phase diagram is the same as the one presented in subsection 3.5 page 52. See [197] for more details.

the Laplacian term in (9) is negligible in the domain bulk. Then $\psi \approx \beta_c/(a+R^{-2})y$, which corresponds to a weak westward flow, as illustrated figure 22. Strong recirculating eastward jets occur at northern and southern boundaries, where the Laplacian term is no more negligible.

The original work of Fofonoff was carried independently from statistical mechanics considerations. The linear $q-\psi$ relationship was chosen as a starting point to compute analytically the flow structure. Because both the Salmon–Holloway–Hendershott statistical theory [172] (which is the extension of the Kraichnan energy-enstrophy theory in presence of topography) and the Bretherton–Haidvoguel minimum enstrophy principle [28] did predict a linear relationship between vorticity and streamfunction, it has been argued that statistical equilibrium theory predicts the emergence of the classical Fofonoff flows, which had effectively been reported in numerical simulations of freely decaying barotropic flows on a beta plane for some range of parameters [200].

We have seen in the last paragraph of subsection 2.3.4 page 34 and at the end of subsection 3.1.3 page 47 that all those theories are particular cases of the RSM statistical mechanics theory. On the one hand it has been actually proven that the classical Fofonoff solutions are indeed RSM statistical equilibria in the limit of low energies [197]. On the other hand, as illustrated by the results of this section, there exists a much richer variety of RSM equilibrium states than the sole classical Fofonoff solution. Even in the case of a linear $q-\psi$ relation, high energy statistical equilibrium states are characterized by a flow structure that differs notably from the original Fofonoff solution , as illustrated figure 22. These high energy states correpond actually to the RSM equilibrium states of the Euler equation, originally computed by [47]. The transition from classical Fofonoff solutions to those high energy states has been related the the occurrence of ensemble inequivalence [197]. This explains also why such high energy states have not been

reported in earlier studies, where computations were always performed in the (unconstrained) canonical ensemble (see the discussion at the end of subsection 2.3.4 page 34).

The early work of Fofonoff [80] and the equilibrium statistical mechanics of geophysical flows presented in this review are often referred to as the inertial approach of oceanic circulation, meaning that the effect of the forcing and the dissipation are neglected.

Ocean dynamics is actually much influenced by the forcing and the dissipation. For instance the mass flux of a current like the Gulf Stream is mainly explained by the Sverdrup transport. Indeed in the bulk of the ocean, a balance between wind stress forcing and beta effect (the Sverdrup balance) lead to a meridional global mass flux (for instance toward the south on the southern part of the Atlantic ocean. This fluxes is then oriented westward and explain a large part of the Gulf Stream mass transport. This mechanism is at the base of the classical theories for ocean dynamics [157]. Because it is not an conservative process, the inertial approach does not take this essential aspect into account. Conversely, the traditional theory explains the Sverdrup transport, the westward intensification and boundary current, but gives no clear explanation of the structure of the inertial part of the current: the strongly eastward jets.

Each of the classical ocean theory [157] or of the equilibrium statistical mechanics point of view give an incomplete picture, and complement each other. Another interesting approach consider the dynamics from the point of view of bifurcation theory when the Reynolds number (or some other controlled parameters) are increased. These three types of approaches seem complimentary and we hope they may be combined in the future in a more comprehensive non-equilibrium theory.

6. Non-equilibrium statistical mechanics of two-dimensional and geophysical flows

In the previous chapters, we dealt with equilibrium statistical mechanics for two-dimensional and geophysical flows. Assuming ergodicity, equilibrium statistical mechanics describes long time outcome of the evolution of the 2D Euler equations or the quasi-geostrophic equations. Ergodicity was then our only assumption, and all the presented results can be derived rigorously.

In laboratory experiments or geophysical situations, most flows are however subjected to dissipative processes. Very often such flows are in statistically steady states, where forcing balance dissipation on average, and where fluxes of energy and other conserved quantities characterize the system. This is a situation of Non Equilibrium Steady States (NESS), following the terminology of statistical mechanics.

In many situations of interest the action of forces and dissipation mechanisms are weak compared to the inertial (Hamiltonian) part of the dynamics. For instance, the turnover time scale can be small compared to forcing time scale (i.e. a typical time needed to create the structure starting from rest) or to a dissipation time scale (i.e. a typical time needed to dissipate the structure if the force would be switched off). In such situations of weak forces and dissipation, at leading order one recovers the inertial dynamics: the Euler equations or the quasi-geostrophic dynamics. Then a natural question is to know whether we are close or not to some statistical equilibria, and if statistical equilibrium could learn us something for these non-equilibrium situations.

A further objective is to make an non-equilibrium theory that could predict the invariant measure and to predict the properties of this NESS directly from the dynamics, for instance using a kinetic theory approach.

In order to discuss these issues more precisely, we consider in the following the 2D Navier-Stokes equations with viscous dissipation ν, linear friction α and stochastic forces η:

$$\partial_t \omega + (\mathbf{v}\cdot\nabla)\omega = \nu\Delta\omega - \alpha\omega + \sqrt{\sigma}\eta(t,\mathbf{x}); \tag{91}$$

where σ is the average energy injection rate by the stochastic force η (η will be defined precisely latter on; η is actually the curl of a force, but without ambiguity we call it a stochastic force in the following). We recall that $\omega = \Delta\psi$ is the vorticity, and $\mathbf{v} = \mathbf{e}_z \times \nabla\psi$ the two-dimensional velocity field.

This is the most simple model for discussing the statistics of the large scales of 2D and geophysical flows, in a statistically steady regime. The type of reasoning presented in the following can be easily generalized to other models.

In the case $\alpha = 0$, many interesting mathematical results have been recently obtained for the stochastic Navier-Stokes equations (91): the existence of an invariant measure, its properties in the Euler limit $\nu \to 0$, the validity of the law of large numbers, central limit theorems, ergodicity (see [116, 114, 115, 29, 203, 134] and references therein). We do not describe these results, but only cite them when they are related to the more physical studies bellow.

This chapter is organized as follows. In section 6.1 we explain that two different regimes exist for the NESS of the 2D Navier-Stokes equations, depending on the values of the forcing parameter σ and the linear friction parameter α. The first one is the classical regime of the self

similar direct cascade of enstrophy and inverse cascade of energy, first predicted by Kraichnan and studied thoroughly during the last three decades. The second one is the regime dominated by the largest scales of the flow. This turbulent large scale regime is the interesting one as soon as one is interested in predicting the statistics of the largest scales of geophysical flows. We explain that it is natural to guess that this regime has some relations with equilibrium statistical mechanics of the Euler equations, even if the microcanonical measure does not describe its statistics.

In section 6.4, we explain that we can predict many properties of this turbulent large scale regime from the equilibrium statistical mechanics, for instance the topology of the average velocity field. For instance, we show that we can predict non-equilibrium phase transitions: situations of bistability between two different topologies of the velocity fields. We also explain the strong limitations to the use of equilibrium theory for such non-equilibrium situations.

In section 6.5, we explain how a kinetic theory could be developed to describe the turbulent large scales of turbulent flows in a non-equilibrium steady state. We explain what would be the minimal requirements for such a theory, and the associated difficulties. In section 6.6 we describe recent progresses in this direction.

6.1. Non-Equilibrium Steady States (NESS) for forced and dissipated turbulence

In this subsection, we show that depending on the values of the friction parameter α and the forcing parameter σ, there are two main regimes for the stochastic Navier-Stokes equations (91). We begin by some general considerations on the balance of energy and other conserved quantities.

6.1.1. Stochastic forces

We first define the stochastic force $\eta(t,\mathbf{x})$. It is a sum of random noises:

$$\eta(t,\mathbf{x}) = \sum_k f_k \mathbf{e}_k(x,y)\,\eta_k(t),$$

where $\{e_k\}$ is the orthonormal basis of the Laplacian eigenvectors with Dirichlet boundary conditions for the domain $\mathscr{D}$: $-\Delta \mathbf{e}_k = \lambda_k \mathbf{e}_k$ with $\int_{\mathscr{D}} d\mathbf{r} \mathbf{e}_k \mathbf{e}_{k'} = \delta_{kk'}$. For a doubly periodic domain of size (L_x,L_y) we have $\mathbf{k} = 2\pi(n_x/L_x, n_y/L_y)$ with integers n_x and n_y, $e_{\mathbf{k}}(\mathbf{r}) = \exp(i\mathbf{k}.\mathbf{r})/L_xL_y$ and $\lambda_k = |\mathbf{k}|^2$. The terms η_k are independent white noises $\langle \eta_k(t)\,\eta_{k'}(t)\rangle = \delta_{kk'}\delta(t-t')$, f_k is the force spectrum and σ is the force amplitude that will be related to the energy and enstrophy injection rate later on. In all the following we assume that f_k decays rapidly for large k: the stochastic force is white in time and smooth in space.

We rewrite (91) in the usual stochastic form:

$$d\omega = [-(\mathbf{u}\cdot\nabla)\omega + \nu\Delta\omega - \alpha\omega]\,dt + \sqrt{\sigma}\sum_k f_k \mathbf{e}_k dW_k, \tag{92}$$

where dW_k are the Wiener processes associated with η_k.

6.1.2. Energy balance

For the deterministic dynamics (i.e. without stochastic forcing, $\sigma = 0$), the energy balance reads

$$\frac{dE}{dt} = -\nu Z - 2\alpha E,$$

where $E = \frac{1}{2}\int_{\mathscr{D}} \mathrm{d}\mathbf{r}\, \mathbf{v}^2$ is the energy (3) and $Z = \int_{\mathscr{D}} \mathrm{d}\mathbf{r}\, \omega^2$ is the enstrophy (19). For the stochastic dynamics, application of the Ito formula to the energy evolution, starting from (92), leads to

$$\frac{d\langle E\rangle}{dt} = -\nu\langle Z\rangle - 2\alpha\langle E_c\rangle + \sigma, \tag{93}$$

where the brackets are averages over the white noises realizations and where we assume

$$B_0 \equiv \frac{1}{2}\sum_k \frac{|f_k|^2}{\lambda_k} = 1. \tag{94}$$

We see from (93) that σ is the average energy injection rate; the assumption $B_0 = 1$ is just equivalent to defining σ. The energy E is on units of $\mathrm{m}^4\,\mathrm{s}^{-2}$, so the units for σ are $\mathrm{m}^4\,\mathrm{s}^{-3}$ and the units for f_k are m^{-1}.

Similar balance relations can be easily derived for all the other conserved quantities. We do not discuss these relations here as we will not need them in the following. More details can be found in [114] and [143].

6.2. First regime: the Kraichnan self-similar cascades

We first consider the case where the force spectrum is peaked around a given wave number k_f. Following Kolmogorov type of reasoning, if α and ν are small enough, it is then possible to define inertial ranges in which the effects of forcing and dissipation will be negligible. Such inertial ranges will then be characterized by fluxes of conserved quantities, for instance energy and enstrophy. When the fluxes are dominated by dynamical processes which are local in Fourier space, this is called a cascade regime. Such cascades, in two-dimensional turbulence, have first been studied by Kraichnan using ideas similar to Kolmogorov ideas for 3D turbulence. We give here a very rapid account, mainly based on dimensional arguments. More details can be found in [113] and in more recent reviews or lectures. Interesting recent results in this domain include study of statistics of zero vorticity lines in relation with the stochastic Loewner equation (SLE) [8] and precise conditions for locality of turbulent cascades with applications also to two-dimensional turbulence **[73, 74, 3]**.

The system is forced at wave number k_f with an energy injection rate per unit surface ε_f. Following the notations of the previous subsection, we have $\varepsilon = \sigma/L^2$. This corresponds to an enstrophy production rate $\eta \sim k_f^2\varepsilon$. We suppose that the system has reached a statistically steady state and that the energy is limited to scales k^{-1} much smaller that the domain size L. A more precise statement of this hypothesis, and a condition for its validity will be given at the end of this section. In the following of this section, we assume cascade regimes (for inertial scales

$k \gg k_f$ and $k \ll k_f$, we assume constant fluxes of conserved quantities due to local dynamical processes in Fourier space).

In the limit where the large scale separation $Lk_f \gg 1$, it is then relevant to write the total energy per unit surface $E_s = E/L^2$ on the form of a continuous spectrum: $E_s = \int E(k)dk$ (see section 2.3.2 for the definition of $E(k)$). We consider the energy fluxes at scale k (the energy going from modes with wave numbers larger than k to wave numbers smaller than k, for a precise definition see [83]). One could imagine a situation with both an upscale energy flux ($k < k_f$) and a downscale one ($k > k_f$), both of the order of ε. However, at small scale (large k), this would imply an enstrophy flux of order εk^2. But because $\varepsilon k^2 \gg \varepsilon k_f^2 \sim \eta$, this would contradict the hypothesis of a steady regime, since there would be much more enstrophy going downscale than the enstrophy injected. We conclude that the energy injected at k_f goes mostly toward large scales, at a fixed rate ε. Using a similar argument where the energy and enstrophy play a reverse role, we conclude that in the limit or large scale separation $Lk_f \gg 1$, enstrophy injected at scale k_f flows mostly toward small scales at a rate η.

We thus conclude that for statistically steady states, energy flows mainly upscale and enstrophy mainly downscale; more precisely in the limit of infinite inertial ranges all the energy flows upscale and all enstrophy downscale. In section 2.3.2, using Fjortoft argument, we obtained a qualitatively similar result for the dynamics of decaying turbulence. In sections 2.3.4 and 2.3.5 we explained that for the Euler equation, statistical mechanics predicts that all energy is concentrated in the largest scale and the all the enstrophy or other invariant excess (a precise meaning being given by the entropy) flows towards smaller and smaller scales. We see that these three precise results, for three different situations, give a precise meaning to the statement that energy goes towards large scales and enstrophy towards small scales in two dimensional turbulence.

By using a dimensional analysis, Kraichnan gave a prediction for the slope of the energy spectrum $E_s(k)$ in the inertial ranges, in the cascade regimes. Let us first consider the inertial range for scales above the injection scale ($k < k_f$). This is the inverse energy cascade, as energy goes upscale in this region, with a given flux ε (with unit $m^2.s^{-3}$), and enstrophy flux is negligible. Because of the locality hypothesis, at scale k^{-1} (unit L), the energy spectrum $E_s(k)$ (unit $m^3.s^{-2}$) can then depend only on ε and k. Dimensional analysis then gives

$$E_s(k) \sim \varepsilon^{2/3} k^{-5/3} \quad \text{for} \quad k \ll k_f \ .$$

Let us now consider the inertial region for scales below the injection scale. This the enstrophy cascade inertial range as the enstrophy goes downscale in this region, with a given flux η (with unit s^{-2}), and the energy flux is negligible. The energy spectrum at scale k^{-1} can then depend only on k and η. Dimensional analysis then gives

$$E_s(k) \sim \eta^{2/3} k^{-3} \quad \text{for} \quad k \gg k_f .$$

Predictions of the self-similar cascade theory have been followed by numerous experimental studies in many different settings over the last three decades (see [8, 9] and references therein),

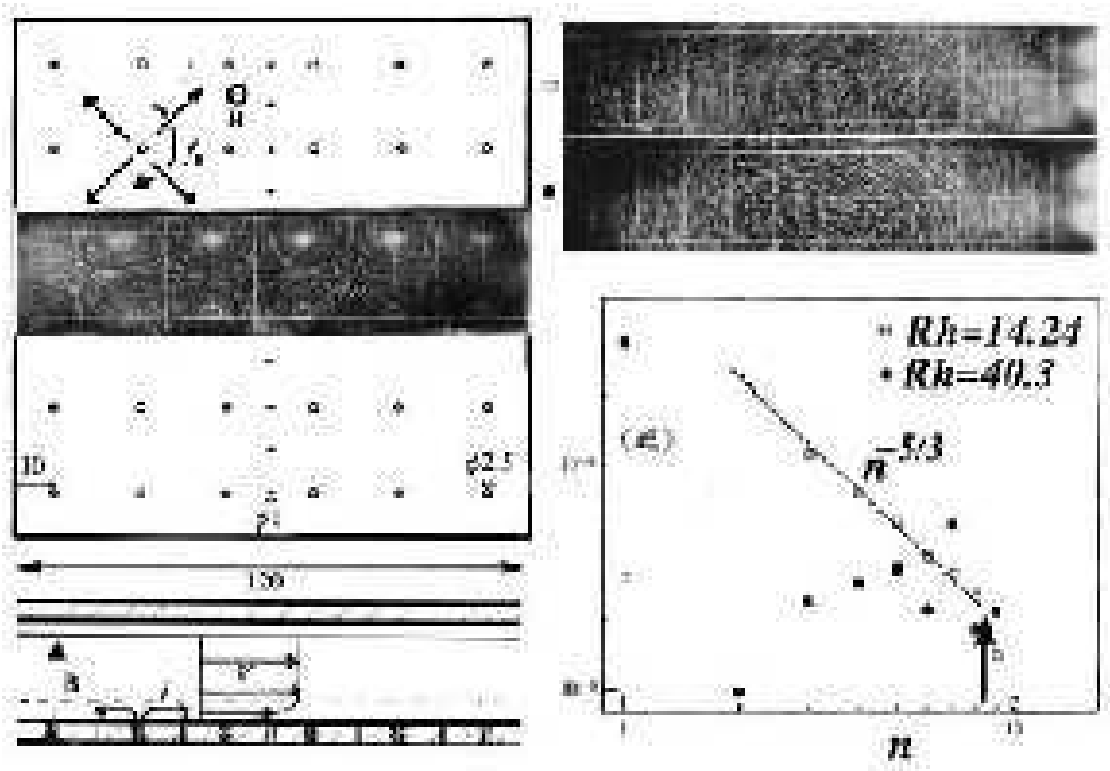

Figure 23: First experimental observation of the inverse energy cascade and the associated $k^{-5/3}$ spectrum, from [179]. The 2D turbulent flow is approached here by a thin layer of mercury and a further ordering from a transverse magnetic field. The flow is forced by an array of electrodes at the bottom, with an oscillating electric field. The parameter Rh is the ratio between inertial to bottom friction terms. At low *Rh* the flow has the structure of the forcing (left panel). At sufficiently high *Rh* the prediction of the self similar cascade theory is well observed (right panel, bottom), and at even higher *Rh*, the break up of the self similar theory along with the organization of the flow into a coherent large scale flow is observed (see right panel above).

and this has led to beautiful experimental results [180, 155]. Among others, there have been measurements of the $-5/3$ slope of the backward energy cascade part of the spectrum [179, 155] (see also figures 23 and 24), as well as of the -3 slope of the forward enstrophy cascade part of the spectrum [154].

In the previous paragraph, we dealt with the inertial range energy spectrum. For large enough scales, the friction $-\alpha\omega$ is no more be negligible and the inertial range hypothesis no more valid. The energy is then be dissipated and no more flow towards larger and larger scales. In experiments, this is visible as a maximum in the energy spectrum $E_s(k)$. Using a classical argument based on dimensional analysis [124] (see also [58] for a critical discussion, or [195]), we predict the scale L_I at which the cascade stops. This scale can depend only on ε ($m^2.s^{-3}$) and on the friction α (s^{-1}):

$$L_I = c\frac{\varepsilon^{1/2}}{\alpha^{3/2}}, \tag{95}$$

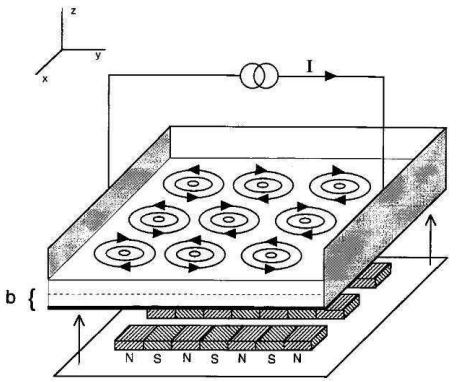

FIG. 1. The experimental set-up.

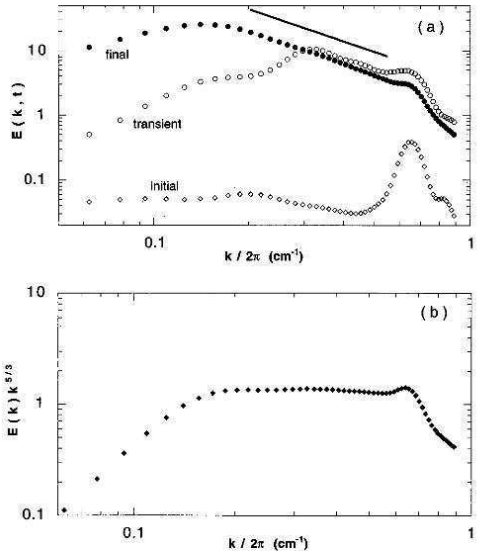

FIG. 2. Energy spectra. (a) Temporal evolution; (b) compensated energy spectrum for the stationary regime.

Figure 24: Another experimental observation of the inverse energy cascade and the associated $k^{-5/3}$, from [155]. The 2D turbulent flow is approached by a thin layer of (light) salty water lying above another thin layer of (dense) salty water. The stable stratification provides a further ordering. The flow is stirred at small scales by the interaction between an horizontal electric field imposed across the experimental cell and a vertical magnetic field imposed by an array of magnets located below the experimental cell. We see on the right panel that predictions of self-similar inverse energy cascade (the $k^{-5/3}$ spectrum) are well observed. Please note also the interesting transient evolution of the energy spectrum.

where c is a non-dimensional constant.

If the dynamics takes place in a finite box of size L, the energy flux towards largest scales can be stopped by the box before it is dissipated by the friction. In such a case the energy pile up at the largest scale. The self-similar hypothesis for the spectrum then break down, and we actually observe that energy fluxes are no more local. The Kraichnan picture then break down. In a finite box, the Kraichnan picture can be valid only if the scale L_I is much smaller than the box size L. Recalling that $\sigma = \varepsilon L^2$, we thus conclude a necessary condition to observe a universal inverse energy cascade is[21]

$$R_\alpha = \sqrt{2}\frac{\sigma^{1/2}}{L^2\alpha^{3/2}} \ll 1. \tag{96}$$

In the opposite case, $R_\alpha \gg 1$, for instance for too strong energy injection or too weak dissipation for a given box size, the energy cascade will not be arrested by friction, but will begin to pile up

[21] The $\sqrt{2}$ is unimportant and is added for convenience in latter computations.

at the largest scales. Then the largest scales self-organize and create coherent vortices and jets. This is the second regime of two dimensional turbulence, to be discussed in the next sections.

6.3. Second regime: the coherent large scale flow

We are now interested in the regime where the flow self organize at the largest scale L. Because the energy will flow towards the largest scales; it is natural to neglect the energy dissipation by viscous effect. We will give a more precise criterion for this to be valid later on. From the energy balance (93), neglecting viscous effect, we have

$$\langle E_c \rangle \simeq \frac{\sigma}{2\alpha}.$$

A typical velocity for the large scale flow is thus $U = \sqrt{\langle E_c \rangle}/L = \frac{1}{L}\sqrt{\frac{\sigma}{2\alpha}}$. A typical time scale for the largest scales (a turnover time) is then $\tau = L/U = L^2\sqrt{\frac{2\alpha}{\sigma}}$. A natural non-dimensional parameter is R_α the ratio of the dissipation time scale $1/\alpha$ over the turnover time scale τ

$$R_\alpha = \sqrt{2}\frac{\sigma^{1/2}}{\alpha^{3/2}L^2}.$$

R_α is indeed a Reynolds number based on the linear friction α and the large scale flow velocities and length scale. We note that the criteria for observing self-organization of the energy at the largest scale (96) is $R_\alpha > 1$, as could have been expected. The limit of large time scale separation, $R_\alpha \gg 1$, is particularly interesting.

It is natural to write non-dimensional dynamical equations using as a length unit the domain size L and as a time unit a typical large scale turnover time $\tau = L^2\sqrt{\frac{2\alpha}{\sigma}}$: $t = \tau t'$ and $(x,y) = L(x',y')$. In these non-dimensional units the dynamical equations are

$$\begin{aligned} &\partial_{t'}\omega' + (\mathbf{u}'\cdot\nabla')\omega' = \tfrac{1}{Re}\Delta'\omega' - \tfrac{1}{R_\alpha}\omega' + \sqrt{\tfrac{2}{R_\alpha}}\eta', \\ &\text{with } \omega' = \Delta'\psi', \end{aligned}$$

where

$$Re = UL/\nu = \sigma^{1/2}/(2\alpha)^{1/2}\nu$$

is the Reynolds number based on the large scale velocity and domain size.

We rewrite the non-dimensional equations dropping the primes and identifying α to $1/R_\alpha$, A to a and ν to $1/Re$. We then obtain

$$\begin{aligned} &\partial_t\omega + (\mathbf{u}\cdot\nabla)\omega = \nu\Delta\omega - \alpha\omega + \sqrt{2\alpha}\eta, \\ &\text{with } \omega = \Delta\psi \end{aligned} \tag{97}$$

and with

$$\eta(t,\mathbf{x}) = \sum_k f_k \mathbf{e}_k(x,y)\,\eta_k(t), \tag{98}$$

where $\{f_k\}$ verifies the constraint (94).

We are interested in the limit where the viscous Reynolds number Re is much larger than the Reynolds number based on the linear friction R_α (meaning that, as far as the large scales are concerned, viscous dissipation is negligible compared to linear friction dissipation). In these non-dimensional units, this condition reads $\nu \ll \alpha$. The regime of large scale self organization is $\alpha \ll 1$. We will thus study the limit $\nu \ll \alpha \ll 1$. We call this the limit of weak forces and dissipation.

In the non-dimensional units, the energy balance (93) is

$$\frac{d\langle E\rangle}{dt} = -2\nu\langle Z\rangle + 2\alpha\left(1-\langle E\rangle\right), \tag{99}$$

giving the stationary balance

$$\langle E\rangle_S = 1 - \frac{\nu}{\alpha}\langle Z\rangle_S \leq 1. \tag{100}$$

We study the dynamics of the coherent large scale flow regime in the next sections.

6.4. Equilibrium statistical mechanics and NESS; prediction of non-equilibrium phase transitions

6.4.1. Are the largest scales of the 2D Navier-Stokes equations close to statistical equilibrium, in the limit of weak forces and dissipation?

We have stressed in the introduction that the Non Equilibrium Steady States (NESS) of the two-dimensional equation break detailed balance, and are the place of fluxes of conserved quantities. The microcanonical measure we built from the Liouville theorem in section 2.2.3 and the equilibrium states we have studied in sections 3, 4 and 5 have no such fluxes. Then the microcanonical measure can not describe the details of the statistics of these NESS. There is however the possibility that the stationary measure be close to the microcanonical equilibrium one in the limit of weak forces and dissipation. We discuss this subtle issue now.

In the limit of weak forces and dissipation, $\nu \ll \alpha \ll 1$, the non-Hamiltonian terms in the stochastic Navier-Stokes equation (97) are vanishingly small. The associated fluxes are also vanishingly small. Because of these small parameters, it is then natural to assume that the flows will be concentrated near to statistical equilibria. As the equilibrium statistical mechanics predicts that the flow is concentrated close to stationary solutions to the 2D Euler equations, a natural conjecture is that in the limit $\nu \ll \alpha \ll 1$, the stationary measure of the stochastic Navier-Stokes equations will be also concentrated close to ensembles of stationary solutions to the 2D Euler equations.

That such a behavior is plausible is actually supported by several theorems. At the dynamical level, the Navier-Stokes equation is actually well behaved in the limit $\nu \ll \alpha \ll 1$: for arbitrary large but finite times, its solutions remain close to the solutions of the Euler equation. This is also true at a statistical level, as recently proved by S. Kuksin for the case $\alpha = 0$ [116]: in the limit $\nu \to 0$ the invariant measure for the stochastic Navier-Stokes equation is described by solutions to the Euler equation. These mathematical theorems support the idea that the invariant

measure will be related to the statistics of Euler dynamics, but they do not prove that the measure is concentrated close to ensemble of stationary solutions to the Euler equations. This remains a challenge for further mathematical results.

We note that the situation is completely different in three dimensional turbulence: as explained in section 2.3.4, equilibrium statistical mechanics of the 3D Euler equations predicts a trivial measure with no flow. Then 3D turbulence is intrinsically a non-equilibrium problem.

As we will see in the following, the conjecture that the invariant measure is concentrated near stationary solutions to the 2D Euler equations is supported both by numerical simulations and experiments. Even in this non-equilibrium context equilibrium statistical mechanics is useful. This is a common situation in statistical physics. For instance in systems with short range interactions driven non-equilibrium, one expects local thermodynamic equilibrium to hold, when the temperature gradient is small enough. In our case, interactions are non local, but in the limit $\nu \ll \alpha \ll 1$, we expect to be close to statistical equilibria. We see this as a zeroth order prediction from equilibrium statistical mechanics in a non-equilibrium situation.

This zeroth order prediction already gives us strong qualitative results about the non-equilibrium dynamics. However the predictive range of these arguments is very limited. For instance the energy distribution and Casimir distributions will be determined by non Hamiltonian processes. They can not be derived from equilibrium processes. As energy and Casimirs are the control parameters of the equilibrium statistical mechanics, we thus conclude that we can guess from equilibrium statistical mechanics that we should be close to some ensemble of stationary solutions to the 2D Euler equations, but that non-equilibrium theory is needed to predict which ones and with which probability.

Moreover as soon as statistics of fluctuations is concerned, it is meaningless to try to make predictions based on equilibrium statistical mechanics, as fluctuations statistics will have to be consistent with non-equilibrium fluxes.

We thus conclude that we expect the stochastic Navier-Stokes invariant measure to be concentrated close to ensemble of statistical equilibria (which are also stationary solutions of the 2D Euler equations). In section 6.4.2 we show that this is confirmed by numerical simulations and experiments. In section 6.4.3, we show that this allows to predict non-equilibrium phase transitions. To know which of the dynamical equilibrium states of the Euler equations is selected by forcing and dissipation, and to predict the fluctuation statistics, one needs an non-equilibrium theory. Possible candidates for such theories will be discussed in section 6.5.

6.4.2. Non-equilibrium flows are close to statistical equilibria

In order to illustrate this discussion, we discuss the case of a doubly periodic domain. Whereas this case has no experimental counterpart, it is extremely interesting from an academic point of view. Indeed because of the absence of boundaries, boundary layers are absent and make the dynamical situation much more simple. Moreover, pseudo-spectral codes allows for much more precise numerical simulations than in any other geometries.

Numerical simulations of the 2D Navier-Stokes equations in a self-similar transient regime,

have been presented in [56], for a square periodic box. This paper also show interesting power laws for the vortex profiles, in this regime. In the following, we concentrate on the statistically steady regime and discuss relation with equilibrium statistical mechanics, and non-equilibrium phase transitions [24, 143].

We have described the equilibrium statistical mechanics of the 2D Euler equations in doubly periodic domains in section 3.5. Figure 8, page 60, shows an equilibrium phase diagram. It shows that two types of flow topologies may be expected: dipole flows or parallel flows, a crucial parameter being the aspect ratio of the domain δ.

Direct numerical simulations of the stochastic Navier-Stokes equations in a square domain $\delta = 1$ exhibit a statistically stationary flow ω with a dipole structure (Fig. 25 **a)**), whereas for $\delta \geq 1.1$, nearly unidirectional flows are observed (Fig. 25 **b)**). This result has been confirmed both for $\alpha = 0$ and $\alpha \neq 0$, and for different values of ν and force spectra. The structure of statistical equilibria is thus observed also for non-equilibrium steady states.

As seen in section 3, statistical equilibria are characterized by a functional relationship $\omega = f(\psi)$ between vorticity and streamfunction. One observes in Fig. 25 a $\omega - \psi$ scatter-plot (light blue or gray), for the two cases of a dipole and a unidirectional flow. In the dipole case, the $\omega - \psi$ relationship is well observed for the larger values of $|\omega|$, which corresponds to the core of the vortices. In the area in between the vortices, the relationship between ω and ψ is more scattered. This correspond to the small scale filaments visible on the vorticity picture (see figure 25).

When we average the vorticity fields and the stream-functions over several turnover times, we obtain the black curves which are very nice $\omega - \psi$ relationships. The $\omega - \psi$ relationship has the same convexity as a sinh (but is different from a sinh), in the dipole case and the same convexity as a tan-h in the unidirectional case. We thus conclude that the observed flows are composed of average quasi-stationary large scale structures, dipoles or unidirectional flows, over which are superimposed fluctuations corresponding to small scale filamentation.

In this sense, the structures are close to equilibrium. We note that the parallel flows seems to be farther from equilibrium than the dipole as the average relationship is a quite thick line. In this case this is due to the presence of intermediate scale vortices as seen on the vorticity picture.

This confirms the usefulness of the predictions of equilibrium statistical mechanics in this non-equilibrium context.

More details about the analysis of the proximity of the flow with stationary solutions to the 2D Euler equation for doubly periodic conditions are given in [24, 143]. A similar conclusion can also be drawn from the numerical results [56], even if the notion of stationary solution to the 2D Euler equation is not used in this work.

In the limit of weak forces and dissipation, it is recognized for a long time that the flow should be close to stationary solutions. For instance, the quasi-geostrophic flows on a beta plane are known to form zonal jets, which are dynamical equilibrium states of the quasi-geostrophic equations, and this have been studied a lot recently. In laboratory experiments, the importance of the formation of large scale coherent structure close to stationary solutions has also been recognized for a long time [179].

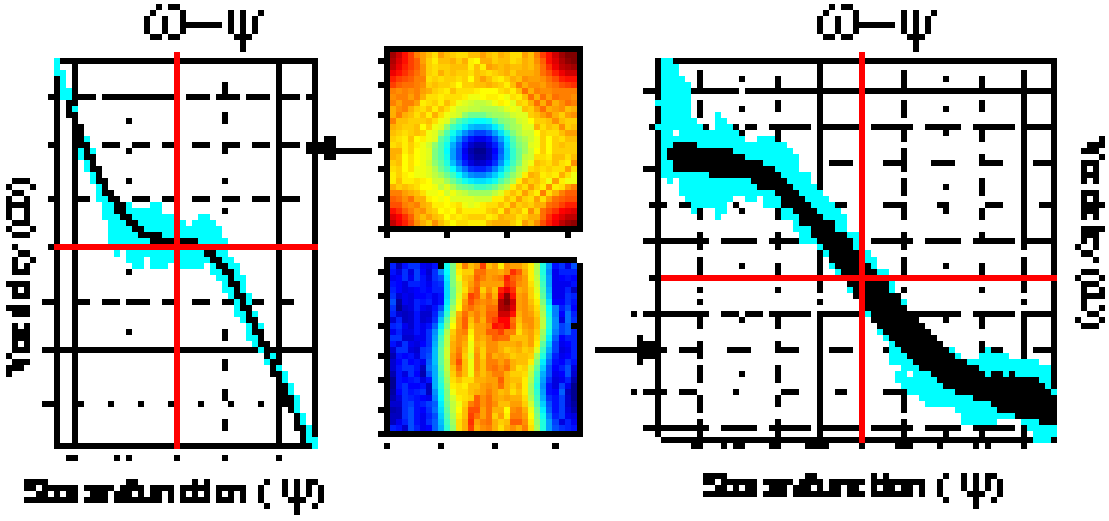

Figure 25: $\omega - \psi$ scatter-plots (cyan) (see color figure on the .pdf version). In black the same after time averaging (averaging windows $1 \ll \tau \ll 1/\nu$, the drift due to translational invariance has been removed). Left: dipole case with $\delta = 1.03$. Right: unidirectional case $\delta = 1.10$.

6.4.3. Non-equilibrium phase transitions in the 2D-Stochastic Navier Stokes equations

Phase transitions are situations where the qualitative properties of the system change drastically. They are thus especially important from a physical and a dynamical point of view.

We have stressed that we are not able to predict the probability of the energy and of the vorticity moments for non-equilibrium situations. However these are the main control parameters of the equilibrium properties. For this reason the use of equilibrium theory for slightly non-equilibrium situations give only qualitative results and does not provide a precise prediction. However phase transitions give such drastic changes that they should also be clearly identified even in non-equilibrium steady states.

We illustrate this idea in the case of 2D Navier-Stokes equations in the doubly periodic domain. Figure 8, page 60 shows that a phase transition occur between dipoles and parallel flows at equilibrium. A natural order parameter is $|z_1|$, where $z_1 = \frac{1}{(2\pi)^2} \int_{\mathscr{D}} \mathbf{dr}\, \omega(x,y) \exp(iy)$. Indeed, for unidirectional flow $\omega = ae_1$, $z_1 = 0$, whereas for a dipole $\omega = a(e_1 + e_2)$, $|z_1| = a$.

We have thus empirically looked for a non-equilibrium phase transition (for the Navier-Stokes equations with random forces) that is the trace of the equilibrium phase transition. A crucial control parameter is the aspect ratio of the domain. We have made numerical simulations for different values of δ. Figure 26 shows $|z_1|$ time series for $\delta = 1.02$ and $\delta = 1.04$. The remarkable observation is the bimodal behavior in this transition range. The switches from $|z_1|$ values close to zero to values of order of 0.6 correspond to genuine transitions between unidirectional and dipole flows. The probability distribution function (PDF) of the complex variable z_1 (Fig. 26) exhibits a circle corresponding to the dipole state (a slow dipole random translation corresponds into to a phase drift for z_1, explaining the circular symmetry). The parallel flow state corresponds to the central peak. As δ increases, one observes less occurrences of the dipole.

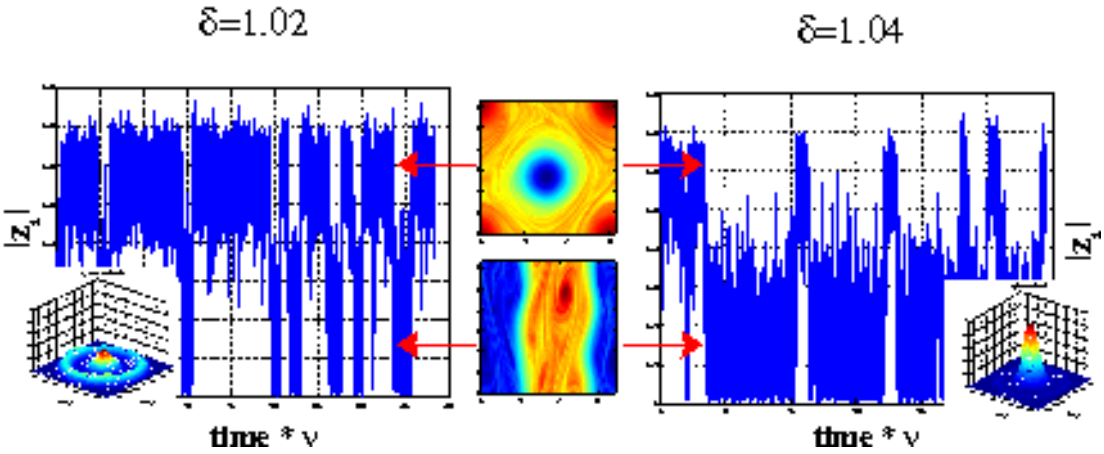

Figure 26: Dynamics of the 2D Navier–Stokes equations with stochastic forces in a doubly periodic domain of aspect ratio δ, in a non-equilibrium phase transition regime. The two main plots are the time series and probability density functions (PDFs) of the modulus of the Fourier component $z_1 = \frac{1}{(2\pi)^2}\int_{\mathscr{D}} \mathbf{dr}\,\omega(x,y)\exp(iy)$ illustrating random changes between dipoles ($|z_1| \simeq 0.55$) and unidirectional flows ($|z_1| \simeq 0.55$). As discussed in section 6.4.3, the existence of such a non-equilibrium phase transition can be guessed from equilibrium phase diagrams (see figure 8)

We thus conclude that situations of phase transitions are extremely important. Prediction of equilibrium phase transition help at locating non-equilibrium phase transitions in slightly non-equilibrium situations. The ideas developed here in the context of the 2D Navier-Stokes equation can be applied in a much broader context, for quasi-geostrophic or shallow-water dynamics. Indeed we conjecture that this would explain the observed bistability in recent quasi-geostrophic experiments [190, 201] (see figure 27).

We also conjecture that this is an explanation of the bistability of the Kuroshio current (Pacific ocean, east of Japan) (see figures 28, 29 and 30).

6.5. Towards a kinetic theory of NESS

We have explained in the previous sections that in the limit of weak forces and dissipation, we expect to be close to some statistical equilibria. This allows to predict qualitative properties of the flow and non-equilibrium phase transitions. However, in order to be able to predict which of these equilibria will be selected and to be able to make predictions about the statistics of fluctuations, we cannot rely on the equilibrium theory and we have to develop a non-equilibrium theory. A way to proceed is to make a kinetic theory of these Non-Equilibrium Steady States.

Such a kinetic theory approach, as any kinetic theory, will be based on an asymptotic expansion. Usually the small parameter is the ratio of the typical time scale for the small scale fluctuations over the typical time scale for the evolution of kinetic variables. For the 2D-stochastic Navier-Stokes equations, in the limit of small forces and dissipation $\nu \ll \alpha \ll 1$, the natural small parameter is the friction coefficient α. It is indeed the ratio of the turnover time scale (the timescale at which fluctuation are advected) over the time scale over which energy and other

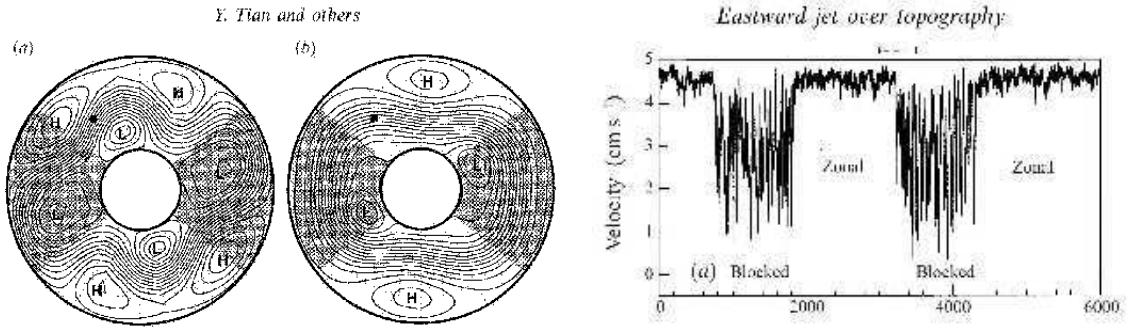

Figure 27: Bistability in a rotating tank experiment with topography (shaded area)[190, 201]. The dynamics in this experiment would be well modelled by a 2D barotropic model with topography (the quasi-geostrophic model with $R = \infty$). The flow is alternatively close to two very distinct states, with random switches from one state to the other. Left: the streamfunction of each of these two states. Right: the time series of the velocity measured at the location of the black square on the left figure, illustrating clearly the bistable behavior. The similar theoretical structures for the 2D Euler equations on one hand and the quasi-geostrophic model on the other hand, suggest that the bistability in this experiment can be explained as a non equilibrium phase transition, as done in section 6.4.3 (see also figure 26)

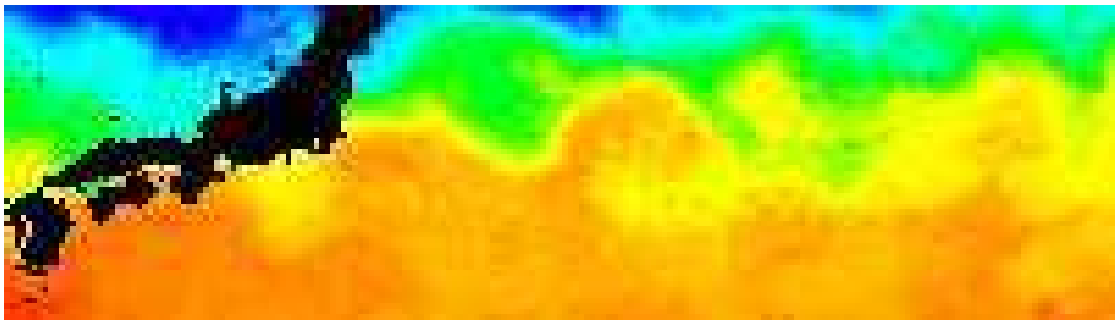

Figure 28: Kuroshio: sea surface temperature of the pacific ocean east of Japan, February 18, 2009, infra-red radiometer from satellite (AVHRR, MODIS) (New Generation Sea Surface Temperature (NGSST), data from JAXA (Japan Aerospace Exploration Agency)).
The Kuroshio is a very strong current flowing along the coast, south of Japan, before penetrating into the Pacific ocean. It is similar to the Gulf Stream in the North Atlantic. In the picture, The strong meandering color gradient (transition from yellow to green) delineates the path of the strong jet (the Kuroshio extension) flowing eastward from the coast of Japan into the Pacific ocean.
South of Japan, the yellowish area is the sign that, at the time of this picture, the path of the Kuroshio had detached from the Japan coast and was in a meandering state, like in the 1959-1962 period (see figure 29)

invariant of the inertial dynamics evolve.

In the limit of weak forces and dissipation, the flow remains close to statistically quasi stationary states (evolving on a time of order $1/\alpha$, for instance dipoles or parallel flows in the case of doubly periodic conditions, discussed in section 6.4.2), with vorticity $\Omega_0(\mathbf{r},t)$ and velocity $\mathbf{V}_0(\mathbf{r},t)$. At leading order in the theory, we naturally obtain that Ω_0 must be a dynamical equilibrium state of the Euler equations $\mathbf{V}_0.\nabla\Omega_0 = 0$. For it to be quasi-stationary, it also has to be dynamically stable.

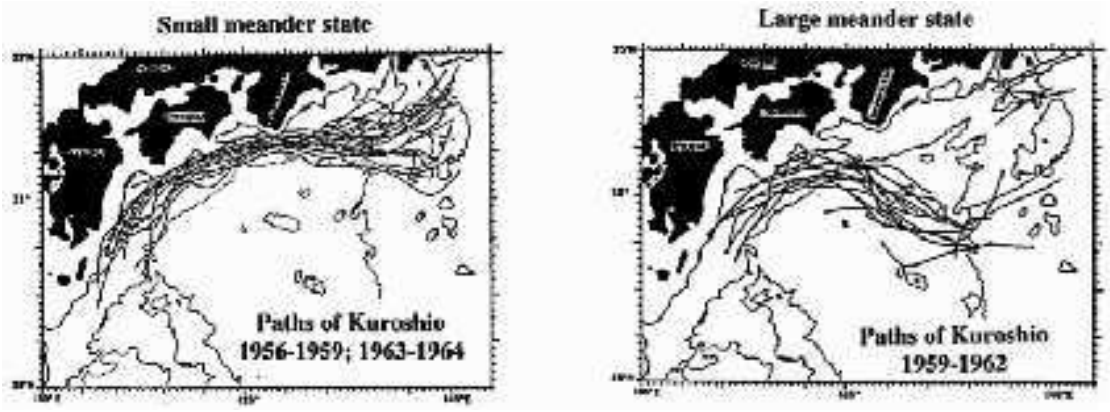

Figure 29: Bistability of the paths of the Kuroshio during the 1956-1962 period : paths of the Kuroshio in (left) its small meander state and (right) its large meander state. The 1000-m (solid) and 4000-m (dotted) contours are also shown. (figure from Schmeits and Dijkstraa [175], adapted from Taft 1972).

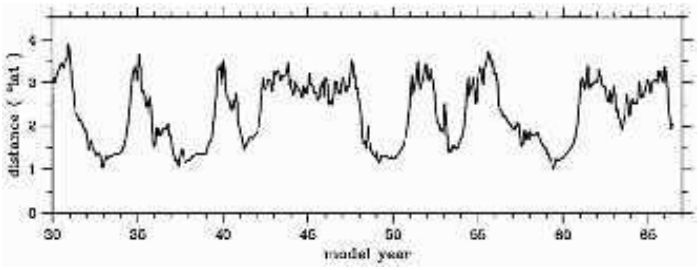

Figure 30: Bistability of the paths of the Kuroshio, from Qiu and Miao [161]: time series of the distance of the Kuroshio jet axes from the coast, averaged other the part of the coast between 132 degree and 140 degrees East, from a numerical simulation using a two layer primitive equation model.

The fluctuations evolve rapidly. The velocity fluctuations are expected to be much smaller that the velocity V_0. It is then tempting to try a perturbative expansion using this time scale separation. We thus decompose the fields as

$$\omega = \Omega_0 + \delta\omega \text{ and } \mathbf{v} = \mathbf{V}_0 + \delta\mathbf{v}. \tag{101}$$

In the more general case, Ω_0 evolves slowly over time. It may also exist cases where Ω_0 is actually stationary. For technical reasons, it will be simpler to discuss in the following the case where Ω_0 is stationary; however the generalization to the quasi-stationary case or to situations with self-similar growth is straightforward. We define $\langle . \rangle$ as an average over the noise realization. Then $\Omega_0 = \langle \omega \rangle$.

We start from the stochastic Navier-Stokes equations

$$\partial_t \omega + (\mathbf{v}\cdot\nabla)\omega = \nu\Delta\omega - \alpha\omega + \sqrt{2\alpha}\eta(t,\mathbf{x}). \tag{102}$$

We will need along the discussion the linearized Navier-Stokes equation close to the base vorticity profile Ω_0

$$\partial_t \delta\omega + L[\delta\omega] = \text{ with } L[\delta\omega] = \mathbf{V}_0.\nabla\delta\omega + \delta\mathbf{v}\cdot\nabla\Omega_0 - \nu\Delta\omega + \alpha\omega. \tag{103}$$

We decompose the fields as average plus fluctuations (101) ; The 2D Navier-Stokes equations 102 are then equivalent to the dynamics of the fluctuations, given by

$$\partial_t \delta\omega + L[\delta\omega] = \sqrt{2\alpha}\eta(t,\mathbf{x}) - \delta\mathbf{v}\cdot\nabla\delta\omega - \alpha\Omega_0 + \nu\Delta\Omega_0 \tag{104}$$

Taking the average of (104) gives

$$\langle\delta\mathbf{v}\cdot\nabla\delta\omega\rangle = -\alpha\Omega_0 + \nu\Delta\Omega_0.$$

This important equation just expresses that the mean vorticity profile is determined by a balance between the average of the nonlinear contributions of the fluctuations (Reynolds stresses) on one hand and the dissipation on the other hand. The challenge is then to find a theory to compute these Reynolds stresses.

The Reynolds stress $\langle\delta\mathbf{v}.\nabla\delta\omega\rangle$ is a quadratic quantity; it can thus be evaluated from the two point correlation function $\phi_2(\mathbf{r}_1,\mathbf{r}_2,t) = \langle\delta\omega(\mathbf{r}_1,t)\,\delta\omega(\mathbf{r}_2,t)\rangle$. The equation for the time evolution of the two-point correlation function is easily obtained from (102), using the Ito formula and averaging. We obtain

$$\partial_t\phi_2 + L_1\phi_2 + L_2\phi_2 = 2\alpha F_2 + NL_2, \tag{105}$$

where L_1 (resp L_2) is the linearized Euler operator L (103) acting on the variable $\mathbf{r}_1$ (resp $\mathbf{r_2}$), $NL_2(\mathbf{r}_1,\mathbf{r}_2) = -\langle\delta\mathbf{v}(\mathbf{r}_1).\nabla\delta\omega(\mathbf{r}_1)\,\delta\omega(\mathbf{r}_2)\rangle - \langle\delta\mathbf{v}(\mathbf{r}_2).\nabla\delta\omega(\mathbf{r}_2)\,\delta\omega(\mathbf{r}_1)\rangle$ is the contribution of the nonlinear term and $2\alpha F_2$ is average effect of the stochastic force on the two-point correlation function (with the stochastic force (98), page 94, we have $F_2(\mathbf{r}_1,\mathbf{r}_2) = \sum_k f_k^2 e_k(\mathbf{r}_1)\,e_k(\mathbf{r}_2)$).

Due to the nonlinearity, the equation for the two points correlation function (105) involves a three point quantity NL_2. One could easily write the whole hierarchy for the n-point correlators. Any truncation of such a hierarchy is arbitrary, except in cases where a small parameter allows to neglect the nonlinear terms in a self-consistent way. Such a situation occurs for instance in kinetic theory, more specifically in the kinetic theory of systems with long range interactions [20] that share deep analogies with the present problem, one example being the kinetic theory of the point vortex model [43] (an application of similar idea to the relaxation towards equilibrium of the 2D Euler equation as also been discussed, see [42] and further discussion in section 6.6). We then call such an approach a kinetic approach.

Such a kinetic theory approach is a classical one. Similar ideas have been discussed back in the seventies and eighties in other contexts and are still studied currently (quasi-normal closures, rapid distortion theories, second order cumulant truncations, and other related approaches). Very few of these works however consider inhomogeneous flows dominated by the large scales, as is our interest here. Some exceptions are a series of theoretical and numerical works made during

last decade [68, 119, 150, 149, 42], among them a very interesting model of 2D wall turbulence [149]. In the case of the large scales of geophysical flows, recent interesting works have used numerical simulations, for instance to study the limits of second order cumulants expansion [132], or to study numerically a self consistent closure describing the coupling of the mean flow and of the second order cumulant [77]. Another line of research, on related issues, has been to search for crude closures [88, 89], or more precise mathematical results [130], when the system is subjected to random bombardments

In all of the previous works, some hypothesis of a phenomenological nature are made in order to simplify the problem at some point (closure without small parameter, assumption of scale separations, Markovianization), that allows interesting studies to be pushed forward. However, there still remains a lot of work to assess either numerically or theoretically the validity or not of these hypothesis, and thus to be really able to propose a clear theory of the large scales of two dimensional and geophysical flows. Our belief is that any progress in this direction requires a better theoretical understanding of the basic objects appearing in the theory.

For instance any progress in the kinetic theory requires the understanding of equation (105), and thus requires a theoretical understanding of the two-point linear operator on the rhs: $\partial_t \phi_2 + L_1\phi_2 + L_2\phi_2 = F$. Similar n-point linear operators, implying the linearized operator L, appear at each level of the hierarchy of the equations for the n point correlation function. A prerequisite for any understanding of this linear operator is a detailed understanding of the linearized Euler equation and of its asymptotic behavior. The current theoretical understanding of L is readily not sufficient to go forward with the kinetic theory.

The results for the behavior of L can not be universal. They depend a lot on the boundary conditions, on the topology of the streamlines and on the specific model (Euler, quasi-geostrophic, etc...). For instance, any theory that would not depend explicitly on boundary conditions would be promised to failure. The theoretical analysis of the linear operator L is one of the aims of next section.

6.6. Relaxation towards equilibrium and asymptotic behavior of the 2D Euler and linearized Euler equation

6.6.1. Irreversibility of reversible dynamical systems

The 2D Euler equations

$$\partial_t \omega + (\mathbf{v}\cdot\nabla)\omega = 0 \tag{106}$$

is time reversible: it is invariant over the time reversal symmetry $t \to -t$, $\omega \to -\omega$ (or equivalently $\mathbf{v} \to -\mathbf{v}$). However, it has anyway an irreversible behavior. Indeed, as explained in section 2, for large times, enstrophy and other Casimir invariant cascade towards lower and lower scales and the largest scales of the flow converge towards a stationary solution to the 2D Euler equations. Such an apparent paradox between the time reversal symmetry of the microscopic dynamics (here the Euler equations) and the irreversible evolution of macroscopic variables (here the largest scales of the flow) is a classic problem of statistical mechanics.

This reversibility paradox is usually satisfactorily explained by introducing in the discussion, the discussion of relative probabilities of types of initial conditions (see for instance the classical discussion [162] about irreversible behavior in electromagnetism). In the statistical mechanics this idea is formalized using the concepts of microscopic versus macroscopic variables and by

introducing the notion of a probability for the macroscopic states. The entropy of a macrostate quantifies the number of microstates corresponding to a given macrostate. Then for a sample of rare initial microscopic conditions (corresponding to a low entropy macrostate), an overwhelming number of the trajectories evolve towards microscopic configurations corresponding to a more probable (higher entropy) macrostate [87].

For this classical explanation of the reversibility paradox to be relevant, a clear distinction between microscopic and macroscopic variable is essential; this requires to consider a limit with a large number of degrees of freedom (usually the thermodynamic limit in classical physical systems). The Euler equation is different from those classical systems in the sense that it is a partial differential equation that has from the beginning an infinite number of degrees of freedom.

Beside the general qualitative explanation of the reversibility paradox, there is only a few examples where one can prove mathematically the irreversible evolution of the macroscopic variable directly from the microscopic dynamics. The most famous example is probably Landford's proof of the validity of the Boltzmann equation (and thus macroscopic irreversibility), for a system of dilute particles (Grad limit), with hard core interactions (see [184] for a very clear presentation). We want to stress that the Euler equation may be another example where an irreversible behavior can be proved for a reversible equation (see [23]).

The aim of the following discussion is to present the results in [23] related to the irreversibility problem. These results moreover include a detailed study of the linearized Euler equation which is directly related to the discussion of section 6.5 about the kinetic theory of the 2D Navier-Stokes equation. The general discussion in [23] is however rather technical, and in this section we only derive the main results for the special case of a constant shear, for which explicit computation are straightforward [41] and state the more general results.

6.6.2. Irreversible relaxation of the linearized Euler equation

We consider in the following the linearized 2D Euler equations close to a stable parallel flows, in a doubly periodic domain or in a channel. We stress however that all the following results should be valid for a stable circular vortex in a disc geometry[22]

Any parallel flow $\mathbf{v}_0$=$U(y)\,\mathbf{e}_x$ is a stationary solution to the 2D Euler equations (106) in a doubly periodic domain or in a channel. We consider the Euler equations with initial conditions close to this base flow: $\Omega = \omega_0 + \omega$ and $\mathbf{V} = \mathbf{v} + \mathbf{v}_0$, where $\omega_0(y) = -U'(y)$ is the base flow vorticity and ω and $\mathbf{v}$ are the perturbation vorticity and velocity, respectively. It reads

$$\partial_t \omega + U(y)\,\partial_x \omega - v_y U''(y) = 0, \tag{107}$$

where v_y is the transverse velocity component.

We assume that the base flow $U(y)$ is linearly stable (there is no unstable mode to the linear equation (107)). We note that any $\omega(y)$ independent of x is a trivial neutral mode of (107). If we decompose ω in Fourier modes along the longitudinal direction $\omega(x,y) = \sum_k \omega_k(y)\,e^{ikx}$, the

[22] For these results to be valid, some further conditions on the behavior of the vorticity at the core of the vortex may be required; this remains to be studied.

linearized Euler equation for ω_k is

$$\partial_t \omega_k + ikU(y)\,\omega_k - ik\psi_k U''(y) = 0, \tag{108}$$

where ψ_k is the Fourier transform of the streamfunction. We assume that for all $k \neq 0$, equations (108) have no neutral modes (this situation of a linear operator with no modes may seem strange, it is however not unusual for a non-normal[23] linear operator; for instance one can prove that that (108) has no mode as soon as U is monotonic in a channel geometry [64], this is also true for the Kolmogorov flow in doubly periodic domains [23]).

The linear shear. Because of its third l.h.s. term, a general discussion of (107) is rather complex and requires the use of complex mathematical tools [23]. It is often argued that this third term can be neglected, but this is usually a very bad approximation (see [23]). However in the special case of a linear shear flow $U(y) = \sigma y$, the third term vanishes and the equation is then very simple

$$\partial_t \omega + \sigma y \partial_x \omega = 0.$$

This equation can be easily solved:

$$\omega(x,y,t) = \omega(x - \sigma y t, y, 0).$$

It is even more simple if we consider perturbation on the form $\omega(x,y,t) = \omega_k(y,t)\exp(ikx)$, then

$$\omega_k(y,t) = \omega_k(y,0)\exp(-ik\sigma y t). \tag{109}$$

The velocity can be expressed from the vorticity using using a Green function formalism. We have

$$\mathbf{v}_k(y,t) = \int \mathrm{d}y'\, \mathbf{G}_k(y,y')\omega_k(y',t), \tag{110}$$

where, using $\omega = \Delta\psi$, $v_x = -\frac{d\psi}{dy}$ and $v_y = \frac{d\psi}{dx}$, $\mathbf{G}_k$ is defined by

$$\mathbf{G}_k(y,y') = \left(-\frac{\partial H_k}{\partial y}, ikH_k\right)(y,y') \text{ with } \frac{\partial^2 H_k}{\partial y^2} - k^2 H_k = \delta(y-y'), \tag{111}$$

with for instance a channel boundary conditions: $y \in (-L,L)$ with $\psi(L) = \psi(-L) = H_k(L) = H_k(-L) = 0$. Using (109), we have

$$\mathbf{v}_k(y,t) = \int dy'\, \mathbf{G}_k(y,y')\,\omega_k(y',0)\exp(-ik\sigma y' t). \tag{112}$$

[23] A linear operator L is said to be normal if it commutes with its adjoint $LL^* = L^*L$. In finite dimensional spaces, a normal operator can always be diagonalized on an orthogonal base. This result often generalize to infinite dimensional space, for instance in the case of bounded self-adjoint operators typical of quantum dynamics. By contrast, non-normal operator may not be diagonalizable, and may not have any mode as illustrated by many examples in fluid mechanics for instance.

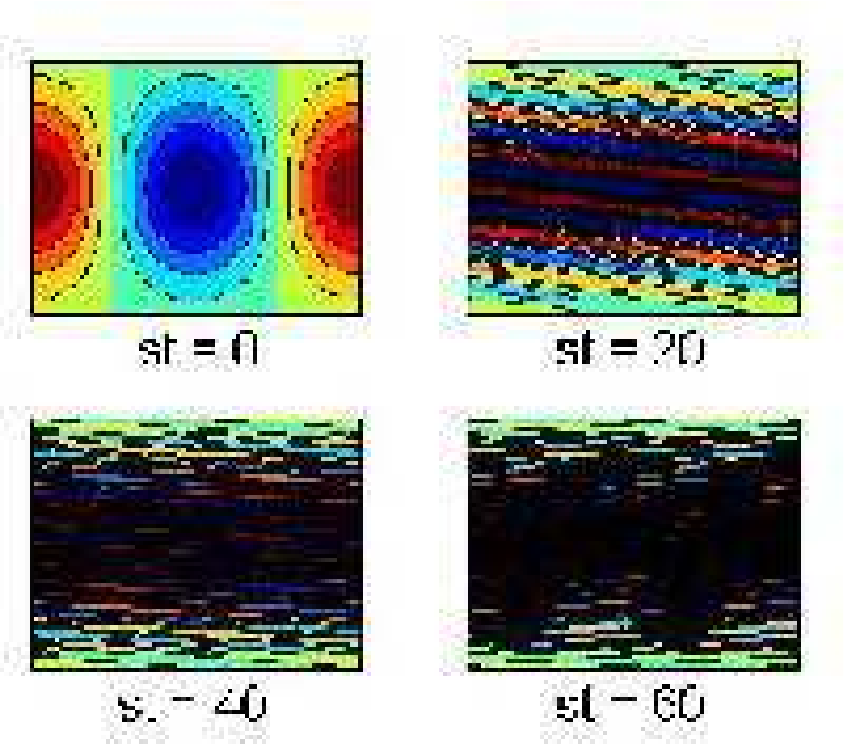

Figure 31: Evolution of $\omega(x,y,t)$ from an initial vorticity perturbation $\omega(x,y,0) = \omega_1(y,0)\cos(x)$, by the linearized 2D Euler equations close to a shear flow $U(y) = \sigma y$. (colors in the .PDF document)

We consider the asymptotic behavior, for large times t, of the oscillating integral (112). Since Kelvin, very classical results do exist for the asymptotic behavior of such integrals, the most well known results being the stationary phase approximation. In our case there is no stationary phase, and the asymptotic behavior of the velocity field is obtained by successive integrations by parts, which lead to

$$v_{k,x}(y,t) \underset{t\to\infty}{\sim} \frac{\omega_k(y,0)}{ik} \frac{\exp(-iky\sigma t)}{\sigma t} \text{ and} \tag{113}$$

$$v_{k,y}(y,t) \underset{t\to\infty}{\sim} \frac{\omega_k(y)}{ik} \frac{\exp(-iky\sigma t)}{\sigma^2 t^2} . \tag{114}$$

The exponents of the algebraic laws $1/t$ for v_x and $1/t^2$ for v_y are related to the singularities of the Green function $\mathbf{G}_k$.

This shows that the velocity field decays algebraically for large time. As illustrated by figure (34) in the case of the Kolmogorov flow, the velocity actually decays much faster (exponentially) for times of order $1/\sigma$ and then the decrease has algebraic tails. This irreversible behavior of the velocity field for a reversible equation (the linearized 2D Euler equations are time reversible (symmetry $t \to -t$, $\omega \to -\omega$, $\mathbf{v} \to -\mathbf{v}$, $U \to -U$ and $\Omega_0 \to -\Omega_0$) is a striking result.

Heuristically, the vorticity field is strongly sheared and produce filaments at finer and finer scales as illustrated by figure (31). The computation of the velocity field from the vorticity field

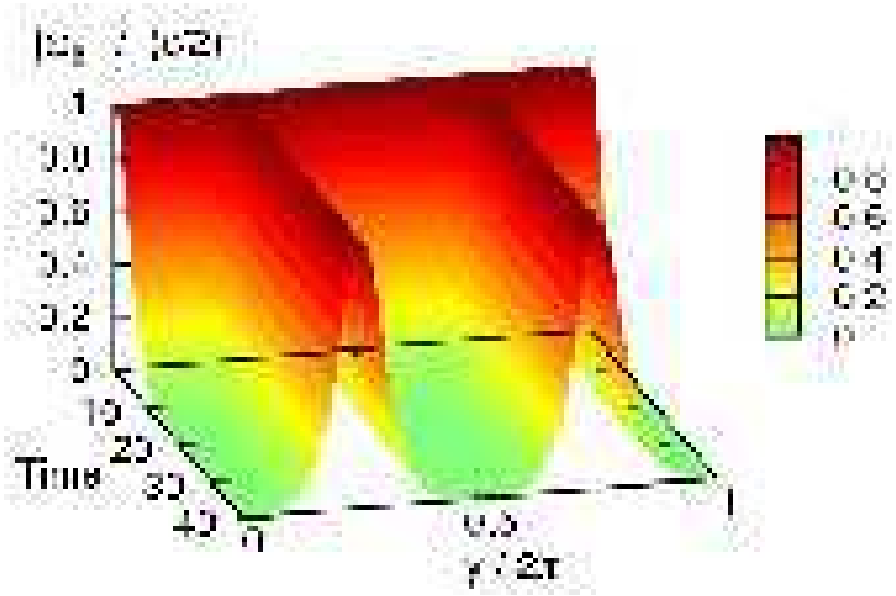

Figure 32: Evolution of the vorticity perturbation $\omega(x,y,t) = \omega(y,t)\exp(ikx)$, close to a parallel flow $\mathbf{v}_0(x,y) = U(y)\mathbf{e}_x$ with $U(y) = \cos(y)$, in a doubly periodic domain with aspect ratio δ. The figure shows the modulus of the perturbation $|\omega(y,t)|$ as a function of time and y. One clearly sees that the vorticity perturbation rapidly converges to zero close to the points where the velocity profile $U(y)$ has extrema ($U'(y_0) = 0$, with $y_o = 0$ and π). This *depletion of the perturbation vorticity* at the stationary streamlines y_0 is a new generic self-consistent mechanism, understood mathematically as the regularization of the critical layer singularities at the edge of the continuous spectrum (see [23]). (colors in the .pdf document)

involves an integration, the contribution of these fine scale filaments is then weaker and weaker.

General parallel flow. The algebraic decay of the velocity field for the linearized 2D Euler equations close to a linear shear has been first obtained by Case [41], using an explicit computation rather than the oscillating integral explanation given above. For more general base flows with strictly monotonic profiles $U(y)$ (without stationary streamline $U'(y_0) = 0$), from classical arguments [170, 30] using the Laplace transform, one expects an asymptotic algebraic decrease of the velocity field with the same $1/t$ and $1/t^2$ laws (see also an ansatz for large time asymptotic in [31]).

In the case of base flows $U(y)$, the oscillating phase in the integral (112) is $ikU(y)t$. Then for base flows with stationary streamlines $U'(y_0) = 0$, the oscillating integral (112) has a stationary phase and one expects other algebraic laws for the asymptotic velocity fields (for instance $1/\sqrt{t}$) (see discussions by [31, 127]). It has however been proved recently that, unexpectedly, the same power laws occur [23]. This is associated with a very surprising non-local mechanism of vorticity depletion at the stationary streamlines, not described before (see [23] and figure 32).

The general result [23], valid for any stable flow $U(y)$ without any mode for (108), is then

$$\omega(y,t) \underset{t\to\infty}{\sim} \omega_\infty(y)\exp(-ikU(y)t) + \mathscr{O}\left(\frac{1}{t^\gamma}\right), \tag{115}$$

with an algebraically decaying velocity for large times

$$v_x(y,t) \underset{t\to\infty}{\sim} \frac{\omega_\infty(y)}{ik}\frac{\exp(-ikU(y)t)}{U'(y)t} \text{ and} \tag{116}$$

$$v_y(y,t) \underset{t\to\infty}{\sim} \frac{\omega_\infty(y)}{ik}\frac{\exp(-ikU(y)t)}{(U'(y)t)^2}; \tag{117}$$

where the asymptotic vorticity profile ω_∞ (see (115), (116) and (117)) can be computed from the Laplace transform of the linearized equation (108) (see [23]). The algebraic decay of the velocity field is illustrated on figures 33 and 34, in the case of the Kolmogorov flow $U(y) = \cos(y)$ on doubly periodic domains.

6.6.3. Relaxation and asymptotic stability of parallel flows for the 2D Euler equations

In the previous section, we have obtained results for the asymptotic behavior of the linearized 2D Euler equations, with initial conditions close to some parallel flows $\mathbf{v}_0(\mathbf{r}) = U(y)\mathbf{e}_x$. We now address the evolution of the same initial conditions by the nonlinear Euler equation (106).

The asymptotic stability of an ensemble of parallel flows means that for any small perturbation of a parallel flow, the velocity converges for large times towards another parallel flow close to the initial one. The aim of this section is to explain why the linearized dynamics is a good approximation for the non-linear dynamics for any time t, and to explain why the flow velocity is asymptotically stable (in kinetic energy norm), for small initial perturbation of the vorticity (in the enstrophy norm). Such an irreversible convergence is a striking phenomena for a reversible equation like the 2D Euler equations.

We consider the initial vorticity $\Omega(x,y,0) = -U'(y) + \varepsilon\omega(x,y,0)$, where ε is small. We suppose, without loss of generality, that $\int dx\,\omega = 0$. The perturbation ω can be decomposed in Fourier modes along the x direction

$$\omega(x,y,t) = \sum_k \omega_k(y,t)\exp(ikx).$$

From the Euler equations (106), the equation for ω_k is

$$\partial_t\omega_k + ikU(y)\omega_k - ik\psi_k U''(y) = -\varepsilon NL$$

$$\text{with } NL = \sum_l \left\{ -ik\frac{\partial\psi_l}{\partial y}(y,t)\,\omega_{k-l}(y,t) + \frac{\partial}{\partial y}\left[il\,\psi_l(y,t)\,\omega_{k-l}(y,t)\right]\right\}. \tag{118}$$

The left hand side is the linearized Euler equation, whereas the right hand side are the nonlinear corrections. We want to prove that, for sufficiently small ε, neglecting the nonlinear terms is self-consistent.

For this we have to prove that the nonlinear terms remain uniformly negligible for large times. We then use the asymptotic results for the linearized equation (115-117) and $\omega_k = d^2\psi_k/dy^2 - k^2\psi_k$. We have, for any k,

$$\psi_{k,L}(y,t) \underset{t\to\infty}{\sim} \frac{\omega_{k,L,\infty}(y)}{(ikU'(y))^2}\frac{\exp(-ikU(y)t)}{t^2}$$

$$\text{and } \omega_{k,L}(y,t) \underset{t\to\infty}{\sim} \omega_{k,L,\infty}(y)\exp(-ikU(y)t), \tag{119}$$

where the subscript L refers to the evolution according to the linearized dynamics. We call a quasilinear approximation for the right hand side of equation (118), the approximation where ψ_k and ω_k would be evaluated according to their linearized evolution close to the base flow $U(y)$. From (119), one would expect at first sight that this quasilinear approximation of the nonlinear term NL_{QL}, would give contributions of order $O(1/t)$. The detailed computation, easily performed from (119), actually shows that the contributions of order $O(1/t)$ identically vanish for large times. This cancellation of terms is a remarkable property with important consequences. Then

$$\varepsilon NL_{k,QL} \underset{t\to\infty}{=} O\left(\frac{\varepsilon}{t^2}\right).$$

This important remark proves that within a quasilinear approximation, the contribution of the nonlinear terms NL_{QL} remains uniformly bounded, and more importantly it is integrable with respect to time.

Then we conjecture that the contribution of the nonlinear terms remains always negligible. More precisely, we conjecture that within the fully nonlinear equation, for sufficiently small ε:

$$\psi_k(y,t) \underset{t\to\infty}{\sim} \frac{\omega_{k,\infty}(y)}{(ikU'(y))^2}\frac{\exp(-ikU(y)t)}{t^2}$$

$$\text{and } \omega_k(y,t) \underset{t\to\infty}{\sim} \omega_{k,\infty}(y)\exp(-ikU(y)t),$$

with

$$\omega_{k,\infty}(y) = \omega_{k,L,\infty}(y) + O(\varepsilon)$$

A similar reasoning in order to evaluate the nonlinear evolution for the profile $U(y)$ would lead to the conclusion that for large times

$$\Omega_0(y,t) \underset{t\to\infty}{\sim} -U'_\infty(y) \text{ with } U'_\infty(y) = U(y) + \delta U(y),$$

where $\delta U = O(\varepsilon^2)$.

This means that the parallel flow quickly stabilizes again towards another parallel flow which is close to the initial one. This stabilization is very rapid, it occurs on times scales of order $1/\sigma$ where σ is a typical shear rate.

We thus conclude that the relaxation towards stationary solutions to the 2D Euler equations is a very fast and simple process, leading to a stationary state on time scales given by the linearized dynamics. The velocity fluctuations are weakened extremely fast by the dynamics, such that their effect becomes soon negligible. This is by contrast with the phenomenology of particle models,

like the point vortex model, where fluctuations are constantly produced due to the singularities of the vorticity field, related to the discrete point particles.

The long term evolution of point vortex models close to quasi-stationary states of the 2D Euler equations is thought to be described by a kinetic equation [43, 4] analogous of the Lenard-Balescu equation of plasma physics. A very natural hypothesis is that a similar kinetic equation could describe the long term evolution of initial conditions close to stationary states of the 2D Euler equations, as interestingly proposed by [42]. Whether this is justified or not, and for which class of solutions, is a very complex issue, that has not been settled yet, neither from a theoretical nor from an empirical point of view. The results described in this section suggest that this is not the case for analytical initial conditions close to parallel flows, as then the fluctuations decays very quickly and the flow settles to a stationary states before a regime of long term quasi-stationary evolution could appear. As far as larger classes of initial conditions are concerned (close to other type of base flow than parallel flows, or with non analytic classes of initial conditions) the answer is unclear yet.

One might then want to compute the modified profile. The preceding analysis leads to the quasilinear expression

$$\delta U(y) = -\varepsilon^2 \int_0^\infty dt\, NL_{0,QL}(t) + o\left(\varepsilon^2\right). \tag{120}$$

This expression involves integrals over times of the linearized Euler equation. It is not amenable to any simple explicit expression, but it can be evaluated using the Laplace transform of (108).

We conclude that for any profile U with no unstable nor neutral modes for (108), any perturbation corresponding to a small vorticity, the assumption that the dynamics can be treated with a quasi-linear approximation is a self consistent hypothesis. Then the velocity converges for large times towards a new parallel velocity profile which is close to the initial profile U. Figures 33 and 35, on page 127, show that numerical computations confirm this conjecture.

From this discussion, we conclude that is natural to conjecture that any profile U verifying the hypothesis of this work (no unstable and no neutral modes for (108)), any perturbation corresponding to a small vorticity will converge at large times towards a new parallel velocity profile which is close to the initial profile U. A possible theorem expressing this more precisely this would require a detailed analysis of subsequent terms in an asymptotic expansion for small ε, in a similar way to the results recently obtained by Mouhot and Villani [145], for the Landau damping in the very close setup of the Vlasov equation. A proof of such a theorem for the Euler equations is not known yet, even in the simplest case of a profile U without stationary points.

On the basis of the previous discussion, a further conjecture would be that the ensemble of shear flows without unstable nor neutral modes for (108) is asymptotically stable [24] in the sense given previously (initial perturbation controlled by a vorticity norm, for instance the enstrophy and large time perturbation controlled in kinetic energy norm) [25].

[24] We think here to the notion of asymptotic stability of an ensemble of stationary solutions of an infinite dimensional Hamiltonian equations, see for example the work [158] where stable solutions slightly perturbed are proved to converge for large times towards another slightly different solution. Asymptotic stability has been proved for other solutions of infinite dimensional Hamiltonian systems.

[25] A classical argument, presented in a rigorous framework by Caglioti and Maffei [34] in the context of the

7. Conclusion and perspectives

Statistical mechanics of two dimensional and geophysical flows brings a new perspective to the study of the self-organization of turbulent flows. It is complimentary to other studies, based on fluid dynamics, non linear dynamics and numerical computations. The successes in modeling Jupiter's troposphere or some aspects of the ocean vortices using the drastic simplification provided by statistical mechanics concepts is very encouraging. One of the current aim is to develop the theory in order extend the range of validity and relevance of the approach, for instance in order to address further problems in geophysical turbulence.

The equilibrium statistical mechanics theory of the 2D Euler and quasi-geostrophic equations is still a actively developing field. Recent results, not presented in this review, include a classification of phase transitions and of ensemble inequivalence [16], which of important practical interest, and extension of the results of stability of stationary solutions [70]. A complete theory of phase transitions, specifically addressing the specificity of two dimensional and quasi-geostrophic turbulence is however still lacking.

Equilibrium statistical mechanics has also been extended recently to magneto-hydrodynamics equations [102, 121], non-linear Schroedinger equations [101, 71], the Shallow-Water model [50], or models of axisymmetric turbulence [122, 142, 148]. In experimental statistically stationary forced and dissipated turbulence, comparison of the PDF of velocity or vorticity fluctuations, with prediction from equilibrium statistical mechanics, is discussed in [104] or in [122, 142, 148].

From a theoretical point of view, these new applications usually have not the same level of rigor as the statistical mechanics of the 2D Euler and quasi-geostrophic equations. More precisely, the classical program of equilibrium statistical mechanics: building from the Liouville theorem the natural invariant measure of the dynamical equations — the microcanonical measure —, and being able to compute the real entropy corresponding to the phase space volume, is not achieved for these models. In some of the works cited above, some very natural hypothesis are made, that will probably be proved to be true in the future; in some others ad-hoc fixes are proposed the logic of which seems sometimes not to be based on clear principles. Still some of the results are quite interesting and lead to very appealing applications. It is thus a very exiting challenge to try to develop the theory for the equilibrium statistical mechanics of these models, in order to understand the validity or not of the previous approaches, and to obtain more physical insights. It is also essential to assess the limits of the range of validity of equilibrium statistical mechanics, also for other models of interest for geophysical flows.

As we explained is this review, equilibrium statistical mechanics may give, in some specific circumstances, interesting results for actual non-equilibrium flows. We discussed the examples

Vlasov equation implies that stationary solutions to the Vlasov equation for which Landau damping would occur, would be unstable in a weak norm. At the core of the argument lies the time reversal symmetry of the equations. These arguments would easily generalize to the Euler equations. This may seem in contradiction with the notion of asymptotic stability. However the notion of stability discussed by Caglioti and Maffei involves weak topology for both the initial conditions and final state. There is no contradiction with our definition of asymptotic stability, as we control here the initial perturbation in a vorticity norm and control the convergence in a velocity norm.

of Jupiter's troposphere where it exists a large separation between the time scales for the inertial (Hamiltonian) and non-inertial aspects of the dynamics (forces and dissipation) or for instance for ocean rings where the dynamical process of their formation is extremely rapid. A large part of the range of interest of equilibrium statistical mechanics, in the laboratory or for geophysical flows, has still to be studied, and many progresses shall be made in this direction in future works.

For many applications, a non-equilibrium statistical mechanics is required. We discussed in the last section recent progresses for the study of the relaxation towards stationary solutions of the 2D Euler equations and recent progresses towards a kinetic description of the 2D Navier Stokes equations with weak forces and dissipation. This is a promising field of research, where theoretical physics and mathematical results are foreseen in a near future. This type of works is essential to explain the large scale organization of geophysical turbulence.

Other approaches for non-equilibrium statistical mechanics, like linear response theory, large deviations or path integral representations of stochastic processes will probably be part of future theories for turbulent flows.

Acknowledgments

We warmly thank M. Corvellec and S. Griffies for their comments about the manuscript.

This work was supported through the ANR program STATFLOW (ANR-06-JCJC-0037-01) and through the ANR program STATOCEAN (ANR-09-SYSC-014).

Freddy Bouchet thanks CNLS and LANL in Los Alamos for hosting him during most of the writing of this review.

References

[1] http://www.whoi.edu/science/PO/people/pberloff/.

[2] R. V. Abramov, A. J. Majda, Statistically relevant conserved quantities for truncated quasigeostrophic flow, Proceedings of the National Academy of Science 100 (2003) 3841–3846.

[3] H. Aluie, G. L. Eyink, Localness of energy cascade in hydrodynamic turbulence. II. Sharp spectral filter, Physics of Fluids 21 (11) (2009) 115108.

[4] H. Aref, 150 Years of vortex dynamics, Theoretical and Computational Fluid Dynamics 24 (2010) 1–7.

[5] V. I. Arnold, On an a-priori estimate in the theory of hydrodynamic stability, Izv. Vyssh. Uchebbn. Zaved. Matematika; Engl. transl.: Am. Math. Soc. Trans. 79 (2) (1966) 267–269.

[6] B. Barnier, G. Madec, T. Penduff, J. Molines, A. Treguier, J. Le Sommer, A. Beckmann, A. Biastoch, C. Böning, J. Dengg, C. Derval, E. Durand, S. Gulev, E. Remy, C. Talandier, S. Theetten, M. Maltrud, J. McClean, B. de Cuevas, Impact of partial steps and momentum advection schemes in a global ocean circulation model at eddy-permitting resolution, Ocean Dynamics 56 (2006) 543–567.

[7] P. Berloff, A. M. Hogg, W. Dewar, The Turbulent Oscillator: A Mechanism of Low-Frequency Variability of the Wind-Driven Ocean Gyres, Journal of Physical Oceanography 37 (2007) 2363.

[8] D. Bernard, G. Boffetta, A. Celani, G. Falkovich, Conformal invariance in two-dimensional turbulence, Nature Physics 2 (2006) 124–128.

[9] D. Bernard, G. Boffetta, A. Celani, G. Falkovich, Inverse Turbulent Cascades and Conformally Invariant Curves, Physi. Rev. Lett. 98 (2) (2007) 024501.

[10] J. Binney, S. Tremaine, Galactic dynamics, Princeton, NJ, Princeton University Press, 1987, 747 p., 1987.

[11] A. Biryuk, On Invariant Measures of the 2D Euler Equation, Journal of Statistical Physics 122 (2006) 597–616.

[12] C. Boucher, R. S. Ellis, B. Turkington, Spatializing Random Measures: Doubly Indexed Processes and the Large Deviation Principle , Annals Prob. 27 (1999) 297–324.

[13] F. Bouchet, Mécanique statistique des écoulements géophysiques, PHD, Université Joseph Fourier-Grenoble, 2001.

[14] F. Bouchet, Parameterization of two dimensionnal turbulence using an anisotropic maximum entropy principle, cond-mat/0305205.

[15] F. Bouchet, Simpler variational problems for statistical equilibria of the 2d euler equation and other systems with long range interactions, Physica D Nonlinear Phenomena 237 (2008) 1976–1981.

[16] F. Bouchet, J. Barré, Classification of Phase Transitions and Ensemble Inequivalence, in Systems with Long Range Interactions, Journal of Statistical Physics 118 (2005) 1073–1105.

[17] F. Bouchet, J. Barre, A. Venaille, Equilibrium and out of equilibrium phase transitions in systems with long range interactions and in 2d flows, in: A. Campa, A. Giansanti, G. Morigi, F. S. Labini (eds.), Dynamics and Thermodynamics of Systems with Long Range Interactions: Theory and Experiments, vol. 970 of American Institute of Physics Conference Series, 2008, pp. 117–152.

[18] F. Bouchet, P. H. Chavanis, J. Sommeria, Statistical mechanics of Jupiter's Great Red Spot in the shallow water model, Preprint, to be submitted.

[19] F. Bouchet, M. Corvellec, Invariant measures of the 2D Euler and Vlasov equations, Journal of Statistical Mechanics: Theory and Experiment 8 (2010) P08021.

[20] F. Bouchet, T. Dauxois, Prediction of anomalous diffusion and algebraic relaxations for long-range interacting systems, using classical statistical mechanics, Phys. Rev. E 72 (4) (2005) 045103.

[21] F. Bouchet, T. Dumont, Emergence of the great red spot of jupiter from random initial conditions, cond-mat/0305206.

[22] F. Bouchet, S. Gupta, D. Mukamel, Thermodynamics and dynamics of systems with long-range interactions, Physica A (2010) 4389–4405.

[23] F. Bouchet, H. Morita, Large time behavior and asymptotic stability of the 2D Euler and linearized Euler equations, Physica D Nonlinear Phenomena 239 (2010) 948–966.

[24] F. Bouchet, E. Simonnet, Random Changes of Flow Topology in Two-Dimensional and Geophysical Turbulence, Physical Review Letters 102 (9) (2009) 094504.

[25] F. Bouchet, J. Sommeria, Emergence of intense jets and Jupiter's Great Red Spot as maximum-entropy structures, Journal of Fluid Mechanics 464 (2002) 165–207.

[26] H. Brands, P. H. Chavanis, R. Pasmanter, J. Sommeria, Maximum entropy versus minimum enstrophy vortices, Physics of Fluids 11 (1999) 3465–3477.

[27] H. Brands, J. Stulemeyer, R. A. Pasmanter, T. J. Schep, A mean field prediction of the asymptotic state of decaying 2D turbulence, Physics of Fluids 9 (1997) 2465–2467.

[28] F. P. Bretherton, D. B. Haidvogel, Two-dimensional turbulence above topography, Journal of Fluid Mechanics 78 (1976) 129–154.

[29] J. Bricmont, A. Kupiainen, R. Lefevere, Ergodicity of the 2D Navier-Stokes Equations with Random Forcing, Com.. Math. Phys. 224 (2001) 65–81.

[30] R. J. Briggs, J. D. Daugherty, R. H. Levy, Role of Landau Damping in Crossed-Field Electron Beams and Inviscid Shear Flow, Physics of Fluids 13 (1970) 421–432.

[31] S. N. Brown, K. Stewartson, On the algebraic decay of disturbances in a stratified linear shear flow, Journal of Fluid Mechanics 100 (1980) 811–816.

[32] C. H. Bruneau, H. Kellay, Experiments and direct numerical simulations of two-dimensional turbulence, Phys. Rev. E71 (4) (2005) 046305.

[33] E. Caglioti, P. L. Lions, C. Marchioro, M. Pulvirenti, A special class of stationary flows for two-dimensional euler equations: A statistical mechanics description. Part II, Commun. Math. Phys. 174 (1995) 229–260.

[34] E. Caglioti, C. Maffei, Time asymptotics for solutions of vlasov poisson equation in a circle., J. Stat. Phys. 92 (1) (1998) 301–323.

[35] E. Caglioti, F. Rousset, Quasi-Stationary States for Particle Systems in the Mean-Field Limit, J. Stat. Phys. 129 (2) (2007) 241–263.

[36] H. B. Callen, Thermodynamics and an Introduction to Thermostatistics, 2nd Edition, 1985.

[37] A. Campa, T. Dauxois, S. Ruffo, Statistical mechanics and dynamics of solvable models with long-range interactions, Phys. Rep. 480 (2009) 57–159.

[38] A. Campa, A. Giansanti, G. Morigi, F. S. Labini (eds.), Dynamics and Thermodynamics of Systems with Long Range Interactions: Theory and Experiments, vol. 970 of American Institute of Physics Conference Series, 2008 (2008).

[39] H. W. Capel, R. A. Pasmanter, Evolution of the vorticity-area density during the formation of coherent structures in two-dimensional flows, Physics of Fluids 12 (2000) 2514–2521.

[40] G. F. Carnevale, J. S. Frederiksen, Nonlinear stability and statistical mechanics of flow over topography, Journal of Fluid Mechanics 175 (1987) 157–181.

[41] K. M. Case, Stability of Inviscid Plane Couette Flow, Physics of Fluids 3 (1960) 143–148.

[42] P. H. Chavanis, Quasilinear Theory of the 2D Euler Equation, Physical Review Letters 84 (2000) 5512–5515.

[43] P. H. Chavanis, Statistical mechanis of two-dimensional vortices and stellar systems, in: T. Dauxois, S. Ruffo, E. Arimondo, M. Wilkens (eds.), Dynamics and Thermodynamics of Systems With Long Range Interactions, vol. 602 of Lecture Notes in Physics, Springer-Verlag, 2002, pp. 208–289.

[44] P. H. Chavanis, Phase Transitions in Self-Gravitating Systems, International Journal of Modern Physics B 20 (2006) 3113–3198.

[45] P. H. Chavanis, Dynamical and thermodynamical stability of two-dimensional flows: variational principles and relaxation equations, European Physical Journal B 70 (2009) 73–105.

[46] P. H. Chavanis, A. Naso, B. Dubrulle, Relaxation equations for two-dimensional turbulent flows with a prior vorticity distribution, European Physical Journal B 77 (2010) 167–186.

[47] P. H. Chavanis, J. Sommeria, Classification of self-organized vortices in two-dimensional turbulence: the case of a bounded domain, J. Fluid Mech. 314 (1996) 267–297.

[48] P. H. Chavanis, J. Sommeria, Thermodynamical Approach for Small-Scale Parametrization in 2D Turbulence, Physical Review Letters 78 (1997) 3302–3305.

[49] P. H. Chavanis, J. Sommeria, Classification of robust isolated vortices in two-dimensional hydrodynamics, Journal of Fluid Mechanics 356 (1998) 259–296.

[50] P. H. Chavanis, J. Sommeria, Statistical mechanics of the shallow water system, Phys. Rev. E 65 (2) (2002) 026302.

[51] P. H. Chavanis, J. Sommeria, R. Robert, Statistical Mechanics of Two-dimensional Vortices and Collisionless Stellar Systems, Astro. Phys. Jour. 471 (1996) 385.

[52] D. B. Chelton, M. G. Schlax, R. M. Samelson, R. A. de Szoeke, Global observations of large oceanic eddies, Geo. Res. Lett.34 (2007) 15606.

[53] P. Chen, M. C. Cross, Phase diagram for coherent vortex formation in the two-dimensional inviscid fluid in circular geometries, Phys. Rev. E50 (1994) 2022–2029.

[54] P. Chen, M. C. Cross, Mean field equilibria of single coherent vortices, Phys. Rev. E54 (1996) 6356–6363.

[55] P. Chen, M. C. Cross, Mixing and Thermal Equilibrium in the Dynamical Relaxation of a Vortex Ring, Physical Review Letters 77 (1996) 4174–4177.

[56] M. Chertkov, C. Connaughton, I. Kolokolov, V. Lebedev, Dynamics of Energy Condensation in Two-Dimensional Turbulence, Phys. Rev. Lett. 99 (2007) 084501.

[57] H. J. H. Clercx, S. R. Maassen, G. J. F. van Heijst, Decaying two-dimensional turbulence in square containers with no-slip or stress-free boundaries, Physics of Fluids 11 (1999) 611–626.

[58] S. Danilov, D. Gurarie, Nonuniversal features of forced two-dimensional turbulence in the energy range, Phys. Rev. E63 (2) (2001) 020203.

[59] T. Dauxois, S. Ruffo, E. Arimondo, M. Wilkens, Dynamics and Thermodynamics of Systems with Long-Range Interactions, vol. 602 of Lecture Notes in Physics, Berlin Springer Verlag, 2002.

[60] M. T. Dibattista, A. J. Majda, An Equilibrium Statistical Theory for Large-Scale Features of Open-Ocean Convection, Journal of Physical Oceanography 30 (2000) 1325–1353.

[61] M. T. Dibattista, A. J. Majda, J. Marshall, A Statistical Theory for the "Patchiness" of Open-Ocean Deep Convection: The Effect of Preconditioning, Journal of Physical Oceanography 32 (2002) 599–626.

[62] T. E. Dowling, Dynamics of jovian atmospheres, Annual Review of Fluid Mechanics 27 (1995) 293–334.

[63] T. E. Dowling, A. P. Ingersoll, Potential vorticity and layer thickness variations in the flow around Jupiter's Great Red SPOT and White Oval BC, Journal of Atmospheric Sciences 45 (1988) 1380–1396.

[64] P. G. Drazin, W. H. Reid, Hydrodynamic stability, Cambridge university press, 2004, second edition.

[65] D. G. Dritschel, M. E. McIntyre, Multiple Jets as PV Staircases: The Phillips Effect and the Resilience of Eddy-Transport Barriers, Journal of Atmospheric Sciences 65 (2008) 855.

[66] D. H. E. Dubin, T. M. O'Neil, Two-dimensional guiding-center transport of a pure electron plasma, Phys. Rev. Lett. 60 (13) (1988) 1286–1289.

[67] S. Dubinkina, J. Frank, Statistical relevance of vorticity conservation in the Hamiltonian particle-mesh method, Journal of Computational Physics 229 (2010) 2634–2648.

[68] B. Dubrulle, S. Nazarenko, Interaction of turbulence and large-scale vortices in incompressible 2D fluids, Physica D 110 (1997) 123–138.

[69] R. S. Ellis, K. Haven, B. Turkington, Large Deviation Principles and Complete Equivalence and Nonequivalence Results for Pure and Mixed Ensembles, J. Stat. Phys. 101 (2000) 999.

[70] R. S. Ellis, K. Haven, B. Turkington, Nonequivalent statistical equilibrium ensembles and refined stability theorems for most probable flows , Nonlinearity 15 (2002) 239–255.

[71] R. S. Ellis, R. Jordan, P. Otto, B. Turkington, A Statistical Approach to the Asymptotic Behavior of a Class of Generalized Nonlinear Schrödinger Equations, Communications in Mathematical Physics 244 (2004) 187–208.

[72] J. G. Esler, The turbulent equilibration of an unstable baroclinic jet, Journal of Fluid Mechanics 599 (2008) 241–268.

[73] G. L. Eyink, Locality of turbulent cascades, Physica D Nonlinear Phenomena 207 (2005) 91–116.

[74] G. L. Eyink, H. Aluie, Localness of energy cascade in hydrodynamic turbulence. I. Smooth coarse graining, Physics of Fluids 21 (11) (2009) 115107.

[75] G. L. Eyink, H. Spohn, Negative-temperature states and large-scale, long-lived vortices in two-dimensional turbulence, Journal of Statistical Physics 70 (1993) 833–886.

[76] G. L. Eyink, K. R. Sreenivasan, Onsager and the theory of hydrodynamic turbulence, Rev. Mod. Phys. 78 (2006) 87–135.

[77] B. F. Farrell, P. J. Ioannou, Structure and Spacing of Jets in Barotropic Turbulence, Journal of Atmospheric Sciences 64 (2007) 3652.

[78] B. F. Farrell, P. J. Ioannou, A Theory of Baroclinic Turbulence, Journal of Atmospheric Sciences 66 (2009) 2444.

[79] R. Fjortoft, On the changes in the spectral distribution of kinetic energy for two-dimensional nondivergent flow, Tellus 5 (1953) 225–230.

[80] N. P. Fofonoff, Steady flow in a frictionless homogeneous ocean., J. Mar. Res. 13 (1954) 254–262.

[81] J. S. Frederiksen, Nonlinear studies on the effects of topography on baroclinic zonal flows, Geophysical and Astrophysical Fluid Dynamics 59 (1991) 57–82.

[82] J. S. Frederiksen, T. J. O'Kane, Entropy, Closures and Subgrid Modeling, Entropy 10 (2008) 635–683.

[83] U. Frisch, Turbulence, Turbulence, by Uriel Frisch, pp. 310. ISBN 0521457130. Cambridge, UK: Cambridge University Press, January 1996., 1996.

[84] U. Frisch, S. Kurien, R. Pandit, W. Pauls, S. S. Ray, A. Wirth, J.-Z. Zhu, Hyperviscosity, galerkin truncation, and bottlenecks in turbulence, Phys. Rev. Lett. 101 (14) (2008) 144501.

[85] A. E. Gill, Atmosphere-Ocean Dynamics, 1982.

[86] A. E. Gill, J. S. A. Green, A. Simmons, Energy partition in the large-scale ocean circulation and the production of mid-ocean eddies, Deep-Sea Research 21 (1974) 499–528.

[87] S. Goldstein, J. L. Lebowitz, On the (Boltzmann) entropy of non-equilibrium systems, Physica D 193 (2004) 53.

[88] M. J. Grote, A. J. Majda, Crude closure dynamics through large scale statistical theories, Physics of Fluids 9 (1997) 3431–3442.

[89] M. J. Grote, A. J. Majda, Crude closure for flow with topography through large-scale statistical theory, Nonlinearity 13 (2000) 569–600.

[90] R. Hallberg, A. Gnanadesikan, The Role of Eddies in Determining the Structure and Response of the Wind-Driven Southern Hemisphere Overturning: Results from the Modeling Eddies in the Southern Ocean (MESO) Project, Journal of Physical Oceanography 36 (2006) 2232.

[91] I. M. Held, V. D. Larichev, A Scaling Theory for Horizontally Homogeneous, Baroclinically Unstable Flow on a Beta Plane., Journal of Atmospheric Sciences 53 (1996) 946–952.

[92] W. Hertel, P. Thirring, Soluble model for a system with negative specific heat, Annals Phys. 63 (1971) 520–533.

[93] N. G. Hogg, H. M. Stommel, The Heton, an Elementary Interaction Between Discrete Baroclinic Geostrophic Vortices, and Its Implications Concerning Eddy Heat-Flow, Royal Society of London Proceedings Series A 397.

[94] G. Holloway, From Classical To Statistical Ocean Dynamics, Surveys in Geophysics 25 (2004) 203–219.

[95] D. D. Holm, J. E. Marsden, T. Ratiu, A. Weinstein, Nonlinear stability of fluid and plasma equilibria, Phys. Rep. 123 (1985) 1–2.

[96] D. D. Holm, J. E. Marsden, T. S. Ratiu, The Euler-Poincare Equations and Semidirect Products with Applications to Continuum Theories, in: eprint arXiv:chao-dyn/9801015, 1998, p. 1015.

[97] A. P. Ingersoll, A. R. Vasavada, Dynamics of Jupiter's atmosphere., IAU Special Session 1 (1998) 1042–1049.

[98] M. B. Isichenko, Nonlinear Landau Damping in Collisionless Plasma and Inviscid Fluid, Physical Review Letters 78 (1997) 2369–2372.

[99] D. Z. Jin, D. H. E. Dubin, Regional Maximum Entropy Theory of Vortex Crystal Formation, Physical Review Letters 80 (1998) 4434–4437.

[100] D. Z. Jin, D. H. E. Dubin, Characteristics of Two-Dimensional Turbulence That Self-Organizes into Vortex Crystals, Phys. Rev. Lett. 84 (2000) 1443–1446.

[101] R. Jordan, C. Josserand, Self-organization in nonlinear wave turbulence, in: eprint arXiv:chao-dyn/9905023, 1999, p. 5023.

[102] R. Jordan, B. Turkington, Statistical mechanics of organized structures in two-dimensional magnetofluid turbulence, vol. 30, 1997, pp. 3629–3636.

[103] G. Joyce, D. Montgomery, Negative temperature states for the two-dimensional guiding-centre plasma, Journal of Plasma Physics 10 (1973) 107.

[104] S. Jung, P. J. Morrison, H. L. Swinney, Statistical mechanics of two-dimensional turbulence, Journal of Fluid Mechanics 554 (2006) 433–456.

[105] B. Jüttner, A. Thess, J. Sommeria, On the symmetry of self-organized structures in two-dimensional turbulence, Physics of Fluids 7 (1995) 2108–2110.

[106] E. Kazantsev, J. Sommeria, J. Verron, Subgrid-Scale Eddy Parameterization by Statistical Mechanics in a Barotropic Ocean Model, Journal of Physical Oceanography 28 (1998) 1017–1042.

[107] H. Kellay, W. I. Goldburg, Two-dimensional turbulence: a review of some recent experiments , Rep. Prog. Phys. 65 (2002) 845–894.

[108] M. Kiessling, Statistical equilibrium dynamics, in: A. Campa, A. Giansanti, G. Morigi, & F. S. Labini (ed.), Dynamics and Thermodynamics of Systems with Long Range Interactions: Theory and Experiments, vol. 970 of American Institute of Physics Conference Series, 2008, pp. 91–108.

[109] M. K. H. Kiessling, J. L. Lebowitz, The Micro-Canonical Point Vortex Ensemble: Beyond Equivalence, Lett. Math. Phys. 42 (1) (1997) 43–56.

[110] J. P. Kossin, W. H. Schubert, Mesovortices, Polygonal Flow Patterns, and Rapid Pressure Falls in Hurricane-Like Vortices., Journal of Atmospheric Sciences 58 (2001) 2196–2209.

[111] R. H. Kraichnan, Inertial Ranges in Two-Dimensional Turbulence, Physics of Fluids 10 (1967) 1417–1423.

[112] R. H. Kraichnan, Inertial Ranges in Two-Dimensional Turbulence, Phys. Fluids 10 (1967) 1417.

[113] R. H. Kraichnan, D. Montgomery, Two-dimensional turbulence, Reports on Progress in Physics 43 (1980) 547–619.

[114] S. Kuksin, . Penrose, A family of balance relations for the two-dimensional Navier-Stokes equations with random forcing, J. Stat. Phys. 118 (3-4) (2005) 437–449.

[115] S. Kuksin, A. Shirikyan, Stochastic Dissipative PDE's and Gibbs Measures, Communications in Mathematical Physics 213 (2000) 291–330.

[116] S. B. Kuksin, The eulerian limit for 2D statistical hydrodynamics, J. Stat. Phys. 115 (2004) 469–492.

[117] L. D. Landau, E. M. Lifshitz, Statistical Physics. Vol. 5 of the Course of Theoretical Physics, Pergamon Press, 1980.

[118] G. Lapeyre, I. M. Held, Diffusivity, Kinetic Energy Dissipation, and Closure Theories for the Poleward Eddy Heat Flux., Journal of Atmospheric Sciences 60 (2003) 2907–2916.

[119] J. Laval, B. Dubrulle, S. Nazarenko, Dynamical modeling of sub-grid scales in 2D turbulence, Physica D Nonlinear Phenomena 142 (2000) 231–253.

[120] Lee, On some statitical properties of hydrodynamical and magnetohydrodynamical fields, Quart. Appl. Math 10 (69).

[121] N. Leprovost, B. Dubrulle, P. H. Chavanis, Thermodynamics of magnetohydrodynamic flows with axial symmetry, Physical Review E 71 (3) (2005) 036311.

[122] N. Leprovost, B. Dubrulle, P. H. Chavanis, Dynamics and thermodynamics of axisymmetric flows: Theory, Phys. Rev. E73 (4) (2006) 046308.

[123] E. M. Lifshitz, L. P. Pitaevskii, Physical kinetics, Course of theoretical physics, Oxford: Pergamon Press, 1981, 1981.

[124] D. K. Lilly, Numerical simulation studies of two-Dimensional turbulence: I. Models of statistically steady turbulence, Geophysical and Astrophysical Fluid Dynamics 3 (1972) 289–319.

[125] C. C. Lim, A long range spherical model and exact solutions of an energy enstrophy theory for two-dimensional turbulence, Physics of Fluids 13 (2001) 1961–1973.

[126] C. C. Lim, R. Singh Mavi, Phase transitions of barotropic flow coupled to a massive rotating sphere. Derivation of a fixed point equation by the Bragg method, Physica A Statistical Mechanics and its Applications 380 (2007) 43–60.

[127] T. S. Lundgren, Strained spiral vortex model for turbulent fine structure, Physics of Fluids 25 (1982) 2193–2203.

[128] D. Lynden-Bell, R. Wood, The gravo-thermal catastrophe in isothermal spheres and the onset of red-giant structure for stellar systems, Mon. Not. R. Astron. Soc. 138 (1968) 495.

[129] A. J. Majda, X. Wang, Nonlinear Dynamics and Statistical Theories for Basic Geophysical Flows, Cambridge University Press, 2006.

[130] A. J. Majda, X. Wang, The emergence of large-scale coherent structure under small-scale random bombardments, Comm. Pure App. Maths 59 (4) (2006) 467–500.

[131] P. S. Marcus, Jupiter's Great Red SPOT and other vortices, Ann. Rev. Astron. Astrophys. 31 (1993) 523–573.

[132] J. B. Marston, E. Conover, T. Schneider, Statistics of an Unstable Barotropic Jet from a Cumulant Expansion, Journal of Atmospheric Sciences 65 (2008) 1955.

[133] D. Marteau, O. Cardoso, P. Tabeling, Equilibrium states of two-dimensional turbulence: An experimental study, Phys. Rev. E51 (1995) 5124–5127.

[134] J. C. Mattingly, Y. G. Sinai, An Elementary Proof of the Existence and Uniqueness Theorem for the Navier-Stokes Equations, ArXiv Mathematics e-prints:math/9903042.

[135] W. J. Merryfield, Effects of stratification on quasi-geostrophic inviscid equilibria, Journal of Fluid Mechanics 354 (1998) 345–356.

[136] W. J. Merryfield, P. F. Cummins, G. Holloway, Equilibrium Statistical Mechanics of Barotropic Flow over Finite Topography, Journal of Physical Oceanography 31 (2001) 1880–1890.

[137] J. Michel, R. Robert, Large deviations for young measures and statistical mechanics of infinite dimensional dynamical systems with conservation law, Communications in Mathematical Physics 159 (1994) 195–215.

[138] J. Michel, R. Robert, Statistical mechanical theory of the great red spot of jupiter, Journal of Statistical Physics 77 (1994) 645–666.

[139] J. Miller, Statistical mechanics of euler equations in two dimensions, Phys. Rev. Lett. 65 (17) (1990) 2137–2140.

[140] J. Miller, P. B. Weichman, M. C. Cross, Statistical mechanics, Euler's equation, and Jupiter's Red Spot, Phys. Rev. A45 (1992) 2328–2359.

[141] L. Modica, The gradient theory of phase transitions and the minimal interface criterion, Archive for Rational Mechanics and Analysis 98 (1987) 123–142.

[142] R. Monchaux, F. Ravelet, B. Dubrulle, A. Chiffaudel, F. Daviaud, Properties of Steady States in Turbulent Axisymmetric Flows, Physical Review Letters 96 (12) (2006) 124502.

[143] H. Morita, E. Simonnet, F. Bouchet, Statistical properties of out of equilibrium phase transitions for the 2D Navier-Stokes equations, Submitted to Phys. Rev. E.

[144] P. J. Morrison, Hamiltonian description of the ideal fluid, Reviews of Modern Physics 70 (1998) 467–521.

[145] C. Mouhot, C. Villani, On the landau damping, arXiv 0904.2760.

[146] A. Naso, P. H. Chavanis, B. Dubrulle, Statistical mechanics of Fofonoff flows in an oceanic basin, ArXiv e-prints:1007.0164.

[147] A. Naso, P. H. Chavanis, B. Dubrulle, Statistical mechanics of two-dimensional Euler flows and minimum enstrophy states, European Physical Journal B 77 (2010) 187–212.

[148] A. Naso, R. Monchaux, P. H. Chavanis, B. Dubrulle, Statistical mechanics of Beltrami flows in axisymmetric geometry: Theory reexamined, Physical Review E 81 (6) (2010) 066318.

[149] S. Nazarenko, Exact solutions for near-wall turbulence theory, Physics Letters A 264 (2000) 444–448.

[150] S. Nazarenko, J.-P. Laval, Non-local two-dimensional turbulence and Batchelor's regime for passive scalars, J. Fluid Mech. 408 (2000) 301–321.

[151] S. Nazarenko, B. Quinn, Triple Cascade Behavior in Quasigeostrophic and Drift Turbulence and Generation of Zonal Jets, Physical Review Letters 103 (11) (2009) 118501.

[152] D. Nicholson, Introduction to plasma theory, Wiley, New-York, 1983.

[153] L. Onsager, Statistical hydrodynamics, Nuovo Cimento 6 (No. 2 (Suppl.)) (1949) 249–286.

[154] J. Paret, M. Jullien, P. Tabeling, Vorticity Statistics in the Two-Dimensional Enstrophy Cascade, Physical Review Letters 83 (1999) 3418–3421.

[155] J. Paret, P. Tabeling, Intermittency in the two-dimensional inverse cascade of energy: Experimental observations, Phys. Fluids 10 (1998) 3126–3136.

[156] J. Pedlosky, Geophysical fluid dynamics, 1982.

[157] J. Pedlosky, Ocean Circulation Theory, New York and Berlin, Springer-Verlag, 1998.

[158] R. L. Pego, M. I. Weinstein, Asymptotic stability of solitary waves, Communications in Mathematical Physics 164 (1994) 305–349.

[159] Y. Pomeau, Statistical approach (to 2D turbulence), in: P. Tabeling, O. Cardoso (eds.), Turbulence: A Tentative Dictionary, Plenum Press, New York, 1995, pp. 117–123.

[160] R. Prieto, W. H. Schubert, Analytical Predictions for Zonally Symmetric Equilibrium States of the Stratospheric Polar Vortex., Journal of Atmospheric Sciences 58 (2001) 2709–2728.

[161] B. Qiu, W. Miao, Kuroshio Path Variations South of Japan: Bimodality as a Self-Sustained Internal Oscillation, Journal of Physical Oceanography 30 (2000) 2124–2137.

[162] W. Ritz, A. Einstein, Zum gegenwärtigen Stand des Strahlungsproblems, Physikalische Zeitschrift 10 (1909) 323–324.

[163] R. Robert, Etats d'équilibre statistique pour l'écoulement bidimensionnel d'un fluide parfait, C. R. Acad. Sci. 1 (1990) 311:575–578.

[164] R. Robert, A maximum-entropy principle for two-dimensional perfect fluid dynamics, J. Stat. Phys. 65 (1991) 531–553.

[165] R. Robert, On the Statistical Mechanics of 2D Euler Equation, Communications in Mathematical Physics 212 (2000) 245–256.

[166] R. Robert, C. Rosier, The modeling of small scales in two-dimensional turbulent flows: A statistical mechanics approach, Journal of Statistical Physics 86 (1997) 481–515.

[167] R. Robert, C. Rosier, Long range predictability of atmospheric flows, Nonlinear Processes in Geophysics 8 (2001) 55–67.

[168] R. Robert, J. Sommeria, Statistical equilibrium states for two-dimensional flows, J. Fluid Mech. 229 (1991) 291–310.

[169] R. Robert, J. Sommeria, Relaxation towards a statistical equilibrium state in two-dimensional perfect fluid dynamics, Phys. Rev. Lett. 69 (19) (1992) 2776–2779.

[170] S. I. Rosencrans, D. H. Sattinger, On the spectrum of an operator occuring in the theory of hydrodynamic stability, J. Math. Phys. 45 (1966) 289–300.

[171] R. Salmon, Lectures on Geophysical Fluid Dynamics, Oxford University Press, 1998.

[172] R. Salmon, G. Holloway, M. C. Hendershott, The equilibrium statistical mechanics of simple quasi-geostrophic models, Journal of Fluid Mechanics 75 (1976) 691–703.

[173] D. A. Schecter, D. H. E. Dubin, A. C. Cass, C. F. Driscoll, I. M. Lansky, T. M. O'Neil, Inviscid damping of asymmetries on a two-dimensional vortex, Physics of Fluids 12 (2000) 2397–2412.

[174] D. A. Schecter, D. H. E. Dubin, K. S. Fine, C. F. Driscoll, Vortex crystals from 2D Euler flow: Experiment and simulation, Phys. Fluids 11 (1999) 905–914.

[175] M. J. Schmeits, H. A. Dijkstraa, Bimodal behavior of the kuroshio and the gulf stream., J. Phys. Oceanogr. 31 (2001) 3425–3456.

[176] E. Segre, S. Kida, Late states of incompressible 2D decaying vorticity fields, in: eprint arXiv:chao-dyn/9709020, 1997, p. 9020.

[177] F. Seychelles, Y. Amarouchene, M. Bessafi, H. Kellay, Thermal Convection and Emergence of Isolated Vortices in Soap Bubbles, Physical Review Letters 100 (14) (2008) 144501.

[178] R. A. Smith, T. M. O'Neil, Nonaxisymmetric thermal equilibria of a cylindrically bounded guiding-center plasma or discrete vortex system, Phys. Fluids B 2 (1990) 2961–2975.

[179] J. Sommeria, Experimental study of the two dimensional inverse energy cascade in a square box, J. Fluid. Mech. 170 (1986) 139–168.

[180] J. Sommeria, Two-Dimensional Turbulence, in: S. Berlin (ed.), New trends in turbulence, vol. 74 of Les Houches, 2001, pp. 385–447.

[181] J. Sommeria, C. Nore, T. Dumont, R. Robert, Statistical theory of the Great Red SPOT of Jupiter, Academie des Science Paris Comptes Rendus Serie B Sciences Physiques 312 (1991) 999–1005.

[182] J. Sommeria, C. Staquet, R. Robert, Final equilibrium state of a two-dimensional shear layer, Journal of Fluid Mechanics 233 (1991) 661–689.

[183] L. Spitzer, Dynamical evolution of Globular Clusters, Princeton University Press, 1991.

[184] H. Spohn, Large Scale Dynamics of Interacting Particles, Springer, New-York, 2002.

[185] D. Stammer, Global Characteristics of Ocean Variability Estimated from Regional TOPEX/POSEIDON Altimeter Measurements, Journal of Physical Oceanography 27 (1997) 1743–1769.

[186] P. Tabeling, Two-dimensional turbulence: a physicist approach, Physics Reports362 (2002) 1–62.

[187] A. Thess, J. Sommeria, B. Jüttner, Inertial organization of a two-dimensional turbulent vortex street, Physics of Fluids 6 (1994) 2417–2429.

[188] A. F. Thompson, W. R. Young, Two-Layer Baroclinic Eddy Heat Fluxes: Zonal Flows and Energy Balance, Journal of Atmospheric Sciences 64 (2007) 3214.

[189] W. Thomson, On the stability of steady and of periodic fluid motion, Philos. Mag. 24 (1887) 188–196.

[190] Y. Tian, E. R. Weeks, K. Ide, J. S. Urbach, C. N. Baroud, M. Ghil, H. L. Swinney, Experimental and numerical studies of an eastward jet over topography, J. Fluid Mech. 438 (2001) 129–157.

[191] B. Turkington, On steady vortex flow in two dimensions, I, Communications in Partial Differential Equations 8 (9) (1983) 999–1030.

[192] B. Turkington, On steady vortex flow in two dimensions, II, Communications in Partial Differential Equations 8 (9) (1983) 999–1030.

[193] B. Turkington, A. Majda, K. Haven, M. Dibattista, Statistical equilibrium predictions of jets and spots on Jupiter, PNAS 98 (2001) 12346–12350.

[194] B. Turkington, N. Whitaker, Statistical equilibrium computations of coherent structures in turbulent shear layers, SIAM J. Sci. Comput. 17 (6) (1996) 1414–1433.

[195] G. K. Vallis, Atmospheric and Oceanic Fluid Dynamics, 2006.

[196] G. K. Vallis, G. F. Carnevale, W. R. Young, Extremal energy properties and construction of stable solutions of the Euler equations, Journal of Fluid Mechanics 207 (1989) 133–152.

[197] A. Venaille, F. Bouchet, Statistical Ensemble Inequivalence and Bicritical Points for Two-Dimensional Flows and Geophysical Flows, Physical Review Letters 102 (10) (2009) 104501.

[198] A. Venaille, F. Bouchet, Oceanic rings and jets as statistical equilibrium states, ArXiv e-prints:1011.2556.

[199] A. Venaille, F. Bouchet, Solvable phase diagrams and ensemble inequivalence for two-dimensional and geophysical turbulent flows, ArXiv e-prints:1011.2309.

[200] J. Wang, G. K. Vallis, Emergence of Fofonoff states in inviscid and viscous ocean circulation models, Journal of Marine Research 52 (1994) 83–127.

[201] E. R. Weeks, Y. Tian, J. S. Urbach, K. Ide, H. L. Swinney, M. Ghil, Transitions Between Blocked and Zonal Flows in a Rotating Annulus, Science 278 (1997) 1598.

[202] P. B. Weichman, Equilibrium theory of coherent vortex and zonal jet formation in a system of nonlinear Rossby waves, Phys. Rev. E73 (3) (2006) 036313.

[203] E. Weinan, J. C. Mattingly, Ergodicity for the Navier-Stokes equation with degenerate random forcing: Finite-dimensional approximation, Comm. Pure Appl. Math. 54 (2001) 1386–1402.

[204] N. Whitaker, B. Turkington, Maximum entropy states for rotating vortex patches, Physics of Fluids 6 (1994) 3963–3973.

[205] G. Wolansky, M. Ghil, Nonlinear Stability for Saddle Solutions of Ideal Flows and Symmetry Breaking, Commun. Math. Phys. 193 (1998) 713–736.

[206] Z. Yin, D. C. Montgomery, H. J. H. Clercx, Alternative statistical-mechanical descriptions of decaying two-dimensional turbulence in terms of “patches” and “points”, Phys. Fluids 15 (2003) 1937–1953.

[207] V. Zeitlin, Finite-mode analogs of 2D ideal hydrodynamics: Coadjoint orbits and local canonical structure, Physica D Nonlinear Phenomena 49 (1991) 353–362.

[208] J. Zou, G. Holloway, Entropy maximization tendency in topographic turbulence, Journal of Fluid Mechanics 263 (1994) 361–374.

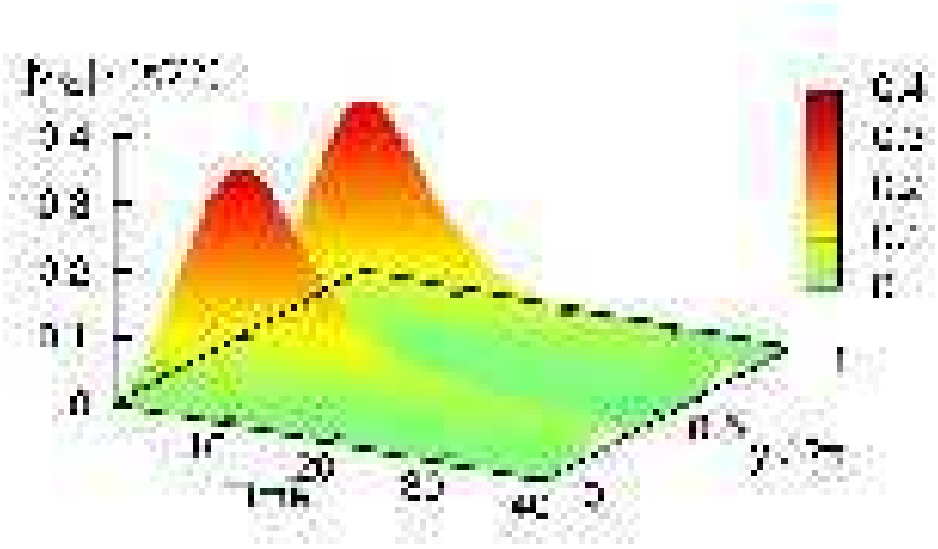

(a)

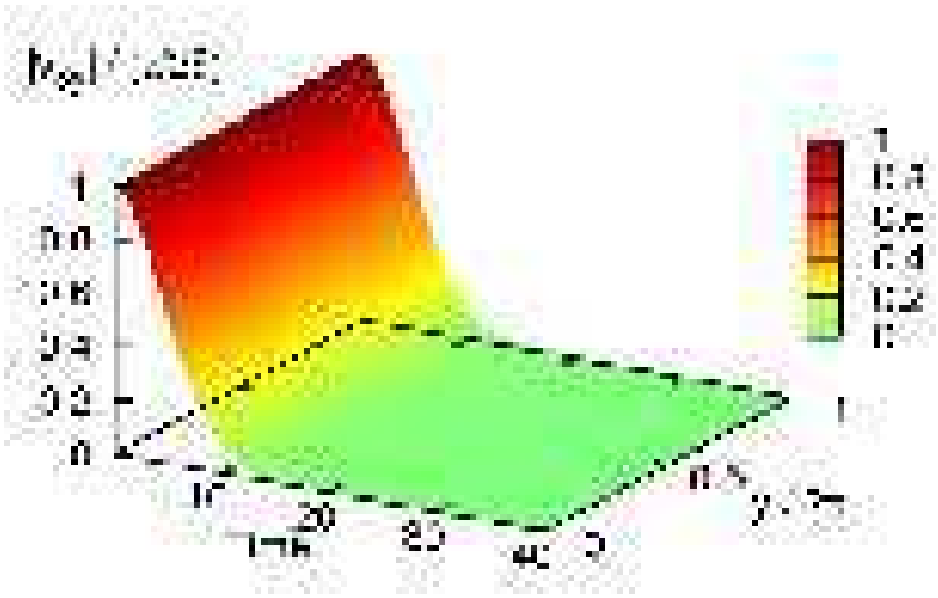

(b)

Figure 33: The space-time series of perturbation velocity components, $|v_{\delta,x}(y,t)|$ (a) and $|v_{\delta,y}(y,t)|$ (b), for the initial perturbation profile $\cos(x/\delta)$ in a doubly periodic domain with aspect ratio $\delta = 1.1$. Both the components relax toward zero, showing the asymptotic stability of the Euler equations. (colors in the .pdf document)

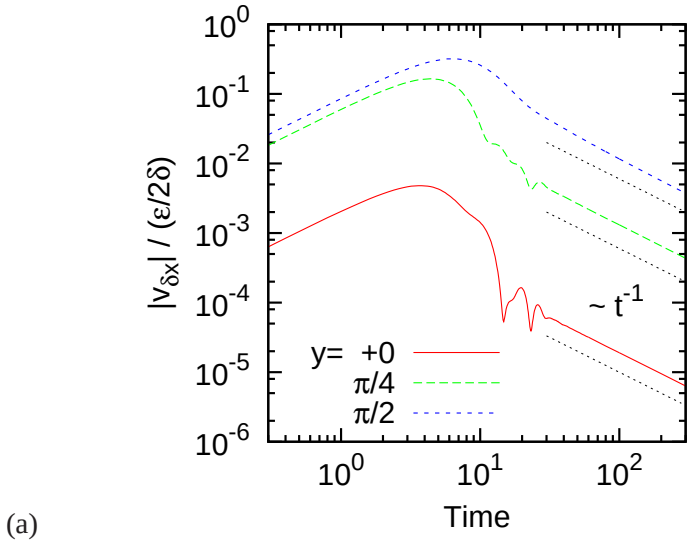

(a)

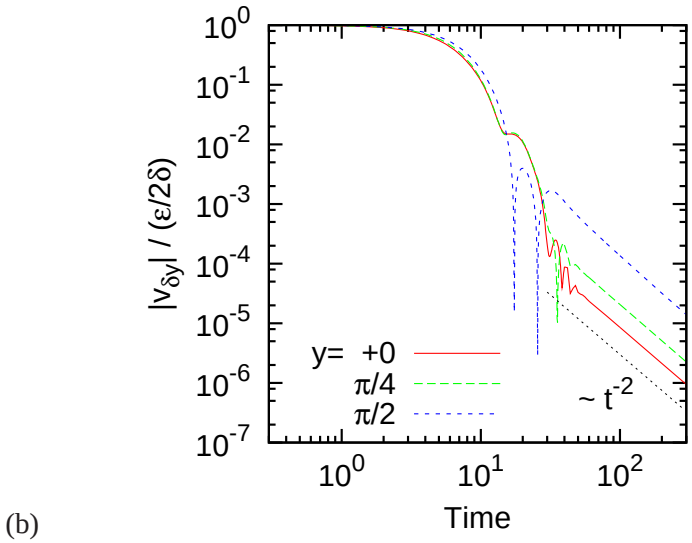

(b)

Figure 34: The time series of perturbation velocity components $|v_{\delta,x}(y,t)|$ (a) and $|v_{\delta,y}(y,t)|$ (b) at three locations, $y = 0$ (vicinity of the stationary streamline) (red), $y = \pi/4$ (green), and $y = \pi/2$ (blue), for the initial perturbation profile $A(y) = 1$ and the aspect ratio $\delta = 1.1$. We observe the asymptotic forms $|v_{\delta,x}(y,t)| \sim t^{-\alpha}$, with $\alpha = 1$, and $|v_{\delta,y}(y,t)| \sim t^{-\beta}$, with $\beta = 2$, in accordance with the theory for the asymptotic behavior of the velocity (equations (113) and (114)). The initial perturbation profile is $\cos(x/\delta)$ in a doubly periodic domain with aspect ratio $\delta = 1.1$. (colors in the .pdf document)

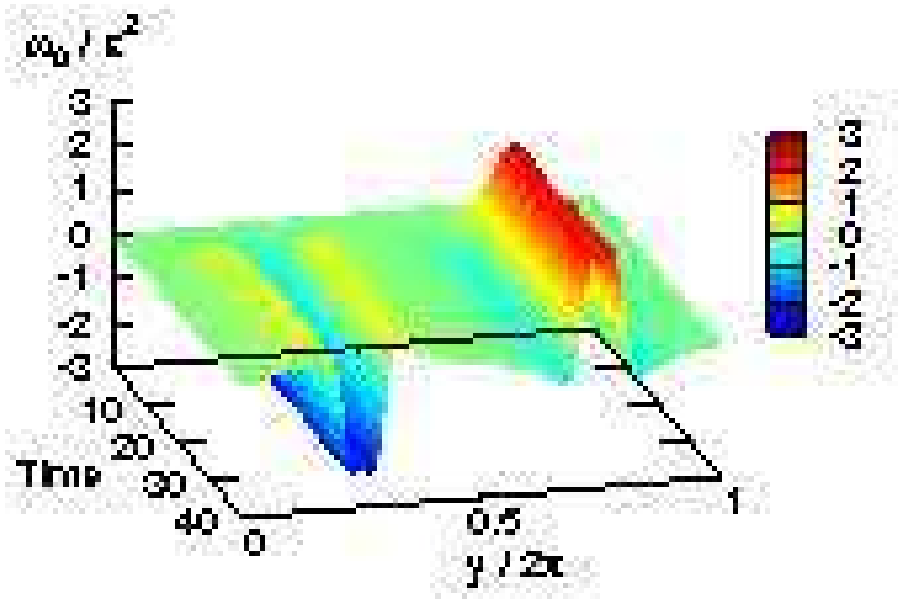

Figure 35: The space-time series of the x-averaged perturbation vorticity, $\omega_0(y,t) = \omega(y,t)$-$\Omega_0(y,0)$. The initial condition is $\omega(y,t) = \Omega_0(y,0) + \varepsilon\cos(x)$, in a doubly periodic domain with aspect ratio $\delta = 1.1$ (colors in the .pdf document).